

ORBITAL MAGNETISM IN THE BALLISTIC REGIME: GEOMETRICAL EFFECTS

Klaus RICHTER^{a, b}, Denis ULLMO^{a, c}, Rodolfo A. JALABERT^{a, d}

^a *Division de Physique Théorique, Institut de Physique, Nucléaire, 91406 Orsay Cedex, France*

^b *Institut für Physik, Memminger Str. 6, 86135 Augsburg, Germany*

^c *AT&T Bell Laboratories, 1D-265, 600 Mountain Avenue, Murray Hill, NJ 07974-0636, USA*

^d *Université Louis Pasteur, IPCMS-GEMME, 23 rue du Loess, 67037 Strasbourg Cedex, France*



ELSEVIER

AMSTERDAM – LAUSANNE – NEW YORK – OXFORD – SHANNON – TOKYO



ELSEVIER

Physics Reports 276 (1996) 1–83

PHYSICS REPORTS

Orbital magnetism in the ballistic regime: geometrical effects

Klaus Richter^{a,b}, Denis Ullmo^{a,c}, Rodolfo A. Jalabert^{a,d}^a *Division de Physique Théorique, Institut de Physique Nucléaire, 91406 Orsay Cedex, France*^b *Institut für Physik, Memminger Str. 6, 86135 Augsburg, Germany*^c *AT&T Bell Laboratories, 1D-265, 600 Mountain Avenue, Murray Hill, NJ 07974-0636, USA*^d *Université Louis Pasteur, IPCMS-GEMME, 23 rue du Loess, 67037 Strasbourg Cedex, France*

Received January 1996; editor: I. Procaccia

Contents

1. Introduction	4	6.1. Generic integrable systems	47
1.1. Historical perspective	4	6.2. Generic chaotic systems	52
1.2. Susceptibility of unconstrained and constrained electron systems	7	6.3. Integrable versus chaotic geometries	57
1.3. Overview of this work	9	7. Non-perturbative fields: bouncing-ball- and de Haas–van Alphen-oscillations	58
2. Thermodynamic formalism	12	7.1. Intermediate fields: Bouncing-ball magnetism	60
2.1. Grand canonical properties	13	7.2. Strong field regime	65
2.2. Canonical ensemble	16	8. Conclusion	67
3. Landau susceptibility	18	A. Convolution of a rapidly oscillat- ing function with the derivative of the Fermi function	71
4. Systems integrable at arbitrary fields	21	B. Semiclassical expansion of the mean density of states	73
4.1. Oscillating density of states for weak field	22	C. Calculation of g_E for a ring billiard	75
4.2. Circular billiards	24	D. Calculation of the determinant D_M at zero field for a generic integrable system	76
4.3. Rings	27	E. Diagonal part of the Green function for a free electron in a constant magnetic field	78
5. Simple regular geometries: the square	33	E.1. Computation of the prefactor of a Green function near a focal point	78
5.1. Oscillating density of states for weak field	34	E.2. Application to the cyclotron motion	80
5.2. The susceptibility: individual samples versus ensemble averages	38	References	81
5.3. Contribution of longer orbits	41		
5.4. Numerical calculations	43		
5.5. Comparison between numerical and semiclassical results	45		
5.6. Comparison with the experiment	46		
6. Generic integrable and chaotic systems	47		

Abstract

We present a general semiclassical theory of the orbital magnetic response of noninteracting electrons confined in two-dimensional potentials. We calculate the magnetic susceptibility of singly-connected and the persistent currents of multiply connected geometries. We concentrate on the geometric effects by studying confinement by perfect (disorder free) potentials stressing the importance of the underlying classical dynamics. We demonstrate that in a constrained geometry the standard Landau diamagnetic response is always present, but is dominated by finite-size corrections of a quasi-random sign which may be orders of magnitude larger. These corrections are very sensitive to the nature of the classical dynamics. Systems which are integrable at zero magnetic field exhibit larger magnetic response than those which are chaotic. This difference arises from the large oscillations of the density of states in integrable systems due to the existence of families of periodic orbits. The connection between quantum and classical behavior naturally arises from the use of semiclassical expansions. This key tool becomes particularly simple and insightful at finite temperature, where only short classical trajectories need to be kept in the expansion. In addition to the general theory for integrable systems, we analyze in detail a few typical examples of experimental relevance: circles, rings and square billiards. In the latter, extensive numerical calculations are used as a check for the success of the semiclassical analysis. We study the weak-field regime where classical trajectories remain essentially unaffected, the intermediate field regime where we identify new oscillations characteristic for ballistic mesoscopic structures, and the high-field regime where the typical de Haas–van Alphen oscillations exhibit finite-size corrections. We address the comparison with experimental data obtained in high-mobility semiconductor microstructures discussing the differences between individual and ensemble measurements, and the applicability of the present model.

PACS: 03.65.Sq; 05.45.+b; 05.30.Fk; 73.20.Dx

1. Introduction

1.1. Historical perspective

The study of orbital magnetism in an electron gas goes back to the 1930s with the pioneering work of Landau [1,2] demonstrating the existence of a small diamagnetic response at weak fields H and low temperatures T (such that $k_B T$ exceeds the typical spacing $\hbar\omega$, $\omega = eH/mc$). Three features of this original proposal contributed to the slowness of its general acceptance. First, it deals with a purely quantum result that can be expressed as a thermodynamic relationship without an explicit \hbar dependence. In contrast to that the Bohr–van Leeuwen theorem [3] establishes the absence of magnetism for a system of classical particles. For finite systems the boundary currents are shown to exactly cancel the diamagnetic contribution from cyclotron orbits of the interior. (This result remains valid even if we consider Fermi or Bose statistics [4].) Secondly, boundary effects (so crucial in obtaining the correct classical behavior) did not enter into Landau’s original derivation. Twenty years later Sondheimer and Wilson [5] presented a more rigorous formulation for the magnetism of *unconstrained* electrons at weak and strong fields without using explicit knowledge of the energy levels, thus avoiding complicated arguments involving boundary electrons. (Here we present a semiclassical derivation of Landau diamagnetism independent of the energy level structure and valid for *constrained* geometries at arbitrary magnetic fields.) Finally, Landau diamagnetism for standard metals yields a small effect (one-third of the Pauli spin paramagnetism) making its experimental observation rather difficult. Peierls [4, 6] showed shortly after Landau’s work that the diamagnetic susceptibility persists when electrons are placed in a periodic potential and its value is obtained by simply using the effective mass instead of the free electron mass. But even if the effective mass is smaller than the bare mass, and the diamagnetic orbital response dominates over the spin paramagnetic susceptibility (as typically happens in doped semiconductors), the detailed comparison with the experimental data on metals was still difficult [5]. This follows from the complicated electronic structure and the fact that taking into account electron–electron interactions in the same way as a periodic potential by renormalizing the effective mass, is a too crude approximation.

While the restriction of the electron gas to a two–dimensional plane (still in the thermodynamic limit) does not pose any new conceptual or calculational difficulty [4, 7], the effect of confining the electron system to a finite volume introduces a new energy scale in the problem (the typical level spacing Δ) and leads to a modification of the Landau susceptibility. The latter point has therefore been the object of several conflicting studies.¹ The investigation of finite-size corrections was motivated by experiments on small metal clusters and dealt with various theoretical models: thin plates [9], thin cylinders [10], confinement by quadratic potentials [11, 12], circular [13] and rectangular boxes [14, 15]. Finite-size effects and corrections to bulk magnetism obviously depend on the relation between the typical size a of the system and other relevant length scales [16]: The thermal length $L_T = \hbar v_F \beta / \pi$ (v_F is the Fermi velocity and $\beta = 1/k_B T$), the elastic mean free path l (with respect to impurity scattering), and the phase-coherence length L_ϕ (taking into account inelastic processes like electron–phonon scattering). Most of the above mentioned studies neglect other scattering mechanisms than that by the boundaries of the device, and deal with the macroscopic (or high temperature) case of $L_T \ll a$. The first assumption severely limits the possible

¹ For the historical account of this tortuous and often contradictory chain of findings see Ref. [8].

comparison with the experimental data of real metal clusters, while in the regime where the second assumption is valid the magnetic response is dominated by its smooth component for which, as generally shown by Robnik [17] and Antoine [18], only small corrections to the diamagnetic bulk susceptibility are found.

Opposite to the macroscopic limit, there had been studies in the extreme quantum limit [19], where the temperature is low enough to enable the resolution of individual levels ($k_B T < \Delta$). In this regime the magnetic susceptibility is dominated by erratic fluctuations that, as we will see later, hinder its unequivocal determination. The purpose of the present work is the study of size corrections in the *mesoscopic* regime [20], intermediate between the two previous limits (that is, for temperatures satisfying $L_T/a > 1 > \beta\Delta$) and where inelastic processes do not inhibit quantum interference effects ($L_\phi > a$). Nowadays this is an experimentally accessible regime receiving considerable attention due to the richness of its physical properties. When $L_\phi > a > l$ we have the mesoscopic *diffusive* regime where the electron motion is dominated by impurity scattering, while for $L_\phi > l > a$ we enter into the *ballistic* regime where electrons are mainly scattered off the walls of a confining potential. A central conclusion of our work is that finite-size corrections to the magnetic susceptibility in the *ballistic* regime can be *orders of magnitude* larger than the bulk values.

One of the reasons for the sustained interest of the last few years in the mesoscopic ballistic regime is the possibility of studying the relation of the underlying classical dynamics and the quantum properties. This issue is precisely the subject of the field known as “quantum chaos” [21, 22]. Since the number of electrons N in a mesoscopic system is always large, particles at the Fermi energy have a De Broglie wavelength λ_F much smaller than the typical size a of the system ($a/\lambda_F \propto k_F a \propto N^{1/d}$, k_F is the Fermi wave vector, d the number of degrees of freedom), and are therefore well in the semiclassical regime. High-mobility mesoscopic semiconductor samples provide an appropriate experimental testing ground in this context and have been recently examined with respect to the role of chaos in transport phenomena (for a review, see [23, 24]). The present work extends the connection between mesoscopic systems and quantum chaos to thermodynamic properties, and analyzes recent experiments [25, 26] measuring the magnetic response of ballistic microstructures. One main concern of our work is to show that mesoscopic finite-size effects depend crucially on the classical dynamics of the ballistic billiard, i.e. whether it is integrable or chaotic, and that the magnetic response provides an experimentally accessible criterion in order to distinguish between integrable and chaotic devices (much more neatly than through the subtle differences found in the transport problem [23, 24]).

The importance of geometrical effects for the finite-size corrections in the above-defined macroscopic limit had already been noticed in terms of the sensitivity of the magnetic susceptibility on the structure of the confining potential [10–12]. The chosen potentials were obviously nongeneric but used due to their calculational simplicity, and therefore it was not possible to anticipate the order-of-magnitude effect that classical dynamics might have on the susceptibility outside the macroscopic limit. The problem of orbital magnetism from a quantum chaos point of view was first addressed by Nakamura and Thomas [27] in their numerical study of the differences in the magnetic response of circular and elliptic billiards at zero temperature. The circular billiard is integrable at arbitrary field, while the ellipse develops chaotic behavior at finite fields. They found a reduction compared to the bulk susceptibility and strong fluctuations (with varying magnetic field), and observed that both effects were stronger for the elliptic billiard. As already mentioned, the difficulty of these studies in the extreme quantum limit (at zero temperature) consists in the existence of strong fluctuations arising from exact or quasi-crossings of energy levels (depending parametrically on the magnetic field)

where the susceptibility diverges. Similar features were obtained for other integrable systems in the quantum limit like the rectangular box [19], the Corbino disk and the cylinder [28]. However, this unphysical behavior is regularized by finite temperature that approximately adjusts the populations of both levels to each other at a crossing (or anti-crossing).

Parallel to the studies of the orbital response in finite size singly connected systems, there have been important developments in the understanding of persistent currents (i.e. the orbital magnetism in multiply connected geometries).² These latter studies started usually from very general considerations without making the connection with the Landau diamagnetism. The pioneering work of Büttiker et al. [29] demonstrating that in the presence of magnetic flux the ground state of a one-dimensional ring has a current flow generated a large theoretical activity, mainly directed towards generalizations of quasi-one-dimensional and diffusive rings [30, 32]. The first experimental evidence of persistent currents in an ensemble of mesoscopic copper rings was given by the 1990 measurement of Lévy et al. [33]. The use of an ensemble was motivated by experimental reasons and brought up important issues about the differences between the canonical and grand canonical ensembles in the mesoscopic regime [34–36] that we will review in the present work. Later experiments achieved the measurement of persistent currents in single disordered [37] and ballistic [26] rings. In Section 4 we analyze in detail the last experiment making the connection with the orbital magnetism of the other sections. The connection between classical mechanics and persistent currents has already been explored in Refs. [38–40].

Small metallic samples at sufficiently low temperatures operate in the diffusive mesoscopic regime, where the classical electron motion is a random walk through the impurity potential. This was the regime of the original experiment on persistent currents [33] and therefore received considerable theoretical attention. The effect of disorder on persistent currents has been evaluated by diagrammatic perturbation theory [36]. A weak disorder potential does not alter the bulk Landau diamagnetism [41] and gives within perturbation theory enhancement factors proportional to $k_F l$ for finite samples [42]. Highly pure semiconductor heterojunctions combined with lithographic techniques allow the realization of samples small enough to be in the mesoscopic ballistic regime where $l > a$. This is the case of the orbital magnetism and persistent current measurements of Refs. [25, 26]. In the ballistic regime electrons move almost straight between collisions with the walls of the confining potential. The small drift between collisions is due to the unavoidable disorder potential existing in real structures. Neglecting completely the effect of disorder, and therefore the associated drift, leads to an ideal or *clean* system which describes simply an electron billiard. A central result of our work is that the application of semiclassical expansions at finite temperature allows one only to consider *short classical periodic trajectories*. Therefore, the clean model provides a reasonable approach to the weak and smooth disorder of the ballistic regime. We will get back to this point in this work, and in a separate paper [43] we examine in detail the role of disorder in ballistic samples.

The previously cited developments, as well as most of the present work, deal with finite-size effects in the orbital response at *weak fields*. At high fields the magnetic response is dominated by the occurrence of Landau levels (whose spacing $\hbar\omega$ is much larger than Δ or $k_B T$) yielding the well known de Haas–van Alphen effect. In 1938 Landau derived (see Refs. [5, 7]) a complete analytical expression for the susceptibility of a degenerate free electron gas including the weak-field diamagnetic response and the de Haas–van Alphen oscillations. Since the latter turned out

² For historical accounts on persistent currents see Refs. [30, 31].

to be a powerful technique to examine the electron structure of metals [44] its study has been at the heart of Condensed Matter Physics for various decades. Its measurement in two-dimensional electron gases has allowed the determination of the density of states at high field [45]. With the advent of Mesoscopic Physics the question of finite-size effects on the de Haas–van Alphen effect was naturally raised, and free electron gases on a disk [46,47] and confined by a parabolic potential [48] were considered at high fields. The semiclassical theory used in the present work provides the finite-temperature susceptibility at arbitrary fields and allows the identification of an intermediate regime characteristic for ballistic samples that we discuss in Section 7.

Our work aims at the convergence of various seemingly disconnected fields: Landau diamagnetism, persistent currents, de Haas–van Alphen effect, finite-size corrections of thermodynamic functions, quantum chaos, and electronic properties of weakly disordered systems. We will show that the semiclassical analysis naturally enters in the problem of the magnetic response of ballistic structures, provided a model of noninteracting electrons is adequate. The expression of the magnetic susceptibility and persistent currents in terms of classical trajectories provides a unifying approach applicable to various geometrical shapes, different temperatures and magnetic field strengths.

1.2. Susceptibility of unconstrained and constrained electron systems

We now present the basic formulas defining the magnetic susceptibility and then compare the unconstrained magnetic response with the susceptibility obtained by confining the electron gas to a finite region to illustrate the subject of our studies in this paper. Let us consider a noninteracting electron gas confined in a volume (area in two dimensions) A at temperature T under a magnetic field H . The magnetic moment of the system in statistical equilibrium is given by the thermodynamic relation

$$\mathcal{M} = -(\partial\Omega/\partial H)_{T,\mu} \quad (1.1)$$

where $\Omega(T, \mu, H)$ is the thermodynamic potential, and μ the chemical potential of the electron gas. The differential magnetic susceptibility is defined by

$$\chi^{\text{GC}} = (1/A)(\partial\mathcal{M}/\partial H)_{T,\mu} = -(1/A)(\partial^2\Omega/\partial H^2)_{T,\mu}. \quad (1.2)$$

The notation with the superscript GC is used in order to emphasize the fact that we are working in the grand canonical ensemble. The choice of the ensemble in the macroscopic limit of N and $A \rightarrow \infty$ is a matter of convenience. As it is well known by now [34–36] the equivalence between the ensembles may break down in the mesoscopic regime that interests us, and this point will be thoroughly discussed in the remaining part of the paper. However, for the purpose of this didactical introduction we will work in the grand canonical ensemble studying the magnetic response of electron systems with fixed chemical potentials. The calculation advantages of the GC ensemble arise from the simple form of the thermodynamic potential

$$\Omega(T, \mu, H) = -\frac{1}{\beta} \int dE d(E) \ln(1 + \exp[\beta(\mu - E)]), \quad (1.3)$$

in terms of the single-particle density of states

$$d(E) = g_s \sum_{\lambda} \delta(E - E_{\lambda}). \quad (1.4)$$

The factor $g_s = 2$ takes into account spin degeneracy, E_i are the eigenenergies of the system. The magnetic susceptibility is directly extracted from the knowledge of the density of states. The case of a free electron gas is particularly simple since the electron eigenstates are Landau states with energies

$$E_k = \hbar w \left(k + \frac{1}{2} \right), \quad k = 0, 1, 2, \dots \quad (1.5)$$

and degeneracies $g_s \Phi / \Phi_0$. The cyclotron frequency is $w = eH/mc$, $\Phi = HA$ is the flux through an area A , and $\Phi_0 = hc/e$ is the elemental flux quantum. Throughout this work we will neglect the Zeeman splitting term due to the electron spin. It can however be incorporated easily when spin–orbit coupling is negligible [49].

Landau's derivation of the magnetic susceptibility of a free electron system arising from the quantization condition (1.5) can be found for the three-dimensional case in standard textbooks [2, 4]. The two-dimensional case [7, 8] follows upon the same lines. In the following we present a sketch of the latter which will be useful towards a semiclassical understanding of the problem. (H is now the component of the field perpendicular to the plane of the electrons.)

By the use of the Poisson summation formula the density of states related to the quantization condition (1.5) can be written as

$$d(E) = g_s \frac{mA}{2\pi\hbar^2} + g_s \frac{mA}{\pi\hbar^2} \sum_{n=1}^{\infty} (-1)^n \cos\left(\frac{2\pi nE}{\hbar w}\right). \quad (1.6)$$

This decomposition is usually interpreted as coming from the Weyl term (given by the volume of the energy manifold in phase space) and the contribution of cyclotron orbits (second term, strongly energy dependent). We stress though that in the bottom of the spectra, from which the Landau diamagnetic component originates, this distinction is essentially meaningless.

In the case of a degenerate electron gas with a weak field such that $\hbar w \ll k_B T \ll \mu$ the energy integral (1.3) is easily performed resulting in

$$\Omega(\mu) \simeq \bar{\Omega}(\mu) = -g_s \frac{mA}{2\pi\hbar^2} \frac{\mu^2}{2} + g_s \frac{e^2}{24\pi mc^2} \frac{AH^2}{2}, \quad (1.7)$$

where $\bar{\Omega}$ is the smooth part (in energy) of the thermodynamic potential. (Note that the second term of Eq. (1.7) comes nevertheless from the integral of the rapidly oscillating term of the density of states.) Thus, we obtain the two-dimensional diamagnetic Landau susceptibility

$$-\chi_L = -g_s e^2 / 24\pi mc^2. \quad (1.8)$$

For high magnetic fields, $k_B T \ll \hbar w$, the energy integrals are slightly more complicated than before since the rapidly oscillating component of Ω is not negligible any longer. This latter can be computed (see Appendix A for the treatment of similar cases) as

$$\Omega^{\text{osc}} = g_s \left(\frac{mA}{\pi\hbar^2} \right) \sum_{n=1}^{\infty} (-1)^n \left(\frac{\hbar w}{2\pi n} \right)^2 \cos\left(\frac{2\pi n\mu}{\hbar w}\right) R_T(n), \quad (1.9)$$

where $R_T(n)$ is a temperature dependent damping factor

$$R_T(n) = 2\pi^2 n k_B T / \hbar w / \sinh(2\pi^2 n k_B T / \hbar w). \quad (1.10)$$

With $\Omega = \bar{\Omega} + \Omega^{\text{osc}}$, we have the Landau and de Haas–van Alphen contributions to the magnetic susceptibility

$$\frac{\chi^{\text{GC}}}{\chi_{\text{L}}} = -1 - 24 \left(\frac{\mu}{\hbar w} \right)^2 \sum_{n=1}^{\infty} (-1)^n \cos \left(\frac{2\pi n \mu}{\hbar w} \right) R_{\text{T}}(n). \quad (1.11)$$

The second term exhibits the characteristic oscillations with period $1/H$ and is exponentially damped with temperature (and the summation index n).³

While going from the bulk two-dimensional case (macroscopic regime) to the constrained case (ballistic mesoscopic) two important changes take place: (i) the confining energy appears as a relevant scale and Eq. (1.5) no longer provides the quantization condition; (ii) since we are not in the thermodynamic limit of N and $A \rightarrow \infty$, the constraint of a constant number of electrons in (isolated) microstructures is no longer equivalent to having a fixed chemical potential. These two effects will be thoroughly discussed in the paper. For didactical purposes we restrict ourselves in this introductory section to only the changes (i) due to the confinement, and we anticipate some of the results that will be later discussed in detail.

We imagine a mesoscopic square of size a connected to an electron reservoir with chemical potential μ . Direct numerical diagonalization in the presence of a magnetic field (Fig. 1(a)) allows us to obtain χ^{GC} (solid line in Fig. 1(b)). In the high-field region ($2r_c < a$, we note $r_c = v_{\text{F}}/\omega$ the cyclotron radius) the characteristic de Haas–van Alphen oscillations are obtained, although not with the amplitude expected from calculations in the bulk (Eq. (1.11)). For lower fields the discrepancy between our numerical results and the bulk Landau diamagnetism is quite striking. Thus, confining deeply alters the orbital response of an electron gas. Without entering into details at this point we remark the fact that the whole curve is quite well reproduced by a finite-temperature semiclassical theory (dashed line) that takes into account only one type of trajectory (see insets) in each of the three regimes: (a) the interference-like regime, dominated by the shortest trajectories with the largest enclosed area for squares at zero magnetic field; (b) the transition regime dominated by the bending of bouncing-ball trajectories between parallel sides of the square; (c) the de Haas–van Alphen regime dominated by cyclotron orbits. It is remarkable how an exceedingly complicated spectrum as that of Fig. 1(a) can be understood within such a simple semiclassical picture once finite temperature acts as a filter selecting only few types of trajectories.

1.3. Overview of this work

The purpose of this paper is to provide an (essentially comprehensive) theory of the orbital magnetic properties of noninteracting spinless electrons in the mesoscopic ballistic regime. We restrict ourselves to the clean limit, where the different behavior of the magnetic response arises as a geometrical effect (shape of the microstructure). We will make extensive use of semiclassical techniques since they appear to be perfectly suited for these problems. For the smooth components (such as in Eq. (1.7)) we will use the general techniques developed by Wigner to obtain higher \hbar corrections to the Weyl term which are field dependent. For the oscillating components, we will rely on the so

³For high fields we cannot in principle separate the orbital and spin effects. The de Haas–van Alphen oscillations are given only by the orbital component, that is the only one that interests us for our model of spinless electrons.

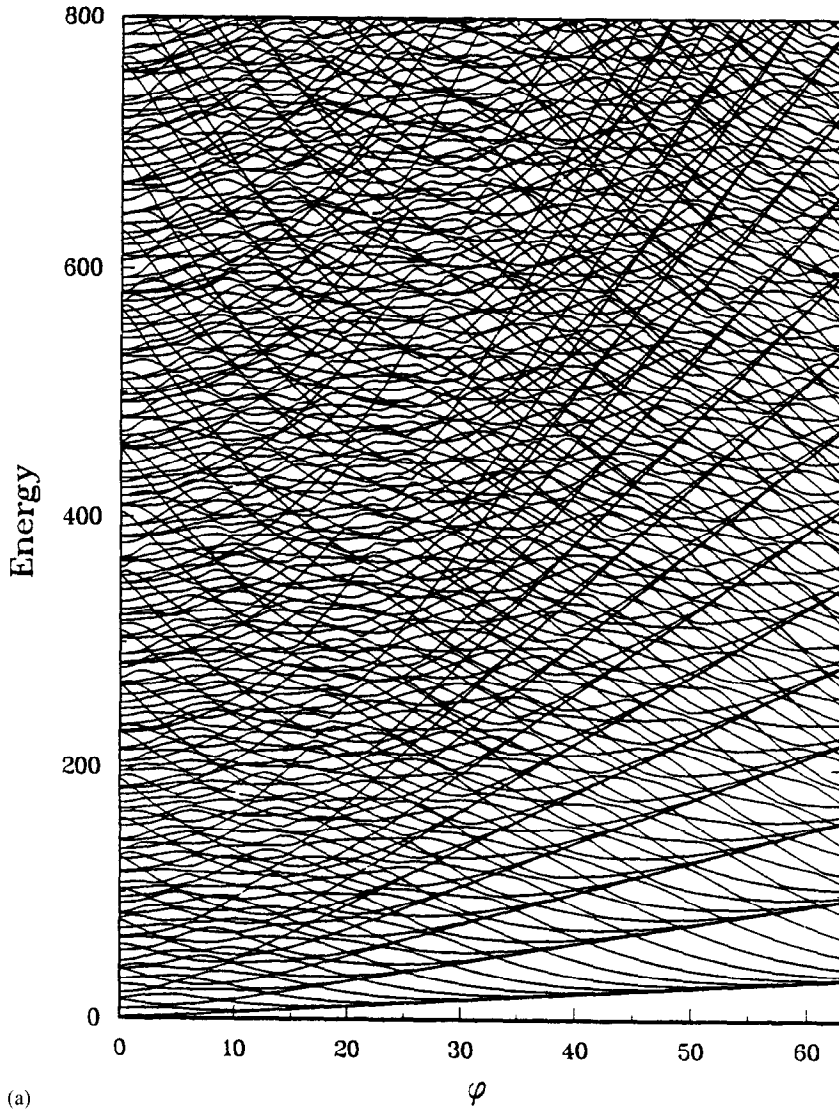


Fig. 1. (a) Evolution of the first 200 energy levels (of one symmetry class (see Section 5.4)) of a square billiard in a uniform perpendicular magnetic field H as a function of the normalized flux $\varphi = Ha^2/\Phi_0$ ($\Phi_0 = hc/e$). The energies are scaled such that the zero field limit gives $E = n_x^2 + n_y^2$. At high fields the levels converge successively to the Landau levels while the nonintegrable intermediate field regime exhibits a complex spectral structure. (b) Full line: Numerically calculated susceptibility of the square at finite temperature at an energy corresponding to ~ 1100 occupied independent particle states. The susceptibility, being strongly enhanced with respect to the bulk value χ_L , exhibits pronounced oscillations which are accurately reproduced by analytical semiclassical expressions (dashed line) based on families of quantized flux enclosing electron orbits (shown in the upper insets for the different magnetic field regimes).

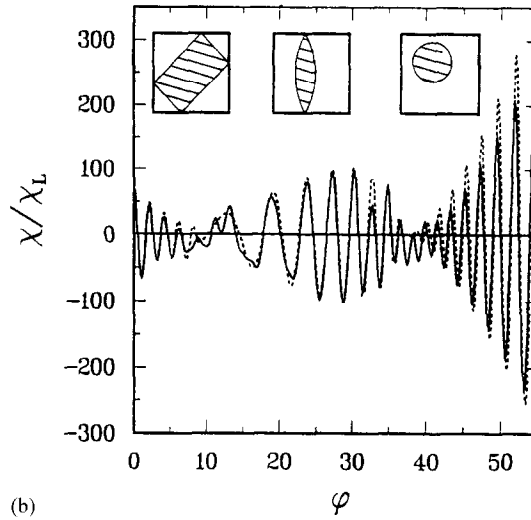


Fig. 1. continued.

called semiclassical trace formulas, which provide simple and intuitive expressions for the density of states as a sum over Fourier-like components associated to closed classical orbits.

In this respect it will be seen that the nature of the classical dynamics, i.e. integrable versus chaotic (and more precisely existence versus absence of continuous families of periodic orbits), plays a major role. Although we will present a complete formalism for both cases, our main emphasis, and in particular all the examples treated explicitly, will concern integrable geometries. The reason for this choice is twofold. First, as we will make clear in the sequel, one expects a much larger magnetic response for integrable systems than for chaotic ones, yielding a more striking effect easier to observe. The second point is that, contrary to what might seem natural a priori, integrable geometries present a few conceptual difficulties in their treatment which are not present for chaotic systems. Indeed integrable systems lack of structural stability, which means that under any small perturbation (such as the one provided by the presence of a magnetic field) they generically do not remain integrable. Chaotic systems on the contrary remain chaotic under a small perturbation. Therefore, as shown in Ref. [50], the Gutzwiller trace formula [21, 51], valid for chaotic systems, can be used at finite fields without further complications. For integrable geometries however, the Berry–Tabor [52, 53] or Balian–Bloch [54] trace formulae valid for integrable systems usually do not apply in the presence of a perturbing magnetic field. It will therefore be necessary, following Ozorio de Almeida [55, 56], to consider the more complicated case of nearly integrable systems, which we will do in detail here.

To perform this program, the present work is organized as follows. In the next section we present the thermodynamic formalism appropriate for working in the canonical and grand canonical ensembles, stressing its semiclassical interpretation and incorporating the changes due to the constancy of the number of electrons in the experimentally relevant microstructures. In Section 3 we consider the smooth magnetic response and show that the Landau diamagnetism is present in any confined geometry at arbitrary fields. In Section 4 we address the magnetic response (susceptibility and persistent currents) in the simplest possible geometries: circles and rings billiards that are integrable with and without magnetic field. In Section 5 we present the calculation of the magnetic susceptibility

for the experimentally relevant case of the square billiard [25] whose integrability at zero field is broken by the effect of an applied magnetic field. An initial study along these lines was presented in Refs. [57, 58] and independently proposed by von Oppen [59]. This geometry and the corresponding experiment have also been analyzed from a completely different point of view by Gefen et al. [60] stressing the importance of the residual disorder (see also Ref. [82]). We consider in Section 6 the generic magnetic response of both integrable and chaotic geometries, stressing the similarities and differences in their behavior and calculating the line-shape of the average magnetization in generic chaotic systems. In Section 7 we demonstrate how the semiclassical formalism we have developed applies not only to the weak-field limit, but also to higher field and in particular to the high field regime of the de Haas–van Alphen oscillations. We treat explicitly the example of the square geometry, including an intermediate field regime dominated by bouncing-ball orbits as depicted in Fig. 1(b). We discuss our conclusions and their experimental relevance in Section 8. The modifications of our results due to the effect of a weak disordered potential are discussed in a separate publication [43].

To keep the focus on the physical concepts developed in the text, a few technical derivations have been relegated to some appendices. Appendix A presents the generic case of the convolution of a rapidly oscillating function with the derivative of the Fermi function. Appendix B gives the calculation of the first field-dependent term of the heat Kernel in an \hbar expansion. In Appendix C we compute the action integrals associated with the dynamics of circular and ring billiards needed to define the energy manifold in action space. Appendix D presents the calculation of the prefactor of the Green function for an integrable system, while in Appendix E we show how to compute the semiclassical Green function at a focal point, and apply the obtained result to the particular case of cyclotron motion.

2. Thermodynamic formalism

One main subject of the present work is the introduction of semiclassical concepts into the thermodynamics of mesoscopic systems. In this section we provide the basic formalism allowing one to obtain the thermodynamic properties (grand potential, free energy) from the quasi-classically calculated single-particle density of states and hence the susceptibility. We begin with general definitions and relations between grand canonical and canonical quantities.

For a system of electrons in a volume (area in two dimensions) A connected to a reservoir of particles with chemical potential μ (grand canonical ensemble) the magnetic susceptibility is obtained, as given by Eq. (1.2), as

$$\chi^{\text{GC}} = -(1/A) (\partial^2 \Omega / \partial H^2)_{T, \mu} .$$

$\Omega(T, \mu, H)$ is the thermodynamic potential, which can be expressed for noninteracting electrons in terms of the single-particle density of states through Eq. (1.3).

For actual microstructures, the number N of particles inside the device might be large but is fixed in contrast to the chemical potential μ . As discussed in the introduction, it will be necessary in some cases, namely when considering the average susceptibility of an ensemble of microstructures, to take explicitly into account the conservation of N , and to work within the canonical ensemble. For such systems with a fixed number N of particles, the relevant thermodynamic function is not the grand

potential Ω , but its Legendre transform, the free energy⁴

$$F(T, H, N) = \mu N + \Omega(T, H, \mu) . \quad (2.1)$$

In particular, the magnetic susceptibility of a system of N electrons is

$$\chi = -1/A (\partial^2 F / \partial H^2)_{T, N} . \quad (2.2)$$

Except for the calculation of the Landau contribution performed in the following section all the computations of the magnetic response of the microstructures to be considered will involve two clearly separated parts. In the first one the (oscillating part of the) density of states will be calculated semiclassically. Depending on the underlying classical dynamics (integrable versus chaotic, with or without breaking of the invariant tori, with or without focal points, etc.), the results as well as their derivation will vary noticeably. In the second stage the integrals over energy yielding the desired thermodynamic properties have to be performed in a leading order in \hbar approximation. To avoid tedious repetitions, we shall consider here in some detail this part of the calculation of the thermodynamic properties, and refer without many additional comments to the results obtained in this section whenever needed. We begin with the grand canonical quantities which exhibit the simplest expressions in terms of the density of states. In a second subsection we shall consider the canonical ensemble following closely the approaches presented in Refs. [36].

2.1. Grand canonical properties

We begin with the standard definition, Eq. (1.4) of the density of states

$$d(E) = g_s \sum_{\lambda} \delta(E - E_{\lambda}) ,$$

($g_s = 2$ is the spin degeneracy, E_{λ} the eigenenergies) and its successive energy integrals. They are the energy staircase

$$n(E) = \int_0^E dE' d(E') , \quad (2.3)$$

and the grand potential at zero temperature

$$\omega(E) = - \int_0^E dE' n(E') . \quad (2.4)$$

These are purely quantum mechanical quantities, depending only on the eigenstates E_{λ} of the system. At finite temperature the corresponding quantities are obtained by convolution with the derivative $f'(E - \mu)$ of the Fermi distribution function

$$f(E - \mu) = 1 / (1 + \exp[\beta(E - \mu)]) . \quad (2.5)$$

⁴In standard thermodynamics, Eq. (2.1) just represents the definition of the grand potential. It should be borne in mind however that from a statistical physics point of view this is not an exact relation, but the result of a stationary-phase evaluation of the average over the occupation number, valid only when $k_B T$ is larger than the typical level spacing. Therefore, we are entitled to use this relation in the mesoscopic regime that interests us, but not in the microscopic regime, where features on the scale of a mean spacing become relevant.

We then have

$$D(\mu) = - \int_0^\infty dE d(E) f'(E-\mu), \quad (2.6a)$$

$$N(\mu) = - \int_0^\infty dE n(E) f'(E-\mu), \quad (2.6b)$$

$$\Omega(\mu) = - \int_0^\infty dE \omega(E) f'(E-\mu). \quad (2.6c)$$

Integration by parts leads to the standard definition (1.3) of the grand potential and the mean number of particles in the GCE with a chemical potential μ , i.e.

$$N(\mu) = \int_0^\infty dE d(E) f(E-\mu). \quad (2.7)$$

That means that the thermodynamic properties (2.6b)–(2.6c) are obtained by performing the energy integrations (2.3)–(2.4) with the Fermi function as a weighting factor.

In the following the separation of the above quantum mechanical and thermodynamic expressions into smooth (noted with a “ $\bar{}$ ”) and oscillating (noted with the superscript “ $^{\text{osc}}$ ”) parts is going to play a major role. It has its origin in the well-known decomposition of the density of states as

$$d(E) = \bar{d}(E) + d^{\text{osc}}(E). \quad (2.8)$$

This decomposition has a rigorous meaning only in the semiclassical ($E \rightarrow \infty$) regime for which the scales of variation of \bar{d} and d^{osc} decouple. To leading order in \hbar , the mean component $\bar{d}(E)$ is the Weyl term reflecting the volume of accessible classical phase space at energy E (zero-length trajectories), while $d^{\text{osc}}(E)$ is given as a sum over periodic orbits (Gutzwiller and Berry-Tabor trace formulas) [21]. Generically, it will be expressed as a sum

$$d^{\text{osc}}(E) = \sum_t d_t(E); \quad d_t(E) = A_t(E) \sin(S_t(E)/\hbar + v_t). \quad (2.9)$$

running over periodic orbits labeled by t where S_t is the action integral along the orbit t , $A_t(E)$ is a slowly varying prefactor and v_t a constant phase.⁵

Using the expression (2.9) for d^{osc} in Eqs. (2.3) and (2.4), n^{osc} and ω^{osc} are obtained to leading order in \hbar as

$$n^{\text{osc}}(E) = \int^E dE' d^{\text{osc}}(E'); \quad \omega^{\text{osc}}(E) = - \int^E dE' n^{\text{osc}}(E'). \quad (2.10)$$

The lower bounds are not specified because the constants of integration are determined by the constraint that n^{osc} and ω^{osc} must have zero mean values. (It should be borne in mind that semiclassical expressions like (2.8), and those that will follow, are not applicable at the bottom of the spectrum.)

In a leading \hbar calculation the integration over energy in Eq. (2.10) has to be applied only to the rapidly oscillating part of each periodic orbit contribution d_t . Noting moreover that if $S_t(E)$ is the

⁵When considering systems whose integrability is broken by a perturbing magnetic field, we shall stress the necessity to consider families of recurrent, but not periodic, orbits of the perturbed system. This will, however, not affect the discussion which follows.

action along a periodic orbit, then $\tau_i(E) \equiv dS_i/dE$ is the period of the orbit, one has in a leading \hbar approximation

$$\int^E A_i(E') \sin(S_i(E')/\hbar + v_i) dE' = \frac{-\hbar}{\tau_i(E)} A_i(E) \cos(S_i(E)/\hbar + v_i) \quad (2.11)$$

as can be checked by differentiating both sides of Eq. (2.11). In order to emphasize that the integration over energy merely yields a multiplication by $(-\hbar/\tau)$, we use the notation $(i_{\otimes} \cdot d_i)$ to assign the contribution d_i of a periodic orbit after shift of the phase by $\pi/2$, i.e. $(i_{\otimes} \cdot [B \sin(S/\hbar)]) = B \cos(S/\hbar)$. We get

$$n^{\text{osc}}(E) = \sum_i n_i(E); \quad n_i(E) = \frac{-\hbar}{\tau_i(E)} (i_{\otimes} \cdot d_i(E)), \quad (2.12)$$

$$\omega^{\text{osc}}(E) = \sum_i \omega_i(E); \quad \omega_i(E) = \left(\frac{\hbar}{\tau_i(E)} \right)^2 d_i(E). \quad (2.13)$$

The thermodynamic functions $D^{\text{osc}}(\mu)$, $N^{\text{osc}}(\mu)$ and $\Omega^{\text{osc}}(\mu)$ are then obtained by application of Eqs. (2.6a) in which the full functions are replaced by their oscillating component. The resulting integrals involve the convolution of functions ($d^{\text{osc}}(E)$, $n^{\text{osc}}(E)$ or $\omega^{\text{osc}}(E)$) oscillating (locally around μ) with a frequency $\tau(\mu)/(2\pi\hbar)$, with the derivative of the Fermi factor $f'(E - \mu)$ being smooth on the scale of $\beta^{-1} = k_B T$. One can therefore already anticipate that this convolution yields an exponential damping of the periodic orbit contribution whenever $\tau(\mu) \gg \hbar\beta$. As shown in Appendix A the temperature smoothing gives rise to an additional factor for each periodic orbit contribution,

$$R_T(\tau_i) = \frac{\tau_i/\tau_c}{\sinh(\tau_i/\tau_c)}; \quad \tau_c = \hbar\beta/\pi, \quad (2.14)$$

in a leading \hbar and β^{-1} approximation (without any assumption concerning the order the limits are taken). In this way we obtain relations between the following useful thermodynamic functions and the semiclassical density of states:

$$D^{\text{osc}}(\mu) = \sum_i D_i(\mu); \quad D_i(\mu) = R_T(\tau_i) d_i(\mu), \quad (2.15a)$$

$$N^{\text{osc}}(\mu) = \sum_i N_i(\mu); \quad N_i(\mu) = R_T(\tau_i) (-\hbar/\tau_i) (i_{\otimes} \cdot d_i(\mu)), \quad (2.15b)$$

$$\Omega^{\text{osc}}(\mu) = \sum_i \Omega_i(\mu); \quad \Omega_i(\mu) = R_T(\tau_i) (\hbar/\tau_i)^2 d_i(\mu). \quad (2.15c)$$

At very low temperature, $R_T \simeq 1 - [(\tau_i\pi)/(\hbar\beta)]^2/6$ which, for billiard-like systems where $\tau_i = L_i/v_F$ (with L_i being the length of the orbit and v_F the Fermi velocity), simply gives the standard Sommerfeld expansion $R_T \simeq 1 - [(L_i\pi)/(\hbar\beta v_F)]^2/6$. For long trajectories or high temperature it yields an exponential suppression and therefore the only trajectories contributing significantly to the thermodynamic functions are those with $\tau_i \leq \tau_c$. Thus, temperature smoothing has a noticeable effect on the oscillating quantities since it effectively suppresses the higher harmonics, which are associated with long classical orbits in a semiclassical treatment. On the contrary, for a degenerate electron

gas ($\beta\mu \gg 1$), finite temperature has no effect on the mean quantities. Temperature is then the tuning parameter for passing from $d(E)$ at $T = 0$ to $\bar{D}(E) = \bar{d}(E)$ at large temperatures (by the progressive reduction of d^{osc}). Similar considerations hold for the energy staircase and the grand potential.

The oscillatory part of the semiclassical susceptibility in the grand-canonical ensemble is finally obtained from Eq. (1.2) by replacing Ω by Ω^{osc} .

2.2. Canonical ensemble

Let us now consider the susceptibility in the canonical ensemble, appropriate for systems with a fixed number of particles. We follow Imry's derivation for persistent currents in ensembles of disordered rings [35]. The only important difference is that we will take averages over the size and the Fermi energy of ballistic structures instead of averages over impurity realizations. We will stress the semiclassical interpretation that will be at the heart of our work, and highlight some of its subtleties.

As mentioned in the introduction the definition Eq. (2.2) of the susceptibility χ is equivalent to χ^{GC} up to $1/N$ (i.e. \hbar corrections). Therefore, in the macroscopic limit of $N \rightarrow \infty$ the choice of the ensemble in which the calculations are done is unimportant. On the other hand, in the mesoscopic regime of small structures (with large but finite N) we have to consider such corrections if we want to take advantage of the computational simplicity of the Grand Canonical Ensemble (GCE). The difference between the two definitions is particularly important when the GCE result is zero as it is the case for the ensemble average of χ^{GC} . The evaluation of the corrective terms can be obtained from the relationship Eq. (2.1) between the thermodynamic functions⁶ $F(N)$ and $\Omega(\mu)$ and the relation $N(\mu) = N$. In the case of finite systems the previous implicit relation is difficult to invert. However, when N is large we can use the decomposition of $N(\mu)$ in a smooth part $\bar{N}(\mu)$ and a small component $N^{\text{osc}}(\mu)$ that fluctuates around the secular part, and we can perturbatively treat the previous implicit relation. The contribution of a given orbit to d^{osc} is always of lower order in \hbar than \bar{d} as can be checked for the various examples we are going to consider and by inspection of semiclassical trace formulae. However, since there are infinitely many of such contributions, we obtain d^{osc} and \bar{d} to be of the same order when adding them up. (This must be the case since the quantum mechanical $d(E)$ is a sum of δ peaks.) Thus, we cannot use d^{osc}/\bar{d} as a small expansion parameter. On the other hand, finite temperature provides an exponential cutoff in the length of the trajectories contributing to D^{osc} so that only a finite number of them must be taken into account. Therefore, D^{osc} is of lower order in \hbar than \bar{D} , and in the semiclassical regime it is possible to expand the free energy F with respect to the small parameter D^{osc}/\bar{D} . The use of a temperature smoothed density of states Eq. (2.6a) closely follows the Balian and Bloch approach [54], where, due to the exponential proliferation of orbits and the impossibility of exchanging the infinite time and semiclassical limits, the semiclassical techniques based on trace formulae are considered meaningful only when applied to smoothed quantities. The decomposition of $D(E)$ is depicted in Fig. 2, where we have taken $\bar{D}(\simeq \bar{d})$ to be energy independent, corresponding to the two-dimensional (potential free) case.

⁶ In the following we will only write the N dependence of F and the μ dependence of Ω , assuming always the T and H dependence of both functions.

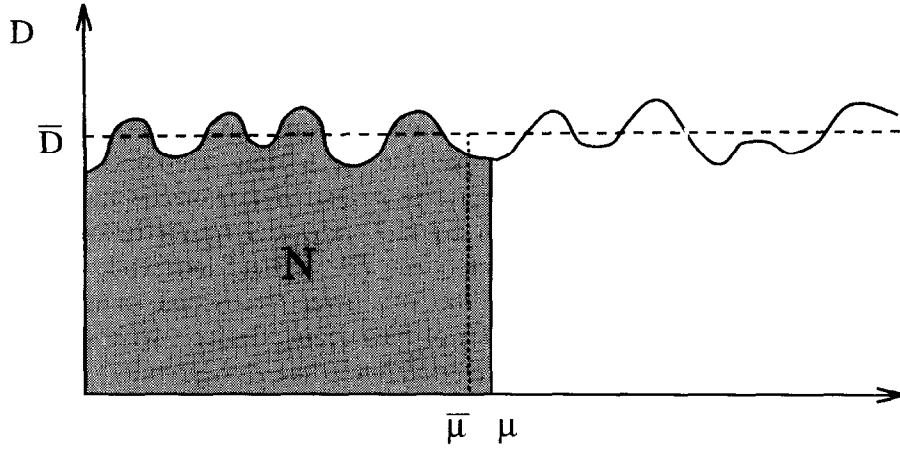


Fig. 2. Schematic illustration of the separation of the density of states $D(\mu)$ (solid line) into a smooth part \bar{D} (dashed line) and an oscillating component. The total number of electrons N is indicated by the shaded area, and equal to the product of \bar{D} and $\bar{\mu}$.

For a perturbative treatment of the mentioned implicit relation we define a mean chemical potential $\bar{\mu}$ by the condition of accommodating N electrons to the mean number of states

$$N = N(\mu) = \bar{N}(\bar{\mu}). \quad (2.16)$$

Expanding this relation to first order in D^{osc}/\bar{D} , and employing that $dN/d\mu = D$, one has

$$\Delta\mu \equiv \mu - \bar{\mu} \simeq -(1/\bar{D}(\bar{\mu}))N^{\text{osc}}(\bar{\mu}). \quad (2.17)$$

The physical interpretation of $\Delta\mu$ is very clear from Fig. 2: The shaded area represents the number of electrons in the system and it is equal to the product $\bar{D} \times \bar{\mu}$.

Expanding the relationship (2.1) to second order in $\Delta\mu$,

$$F(N) \simeq (\bar{\mu} + \Delta\mu)N + \Omega(\bar{\mu}) - N(\bar{\mu})\Delta\mu - D(\bar{\mu})\Delta\mu^2/2, \quad (2.18)$$

using the decomposition of $\Omega(\bar{\mu})$ and $N(\bar{\mu})$ into mean and oscillating parts and eliminating $\Delta\mu$ (Eq. (2.17)) in the second-order term, one obtains the expansion of the free energy to second order in D^{osc}/\bar{D} [35, 36]

$$F(N) \simeq F^0 + \Delta F^{(1)} + \Delta F^{(2)}, \quad (2.19)$$

with

$$F^0 = \bar{\mu}N + \bar{\Omega}(\bar{\mu}), \quad (2.20a)$$

$$\Delta F^{(1)} = \Omega^{\text{osc}}(\bar{\mu}), \quad (2.20b)$$

$$\Delta F^{(2)} = (1/2\bar{D}(\bar{\mu}))(N^{\text{osc}}(\bar{\mu}))^2. \quad (2.20c)$$

Then $\Delta F^{(1)}$ and $\Delta F^{(2)}$ can be expressed in terms of the oscillating part of the density of states by means of Eqs. (2.15b) and (2.15c). The first two terms $F^0 + \Delta F^{(1)}$ yield the magnetic response

calculated in the GCE with an effective chemical potential $\bar{\mu}$. The first “canonical correction” $\Delta F^{(2)}$ has a grand canonical form since it is expressed in terms of a temperature smoothed integral of the density of states (Eq. (2.7)) for a fixed chemical potential $\bar{\mu}$.

It is convenient to use the expansion (2.19) in the calculation of the magnetic susceptibility of a system with a fixed number of particles because the leading \hbar contribution to $\bar{N}(\bar{\mu})$ has no magnetic field dependence, independent of the precise system under consideration. Therefore, *at this level of approximation*, keeping N constant in Eq. (2.2) when taking the derivative with respect to the magnetic field amounts to keep $\bar{\mu}$ constant. Since $F^{(0)}$ is field independent in a leading order semiclassical expansion the weak-field susceptibility of a given mesoscopic sample will be dominated by $\Delta F^{(1)}$. However, when considering ensembles of mesoscopic devices, with slightly different sizes or electron fillings, $\Delta F^{(1)}$ (and its associated contribution to the susceptibility) averages to zero due to its oscillatory behavior independently of the order in \hbar up to which it is calculated.⁷ Then we must consider the next order term $\Delta F^{(2)}$.

As mentioned above, we will essentially work in the semiclassical regime (to leading order in \hbar) where F^0 is field independent. However, in the following section we will examine the next order \hbar correction to $\bar{\Omega}(\bar{\mu})$ (and to F^0), demonstrating that its field dependence gives rise to the standard Landau diamagnetism, independent of any confinement.

3. Landau susceptibility

In the previous section we showed that the various quantum mechanical (i.e. $d(E)$, $n(E)$, $\omega(E)$) and thermodynamic (i.e. $D(\mu)$, $N(\mu)$, $\Omega(\mu)$) properties of a mesoscopic system can be decomposed into smooth and fluctuating parts. In the semiclassical limit, where the Fermi wavelength is much smaller than the system size, each of these quantities allows an asymptotic expansion in powers of \hbar . For most of the purposes it is sufficient to consider only leading order terms while higher-order corrections must only be added if the former vanish for some reason. This is the case for the smooth part $\bar{\Omega}(\mu)$ of the grand potential, which is the dominant term at any temperature, but is magnetic field independent to leading order in \hbar . The present section will be the only part of our work where higher \hbar corrections are considered. We will show that they give rise to the standard Landau susceptibility. Our derivation relies neither, on the quantum side, on the existence of Landau levels, nor, on the classical side, on boundary trajectories or the presence of circular cyclotronic orbits fitting into the confinement potential. This shows that the Landau susceptibility is a property of mesoscopic devices as well as infinite systems, being the dominant contribution at sufficiently high temperature.⁸

We consider a d -dimensional ($d = 2, 3$) system of electrons governed by the quantum Hamiltonian

$$\hat{\mathcal{H}} = \frac{1}{2m} \left(\hat{\mathbf{p}} - \frac{e}{c} \mathbf{A}(\hat{\mathbf{q}}) \right)^2 + V(\hat{\mathbf{q}}), \quad (3.1)$$

where \mathbf{A} is the vector potential generating the magnetic field H and $V(\mathbf{q})$ is the potential which confines the electrons in some region of the space. This region can a priori have any dimension,

⁷ In the following, we shall always calculate $\Delta F^{(1)}$ in a leading order \hbar approximation. Higher-order corrections to $\Delta F^{(1)}$ may be of the same order as $\Delta F^{(2)}$ but will average to zero under ensemble averaging.

⁸ Analog results have been independently obtained by Prado et al. [61]. The Wigner distribution function was previously used by Kubo [83] in the study of Landau diamagnetism.

and it can be smaller than the cyclotron radius. We will only assume in the following that $V(\mathbf{q})$ is *smooth* on the scale of a Fermi wavelength, so that semiclassical asymptotic results can be used. In billiards the effect of *hard* boundaries on the susceptibility is negligible compared to the Landau bulk term [17, 18], and therefore the results obtained below apply there, too.

There exist general techniques to compute the semiclassical expansion of the mean part of the density of states (or of its integrated versions Eqs. (2.3) and (2.4)) up to arbitrary order in \hbar . The most complete approach, which allows one to take into account the effect of sharp boundaries, can be found in the work of Seeley [62]. However, assuming the smoothness of $V(\mathbf{q})$ allows us to follow the standard approach introduced by Wigner in 1932 [63] which is based on the notion of the Wigner transform of an operator. As a starting point we consider the Laplace transform of the level density (or heat Kernel),

$$Z(\lambda) = \int_0^\infty dE e^{-\lambda E} d(E) = \mathbf{g}_s \text{Tr}(e^{-\lambda \hat{\mathcal{H}}}), \quad (3.2)$$

where $\mathbf{g}_s = 2$ takes into account the spin degeneracy. In Appendix B we apply after a brief description the technique to calculate the first two terms of the expansion of $Z(\lambda)$ with respect to λ . They yield under the inverse transformation the first two terms of the expansion of $d(E)$ in powers of \hbar . The oscillating part $d^{\text{osc}}(E)$ of $d(E)$ is not included in this procedure since it is associated with exponentially small terms in $Z(\lambda)$, that is, $Z(\lambda) \simeq \bar{Z}(\lambda)$ for $\lambda \simeq 0$. This well known property can be easily seen from the integral treated in Appendix A by identifying β with λ and using the exponential form of the distribution function in the classical limit of high temperatures ($\beta\mu \ll 1$).

Noting $\mathcal{H}(\mathbf{q}, \mathbf{p})$ the classical Hamiltonian corresponding to Eq. (3.1), the leading-order (Weyl) contribution to $Z(\lambda)$ is given by Eq. (B6),

$$Z_W(\lambda) = \frac{\mathbf{g}_s}{(2\pi\hbar)^d} \int d\mathbf{q} d\mathbf{p} \exp(-\lambda \mathcal{H}(\mathbf{q}, \mathbf{p})), \quad (3.3)$$

and the inverse Laplace transform yields the familiar result

$$d_W(E) = \bar{d}_W(E) = \frac{\mathbf{g}_s}{(2\pi\hbar)^d} \int d\mathbf{q} d\mathbf{p} \delta(E - \mathcal{H}(\mathbf{q}, \mathbf{p})). \quad (3.4)$$

In the above integrals, the substitution

$$\mathbf{p} \rightarrow \mathbf{p}' = \mathbf{p} - (e/c)\mathbf{A} \quad (3.5)$$

eliminates any field dependence. Therefore

$$\omega_W(E) = \bar{\omega}_W(E) = - \int_0^E dE' \int_0^{E'} dE'' d_W(E''), \quad (3.6)$$

as well as the leading term $\bar{\Omega}_W(\mu)$ of the grand potential (obtained in the high-temperature limit of Eq. (2.6c)), are field independent. This is the reason for the absence of orbital magnetism in classical mechanics. To observe a field dependence, one must consider the first correcting term of $Z(\lambda)$ which, as shown in Appendix B (Eq. (B11)), is given by

$$Z_1(\lambda, H) = -\lambda^2 \frac{\mu_B^2 H^2}{6} Z_W + Z_1^0. \quad (3.7)$$

Here, $\mu_B = (e\hbar)/(2mc)$ is the Bohr magneton, and $Z_1^0 = Z_1(H = 0)$ is a field-independent term that we will drop from now on since it does not contribute to the susceptibility.

The integrated functions $n(E)$ and $\omega(E)$ can be obtained from their Laplace transforms

$$n(\lambda) = Z(\lambda)/\lambda, \quad w(\lambda) = -Z(\lambda)/\lambda^2. \quad (3.8)$$

Then the first correction to the zero-temperature grand potential is

$$\omega_1(E) = \bar{\omega}_1(E) = \frac{1}{6}\mu_B^2 H^2 \bar{d}_W(E). \quad (3.9)$$

After convolution with the derivative of the Fermi function (Eq. (2.6c)) we obtain the first corrective term of the grand potential

$$\Omega_1(\mu) = \bar{\Omega}_1(\mu) = \frac{1}{6}\mu_B^2 H^2 \bar{D}_W(\mu). \quad (3.10)$$

In the grand canonical ensemble, the above equation readily gives the leading contribution to the susceptibility

$$\bar{\chi}^{\text{GC}} = -\frac{\mu_B^2}{3A} \bar{D}_W, \quad (3.11)$$

coming from the mean part of the grand potential. In Eq. (3.11) A is the confining volume (area for $d = 2$) of the electrons. Noting that $\bar{D}_W = d\bar{N}_W/d\mu$, one recognizes the familiar result of Landau [1]. For systems without potential (bulk, or billiard systems), it gives in the degenerate case ($\beta\mu \gg 1$) in two, respectively, three dimensions

$$\bar{\chi}_{2d}^{\text{GC}} = -\frac{g_s e^2}{24\pi m c^2}, \quad \bar{\chi}_{3d}^{\text{GC}} = -\frac{g_s e^2 k_F}{24\pi^2 m c^2}. \quad (3.12)$$

In the nondegenerate limit the susceptibility is

$$\bar{\chi}^{\text{GC}} = -\frac{\mu_B^2}{3A} \frac{N}{k_B T}. \quad (3.13)$$

The temperature independence in the degenerate regime and the power-law decay in the nondegenerate limit cause the dominance of the Landau contribution at high temperatures since, as mentioned in the previous section (and demonstrated in Appendix A), the contributions from $\Delta F^{(1)}$ and $\Delta F^{(2)}$ (Eqs. (2.20b) and (2.20c)) are exponentially damped by temperature.

The Landau diamagnetism is usually derived for free electrons or for a quadratic confining potential [2,4]. We have provided here its generalization to any confining potential (including systems smaller than the cyclotron radius).

For a system with fixed number N of electrons, defining a Weyl chemical potential μ_W by

$$N = \bar{N}_W(\mu_W) \quad (3.14)$$

and following the same procedure as in Section 2.2 one can write

$$F^{(0)}(N) \simeq F_W + \bar{\Omega}_1(\mu_W), \quad (3.15)$$

where both μ_W and

$$F_W = \mu_W N + \bar{\Omega}_W(\mu_W) \quad (3.16)$$

are field independent. Therefore, the smooth part of the free energy gives the same contribution than Eq. (3.11): We recover the Landau diamagnetic response in the canonical ensemble, too.

At the end of this section we would like to comment on the case of free electrons in two dimensions. Since Eq. (1.6) represents an exact formula for the density of states, $\bar{d}(E) = (\mathbf{g}_s mA)/(2\pi\hbar^2)$ can be interpreted as the exact mean density of states, and $d^{\text{osc}}(E) = (\mathbf{g}_s mA)/(\pi\hbar^2) \sum_{n=1}^{\infty} (-1)^n \times \cos((2\pi nE)/(\hbar w))$ as the exact oscillating part. However, $\omega(E)$ being obtained by integrating $d(E)$ twice, has a mean value which, in addition to $-\bar{d}E^2/2$, contains the term $(\mu_B^2 H^2/6)\bar{d}$ yielding the Landau susceptibility. In the usual derivation, this term comes from the integration of $d^{\text{osc}}(E)$, more precisely from the boundary contribution at $E = 0$ (i.e. from levels too close to the ground state in order to properly separate the mean value from oscillating parts). One should be aware that $\bar{\omega}(E)$ cannot be defined by Eq. (3.6) as soon as nonleading terms are considered. For this reason some care was required for the definitions of the last section (see the discussion around Eqs. (2.10)–(2.15)).

4. Systems integrable at arbitrary fields

In the remainder of this work we will provide semiclassical approximations for the corrective free-energy terms $\Delta F^{(1)}$ and $\Delta F^{(2)}$ (see Eq. (2.19)) and their associated magnetic responses for systems that react differently under the influence of an applied field. We will be mainly working in the weak-field regime (except in Section 7), where the magnetic field acts as a perturbation almost without altering the classical dynamics. In this regime the nature of the zero-field dynamics (i.e. integrable versus chaotic, or more precisely, the organization of periodic orbits in phase space) becomes the dominant factor determining the behavior and magnitude of the magnetic susceptibility. For systems which are integrable at zero field the generic situation is that the magnetic field breaks the integrability (as any perturbation will do). It is necessary in that case to develop semiclassical methods allowing to deal with nearly, but not exactly, integrable systems. This question will be addressed in Sections 5 and 6. There exist however “non generic” systems where the classical dynamics remains integrable in the presence of the magnetic field. Due to their rotational symmetry, circles and rings (which are the geometries used in many experiments) fall into this category. In these cases (and similarly for the Bohm–Aharonov flux [39]) the Berry–Tabor semiclassical trace formula [52, 53] provides the appropriate path to calculate semiclassically the oscillating part of the density of states d^{osc} , including its field dependence. Thus, $\Delta F^{(1)}$ and $\Delta F^{(2)}$, and their respective contributions to the susceptibility, can be deduced. This is the program we perform in this section, treating specifically the example of circular and ring billiards.

The magnetic susceptibility of the circular billiard can be calculated from its exact quantum mechanical solution in terms of Bessel functions [10, 13, 30]. The magnetic response of long cylinders [32, 64] and narrow rings [32] (the two nontrivial generalizations of one-dimensional rings) can be calculated by neglecting the curvature of the circle and solving the Schrödinger equation for a rectangle with periodic boundary conditions. Our semiclassical derivation provides an intuitive and unifying approach to the magnetic response of circular billiards and rings of any thickness (for individual systems as well as ensembles) and establishes the range of validity of previous studies. Moreover, we present it for completeness since it provides a pedagogical introduction to the more complicated (“generic”) cases of the following sections.

4.1. Oscillating density of states for weak field

By definition, a classical Hamiltonian $\mathcal{H}(\mathbf{p}, \mathbf{q})$ is integrable if there exist as many constants of motion in involution as degrees of freedom. For bounded systems, this implies (see e.g. [65]) that all trajectories are trapped on torus-like manifolds (invariant tori), each of which can be labeled by the action integrals

$$I_i = \frac{1}{2\pi} \oint_{\mathcal{C}_i} \mathbf{p} \, d\mathbf{q} \quad (i = 1, 2), \quad (4.1)$$

taken along two independent paths \mathcal{C}_1 and \mathcal{C}_2 on the torus. (We are dealing with two degrees of freedom.) It is moreover possible to perform a canonical transformation from the original (\mathbf{p}, \mathbf{q}) variables to the action-angle variables (\mathbf{I}, ϕ) where $\mathbf{I} = (I_1, I_2)$ and $\phi = (\varphi_1, \varphi_2)$ with φ_1, φ_2 in $[0, 2\pi]$. Because both, I_1 and I_2 , are constants of motion, the Hamiltonian $\mathcal{H}(I_1, I_2)$ expressed in action-angle variables depends only on the actions.

For a given torus we note $\nu_i = \partial\mathcal{H}/\partial I_i$ ($i = 1, 2$) the angular frequencies, and $\alpha \equiv \nu_1/\nu_2$ the rotation number. A torus is said to be “resonant” when its rotation number is rational ($\alpha = u_1/u_2$ where u_1 and u_2 are coprime integers). In that case all the orbits on the torus are periodic, and the torus itself constitutes a one-parameter family of periodic orbits, each member of the family having the same period and action. The families of periodic orbits can be labeled by the two integers $(M_1, M_2) = (ru_1, ru_2)$ where (u_1, u_2) specifies the primitive orbits and r is the number of repetitions. M_i ($i = 1, 2$) is thus the winding number of φ_i before the orbits close themselves. The pair $\mathbf{M} = (M_1, M_2)$ has been coined the “topology” of the orbits by Berry and Tabor.

For two-dimensional systems, the Berry–Tabor formula can be cast in the form [52, 53]

$$d^{\text{osc}}(E) = \sum_{\mathbf{M} \neq (0,0), \varepsilon} d_{\mathbf{M}, \varepsilon}(E), \quad (4.2)$$

with

$$d_{\mathbf{M}, \varepsilon}(E) = \frac{\mathfrak{g}_s \tau_{\mathbf{M}}}{\pi \hbar^{3/2} M_2^{3/2} |g'_E(I_1^{\mathbf{M}})|^{1/2}} \cos \left(\frac{S_{\mathbf{M}, \varepsilon}}{\hbar} - \hat{\eta}_{\mathbf{M}} \frac{\pi}{2} + \gamma \frac{\pi}{4} \right). \quad (4.3)$$

The sum in Eq. (4.2) runs over all families of closed orbits at energy E , labeled by their topology \mathbf{M} (in the first quadrant, that is M_1 and M_2 are positive integers), and, except for self-retracing orbits, by an additional index ε specifying tori related to each other through time-reversal symmetry and therefore having the same topology. \mathfrak{g}_s represents the spin degeneracy factor, while $S_{\mathbf{M}, \varepsilon}$ and $\tau_{\mathbf{M}}$ are, respectively, the action integral and the period along the periodic trajectories of the family \mathbf{M} . $\hat{\eta}_{\mathbf{M}}$ is the Maslov index which counts the number of caustics of the invariant torus encountered by the trajectories. For billiard systems with Dirichlet boundary conditions, we will also take into account in $\hat{\eta}_{\mathbf{M}}$ the phase π acquired at each bounce of the trajectory on the hard walls (and still refer to $\hat{\eta}_{\mathbf{M}}$ as the Maslov index, although slightly improperly). The energy surface E in action space whose implicit form is $\mathcal{H}(I_1, I_2) = E$, is explicitly defined by the function $I_2 = g_E(I_1)$. We note $\mathbf{I}^{\mathbf{M}} = (I_1^{\mathbf{M}}, I_2^{\mathbf{M}})$ the action variables of the torus where the periodic orbits of topology \mathbf{M} live. They are determined by the resonant-torus condition

$$\alpha = -dg_E(I_1)/dI_1|_{I_1=I_1^{\mathbf{M}}} = M_1/M_2, \quad (4.4)$$

where the first equality arises from the differentiation of $\mathcal{H}(I_1, g_E(I_1)) = E$ with respect to I_1 . Finally, the last contribution to the phase is given by $\gamma = \text{sgn}(g_E''(I_1^M))$.

The (first) derivation of the Berry–Tabor trace formula [52] follows very similar lines as the treatment of the density of states performed in the introduction for the macroscopic Landau susceptibility. The EBK (Einstein, Brillouin, Keller) quantization condition is used instead of the exact form (1.5) of the Landau levels, followed by the application of the Poisson summation rule. While in the latter case this procedure leads to the exact sum of Eq. (1.6), the Berry–Tabor formula is obtained (similar to the treatment of de Haas–van Alphen oscillations for a nonspherical Fermi surface) after a stationary-phase approximation valid in the semiclassical limit where $S \gg \hbar$ (with a stationary-phase condition according to Eq. (4.4)).

Given a two-dimensional electron system whose classical Hamiltonian

$$\mathcal{H}(\mathbf{p}, \mathbf{q}) = \frac{1}{2m} \left(\mathbf{p} - \frac{e}{c} \mathbf{A}(\mathbf{q}) \right)^2 + V(\mathbf{q}) \quad (4.5)$$

remains integrable for finite values of the transverse field $H\hat{z} = \nabla \times \mathbf{A}$, the magnetic response can be obtained, in principle, from the calculation of the various quantities involved in the Berry–Tabor formula at finite fields. However, for weak fields, one can use the fact that the field dependence of each contribution d_M to the oscillating part of the density of states is essentially due to the modification of the classical action, since this latter is multiplied by the large factor $1/\hbar$, while the field dependence of the periods and the curvatures of the energy manifold can be neglected. Therefore, in this regime we will use for τ_M and g_E the values τ_M^0 and g_E^0 at zero field and consider the first order correction δS to the unperturbed action S_M^0 . A general result in classical mechanics [56, 67] states that the change (*at constant energy*) in the action integral along a closed orbit under the effect of a parameter λ of the Hamiltonian is given by

$$(\partial S / \partial \lambda)_E = - \oint dt \partial \mathcal{H} / \partial \lambda, \quad (4.6)$$

where the integral is taken along the *unperturbed* trajectory. Therefore, if the Hamiltonian has the form of Eq. (4.5), classical perturbation theory yields for small magnetic fields H ,

$$\delta S = \frac{e}{c} H \mathcal{A}_i, \quad (4.7)$$

where \mathcal{A}_i is the directed area enclosed by the unperturbed orbit. This expansion is valid for magnetic fields low enough, or energies high enough, such that the cyclotron radius of the electrons is much larger than the typical size of the structure ($r_c = mc v / eH \gg a$, which is e.g. the case for electrons at the Fermi energy in the experiments of Refs. [25, 26]). In this case we neglect the change in the classical dynamics and consider the effect of the applied field only through the change of the action integral.

For a generic integrable system there is no reason, a priori, that all the orbits of a given family M should enclose the same area. However, as pointed out above, a characteristic feature of integrable systems is that the action is a constant for all the periodic orbits of a given resonant torus. Therefore, the fact that a system remains integrable under the effect of a constant magnetic field implies (because of Eq. (4.7)) that all the orbits of a family enclose the same absolute area $\mathcal{A}_{M,\varepsilon}$. Moreover, since the system is time-reversal invariant at zero field, each closed orbit (M, ε) enclosing an area $\mathcal{A}_{M,\varepsilon}$ is

associated with a time-reversed partner having exactly the same characteristics except for an opposite enclosed area (if the orbit is its own time reversal, $\mathcal{A}_M = 0$). Grouping time-reversal trajectories in Eq. (4.2) at $H = 0$ we have

$$d_M^0(E) = \begin{cases} d_{M,\varepsilon}^0(E) & \text{for self-retracing orbits,} \\ \sum_{\varepsilon=\pm 1} d_{M,\varepsilon}^0(E) = 2d_{M,\varepsilon}^0(E) & \text{for non-self-retracing orbits.} \end{cases} \quad (4.8)$$

For weak fields the contribution of self-retracing orbits is unaltered and therefore they do not contribute to the magnetic response. For the non self-retracing ones we have

$$d_M(E, H) = \sum_{\varepsilon=\pm 1} d_{M,\varepsilon}(E, H) = d_M^0(E) \cos\left(\frac{eH}{\hbar c} \mathcal{A}_M\right), \quad \mathcal{A}_M = |\mathcal{A}_{M,\varepsilon}|. \quad (4.9)$$

This is the basic relation to be used in the examples that follow.

4.2. Circular billiards

We now apply the preceding considerations to a two-dimensional gas of electrons moving in a circular billiard of radius a (where the potential $V(\mathbf{q})$ is zero in the region $|\mathbf{q}| < a$ and infinite outside it). Thus we deal with vanishing wavefunctions at the boundary (Dirichlet boundary condition).

In billiards without magnetic field the magnitude p of the momentum is conserved, and it is convenient to introduce the wave number,

$$k = p/\hbar = \sqrt{2mE}/\hbar \quad (4.10)$$

since at $H = 0$ the time of flight and the action integral of a given trajectory can be simply expressed in terms of its length L as

$$\tau^0 = (m/p)L, \quad S^0/\hbar = kL. \quad (4.11)$$

Following Keller and Rubinow [66], we calculate the action integrals $\mathbf{I} = (I_1, I_2)$ by using the independent paths \mathcal{C}_1 and \mathcal{C}_2 displayed in Fig. 17(a). The function g_E is given by (see [66] and Appendix C)

$$g_E(I_1) = \frac{1}{\pi} \left\{ [(pa)^2 - I_1^2]^{1/2} - I_1 \arccos\left(\frac{I_1}{pa}\right) \right\}, \quad (4.12)$$

where I_1 is interpreted as the angular momentum and bounded by $0 \leq I_1 < pa$.

The periodic orbits of the circular billiard are labeled by the topology $\mathbf{M} = (M_1, M_2)$, where M_1 is the number of turns around the circle until coming to the initial point after M_2 bounces. (Obviously $M_2 \geq 2M_1$.) Elementary geometry yields for the length of the topology- \mathbf{M} trajectories

$$L_M = 2M_2 a \sin \delta, \quad (4.13)$$

where $\delta = \pi M_1/M_2$. The resonant-torus condition, Eq. (4.4), allows us to obtain \mathbf{I}^M as

$$I_1^M = pa \cos \delta, \quad (4.14a)$$

$$I_2^M = (pa/\pi) \{ \sin \delta - \delta \cos \delta \}. \quad (4.14b)$$

The Maslov index of the topology- M trajectories is $\hat{\eta}_M = 3M_2$ (M_2 bounces, each of them giving a dephasing of π , and M_2 encounters with the caustic per period). We therefore have all the ingredients necessary to calculate the oscillating part of the density of states at zero field: For the non-self-retracing trajectories we obtain

$$d_M^0(E) = \sqrt{\frac{2}{\pi}} \frac{g_s m L_M^{3/2}}{\hbar^2} \frac{1}{k^{1/2} M_2^2} \cos\left(kL_M + \frac{\pi}{4} - \frac{3\pi}{2}M_2\right). \quad (4.15)$$

The contribution of a self-retracing orbit is just one half of the contribution (4.15). Its field dependent counterpart is obtained from Eq. (4.9) with the area enclosed by the periodic orbits given by

$$\mathcal{A}_M = \frac{1}{2}M_2 a^2 \sin 2\delta. \quad (4.16)$$

The bouncing-ball trajectories $M_2 = 2M_1$ (with zero angular momentum) are self-retracing and have no enclosed area; thus they do not contribute to the low field susceptibility.

Using Eqs. (2.20b) and (2.15c), and noting $k_F = k(\bar{\mu}) = (2/a)(\bar{N}(\bar{\mu})/g_s)^{1/2}$ the Fermi wave vector, we obtain the contribution to the magnetic susceptibility associated with $\Delta F^{(1)}$:

$$\begin{aligned} \frac{\chi^{(1)}}{\chi_L} &= \frac{48}{\sqrt{2\pi}} (k_F a)^{3/2} \\ &\times \sum_{M_1, M_2 > 2M_1} \frac{(\mathcal{A}_M/a^2)^2}{(L_M/a)^{1/2}} \frac{1}{M_2^2} \cos\left(k_F L_M + \frac{\pi}{4} - \frac{3\pi}{2}M_2\right) \cos\left(\frac{eH}{\hbar c} \mathcal{A}_M\right) R_T(L_M). \end{aligned} \quad (4.17)$$

Since we are working with billiards, the temperature factor R_T is given in terms of the trajectory length L_M by Eq. (A5) and the characteristic cutoff length $L_c = \hbar v_F \beta / \pi$. For $M_2 \gg M_1$ we have $L_M \simeq 2\pi M_1 a$ and $\mathcal{A}_M \simeq \pi M_1 a^2$, independent of M_2 . Performing the summation over the index M_2 (for fixed value of M_1) by taking the length and area dependent terms outside the sum we are left with a rapidly convergent series (whose general term is $(-1)^{M_2}/M_2^2$). We can therefore truncate the series after the first few terms. In Fig. 3 the sum (4.17) is evaluated numerically at zero field (solid line) for a cutoff length $L_c = 6a$ which selects only the first ($M_1 = 1$) harmonic, and the beating between the first few periodic orbits is obtained as a function of wave vector k_F . With only the first two primitive orbits ($M_2 = 3$ and 4, dashed line) we give a good account of $\chi^{(1)}$ for most of the k -interval. Taking the first four primitive orbits suffices to reproduce the whole sum. The short period in k_F corresponds approximately to the circle perimeter $L = 2\pi a$. Going to lower temperatures gives an overall increase of the susceptibility but does not modify the structure of the first harmonic contribution since the length of the whispering-gallery trajectories is bounded by L . However, for larger values of L_c higher harmonics, namely up to M_1 of the order of $L_c/2\pi a$, will be observed. The predominance of the first few trajectories also appears in the beating as a function of magnetic field (not shown) that results from the evaluation of (4.17) at finite fields.

From Fig. 3 we see that the susceptibility of a circular billiard oscillates as a function of the number of electrons (or k_F) taking paramagnetic and diamagnetic values. Its overall magnitude is much larger than the two-dimensional Landau susceptibility and grows as $(k_F a)^{3/2}$. We will later show (Section 6) that this finite-size increase with respect to the bulk value is distinctive of systems that are integrable at zero field. In order to characterize the typical value of the magnetic susceptibility

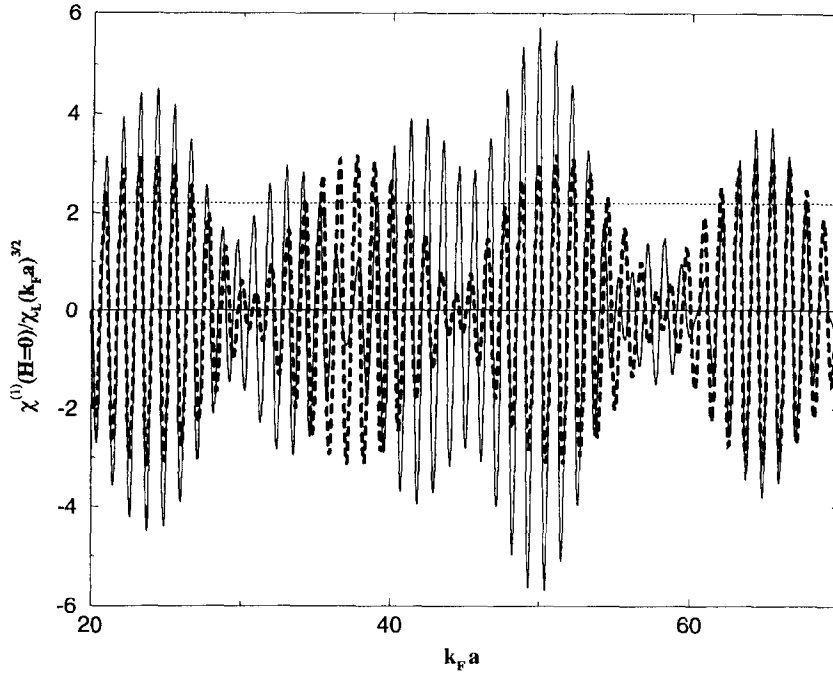


Fig. 3. Magnetic susceptibility at zero field for a circular billiard of radius a as a function of $k_F a$ (solid line) from Eq. (4.17) and as obtained by keeping only the first two terms of the sum (dashed line). The typical susceptibility from Eq. (4.18) is represented by the dotted horizontal line.

we define

$$\chi^{(1)} = \left[\overline{(\chi^{(1)})^2} \right]^{1/2} \quad (4.18)$$

where, as in Section 2, the average is over a $k_F a$ interval classically negligible ($\Delta(k_F a) \ll k_F a$) but quantum mechanically large ($\Delta(k_F a) \gg 2\pi$), so that off-diagonal terms $\cos(k_F L_M) \cos(k_F L_{M'})$ with $M \neq M'$ vanish under averaging. A remark is in order here because at fixed M_1 , L_M goes to $2\pi M_1 a$ as M_2 goes to ∞ , and $(L_{(M_1, M_2)} - L_{(M_1, M'_2)})$ can be made arbitrarily small by increasing M_2 and M'_2 . Therefore, for any interval of $k_F a$ over which the average is taken, some nondiagonal terms should remain unaffected. Nevertheless, because of the rapid decay of the contribution with M_2 , these nondiagonal terms can be neglected in practice for the experimentally relevant temperatures. The typical zero-field susceptibility of the circular billiard is then given by

$$\frac{\chi^{(1)}(H=0)}{\chi_L} \simeq \frac{48}{\sqrt{2\pi}} (k_F a)^{3/2} \left[\frac{1}{2} \sum_{M_1, M_2 > 2M_1} \frac{(\mathcal{A}_M/a^2)^4 R_T^2(L_M)}{L_M/a M_2^4} \right]^{1/2}. \quad (4.19)$$

Numerical evaluation of the first harmonic ($M_1 = 1$) from (4.18) on the $k_F a$ interval of Fig. 3 with $L_c = 6a$ gives $2.20(k_F a)^{3/2} \chi_L$ (dotted horizontal line), while Eq. (4.19) restricted to $M_2 \leq 6$ yields $2.16(k_F a)^{3/2} \chi_L$ illustrating the smallness of the off-diagonal and large- M_2 terms.

For an ensemble made of circular billiards with a dispersion in size or in the number of electrons such that $\Delta(k_F a) > 2\pi$, the term $\chi^{(1)}$ yields a vanishing contribution to the average susceptibility.

In such a case it is necessary to go to the next-order free-energy term $\Delta F^{(2)}$, whose associated contribution $\chi^{(2)}$ yields the average susceptibility by means of Eqs. (2.2) and (2.20c). For the same reason as above one can show that only diagonal terms of $(N^{\text{osc}})^2$ survive the $k_F a$ average, in spite of the degeneracy of the length of the closed orbits as M_2 goes to ∞ . One therefore has

$$\frac{\bar{\chi}}{\chi_L} = \frac{48}{\pi} k_F a \sum_{M_1, M_2 > 2M_1} \frac{(A_M/a^2)^2 (L_M/a)}{M_2^4} \cos\left(\frac{2eH}{\hbar c} \mathcal{A}_M\right) R_T^2(L_M). \quad (4.20)$$

Again, the terms generally decay rapidly with M_2 (as $1/M_2^4$), and for a cutoff length L_c selecting only the terms with $M_1 = 1$ the total amplitude at zero field ($5.2k_F a$) can be obtained from the first few lowest terms. The low field susceptibility of an ensemble of circular billiards is paramagnetic and increases linearly with $k_F a$. As for the $\chi^{(1)}$ contribution, we will show in the sequel that this behavior does not necessitate the integrability at finite fields, but rests only upon the integrability at zero field.

Up to now there have not been measurements of the magnetic response of electrons in circular billiards (individual or ensembles). Our typical (Eq. (4.19)) or average (Eq. (4.20)) susceptibilities exhibit a large enhancement with respect to the bulk values (by powers of $k_F a$). Thus it should be possible to detect experimentally these finite-size effects.

4.3. Rings

The magnetic response of small rings can be calculated along the same lines as in the case of the circles. The ring geometry deserves special interest since it is the preferred configuration for persistent current measurements. In a ring geometry at $H=0$ we have two types of periodic orbits: those which do not touch the inner disk (type-I), and those which do hit it (type-II). (See Fig. 17 of Appendix C; we note by a and b respectively the outer and inner radius of the ring.) The function $g_E(I_1)$ has two branches corresponding to the interval to which the angular momentum I_1 belongs. For $pb < I_1 < pa$, (type-I trajectories) g_E has the same form (4.12) as for the circle, while for $0 \leq I_1 < pb$, (type-II trajectories) we show in Appendix C that

$$g_E(I_1) = \frac{1}{\pi} \left\{ [(pa)^2 - I_1^2]^{1/2} - [(pb)^2 - I_1^2]^{1/2} - I_1 \left[\arccos\left(\frac{I_1}{pa}\right) - \arccos\left(\frac{I_1}{pb}\right) \right] \right\}. \quad (4.21)$$

The type-I trajectories are labeled in the same way as for the circle by the topology $\mathbf{M} = (M_1, M_2)$ representing the number of turns M_1 around the inner circle until returning to the initial point after M_2 bounces on the outer circle. We therefore obtain the resonant-tori condition Eqs. (4.2) and the same contribution (4.15) to the oscillating part of the density of states as in the case of the circle. The only difference is that in the Berry–Tabor trace formula (Eq. (4.2)) the sum corresponding to type-I trajectories is now restricted to $M_2 \geq \hat{M}_2(M_1) = \text{Int}[M_1\pi/\arccos r]$. We note by Int the integer-part function and $r = b/a$. We stress the fact that the minimum value of M_2 is itself a function of M_1 . The previous restriction can also be expressed as $\cos \delta > r$, with $\delta = \pi M_1/M_2$. Type-II trajectories can be labeled by the topology $\mathbf{M} = (M_1, M_2)$, where M_1 is the number of turns around the inner circle in coming to the initial point after M_2 bounces on the *outer* circle. We have the same restriction $M_2 \geq \hat{M}_2(M_1)$ as for type-I trajectories, and we can use $\hat{\eta}_{\mathbf{M}} = 0$ since there are $2M_2$ bounces with the hard walls and no encounters with the caustic. From (4.21) we obtain the

resonant-torus condition

$$l_1^M = pb \frac{\sin \delta}{\sqrt{1+r^2-2r \cos \delta}}, \quad (4.22a)$$

$$l_2^M = \frac{pa}{\pi} \left\{ \sqrt{1+r^2-2r \cos \delta} - \frac{r \delta \sin \delta}{\sqrt{1+r^2-2r \cos \delta}} \right\}. \quad (4.22b)$$

The $H = 0$ contribution to the oscillating part of the density of states from non-self-retracing type-II trajectories with topology M is given by

$$\tilde{d}_M^0(E) = 4 \sqrt{\frac{2}{\pi}} \frac{g_s a^2 m}{\hbar^2} \frac{[(1-r \cos \delta)(r \cos \delta - r^2)]^{1/2}}{(k \tilde{L}_M)^{1/2}} \sin \left(k \tilde{L}_M + \frac{\pi}{4} \right), \quad (4.23)$$

while its length is

$$\tilde{L}_M = 2M_2 a \sqrt{1+r^2-2r \cos \delta}. \quad (4.24)$$

The small field dependence follows from Eq. (4.9) using the enclosed area

$$\tilde{A}_M = M_2 ab \sin \delta. \quad (4.25)$$

In the case of annular geometries it is customary to characterize the magnetic moment \mathcal{M} of the ring by the persistent current

$$I = \frac{c}{A} \mathcal{M} = -c \left(\frac{\partial F}{\partial \Phi} \right)_{T,N}. \quad (4.26)$$

In order to pass from the applied magnetic field H to the flux Φ we use the area A of the outer circle ($\Phi = AH$, $A = \pi a^2$) as defining area. (For thin rings, all periodic orbits with the same repetition number M_1 enclose approximately the same flux $M_1 \Phi$.) Applying Eqs. (2.15c)–(2.20), and calling $I_0 = ev_F/2\pi a$ the typical current of one-dimensional electrons at the Fermi energy, the persistent current of a ring billiard can be expressed as the sum of two contributions corresponding to both types of trajectories:

$$\begin{aligned} \frac{I^{(1)}}{I_0} = g_s (k_F a)^{1/2} \sum_{M_1, M_2 \geq \tilde{M}_2} \left\{ \mathcal{J}_{M, I}^{(1)} \sin \left(\frac{eH}{\hbar c} \mathcal{A}_M \right) R_T(L_M) \right. \\ \left. + \mathcal{J}_{M, II}^{(1)} \sin \left(\frac{eH}{\hbar c} \tilde{\mathcal{A}}_M \right) R_T(\tilde{L}_M) \right\}, \quad (4.27) \end{aligned}$$

$$\mathcal{J}_{M, I}^{(1)} = 2 \sqrt{\frac{2}{\pi}} \frac{1}{M_2^2} \frac{(\mathcal{A}_M/a^2)}{(L_M/a)^{1/2}} \cos \left(k_F L_M + \frac{\pi}{4} - \frac{3\pi}{2} M_2 \right), \quad (4.28a)$$

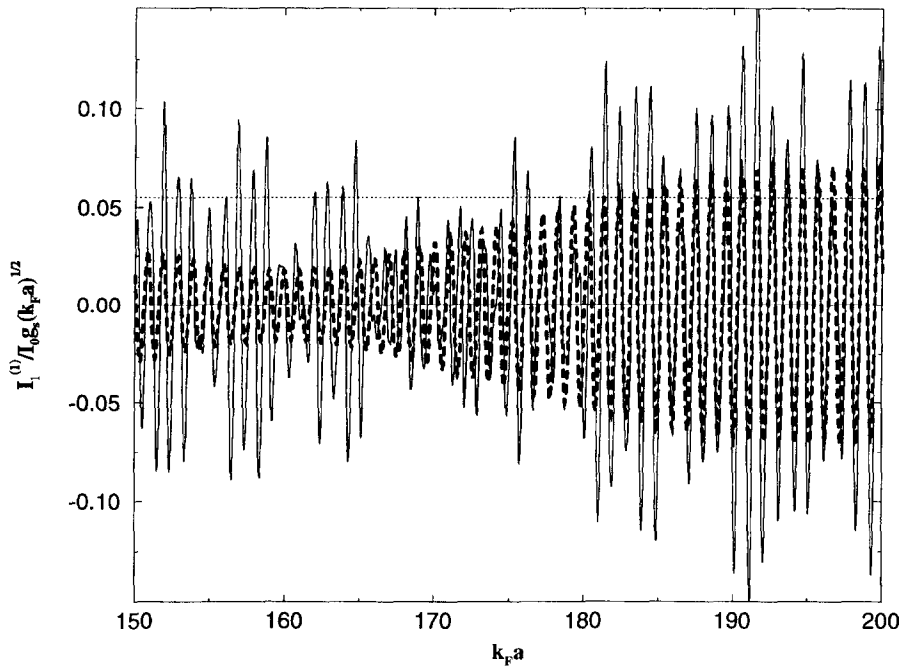


Fig. 4. First harmonic of the persistent current in a ring with $r = b/a = 0.9$ as a function of $k_F a$ (solid line) for a cutoff length $L_c = 6a$ according to Eqs. (4.27)–(4.28) together with the contribution coming from type-I trajectories (dashed line). The typical persistent current from Eq. (4.29) is represented by the dotted horizontal line.

$$\mathcal{I}_{M,II}^{(1)} = 8 \sqrt{\frac{2}{\pi}} \frac{(\tilde{\mathcal{A}}_M/a^2)}{(\tilde{L}_M/a)^{5/2}} [(1 - r \cos \delta)(r \cos \delta - r^2)]^{1/2} \sin \left(k \tilde{L}_M + \frac{\pi}{4} \right). \quad (4.28b)$$

In Fig. 4 we present the first harmonic $I_1^{(1)}$ of the persistent current for a thin ring and a cutoff length $L_c = 6a$ (solid line). (I.e., we are considering the winding number $M_1 = 1$.) The contribution of type-I trajectories (dashed line) is similar as in the case of the circle: a rapidly convergent sum showing as a function of k_F the beating between the first two trajectories (\hat{M}_2 and $\hat{M}_2 + 1$). On the other hand, Eq. (4.28b) shows that the trajectories with low values of M_2 (i.e. $M_2 \sim \hat{M}_2$) contributing to $\mathcal{I}_{M,II}^{(1)}$ have negligible weight due to the small stability prefactor caused by the defocusing effect exerted by the inner disk ($\cos \delta \simeq r$). The sum is dominated by trajectories with $M_2 > \hat{M}_2$ and therefore we loose the previous beating structure in the total $I_1^{(1)}$. The short period in k_F still corresponds to the circle perimeter L .

As in the previous subsection, we characterize the typical value of the magnetic response by averaging $(I^{(1)})^2$ over a $k_F a$ -interval containing many oscillations, but yet negligible on the classical scale.

$$I^{(0)} = \left[\overline{(I^{(1)})^2} \right]^{1/2}. \quad (4.29)$$

In the same way as for the circular billiard, one can in practice consider that, despite the degeneracy in the length of type-I trajectories for large M_2 , only diagonal terms (in both index \mathbf{M} and trajectory-

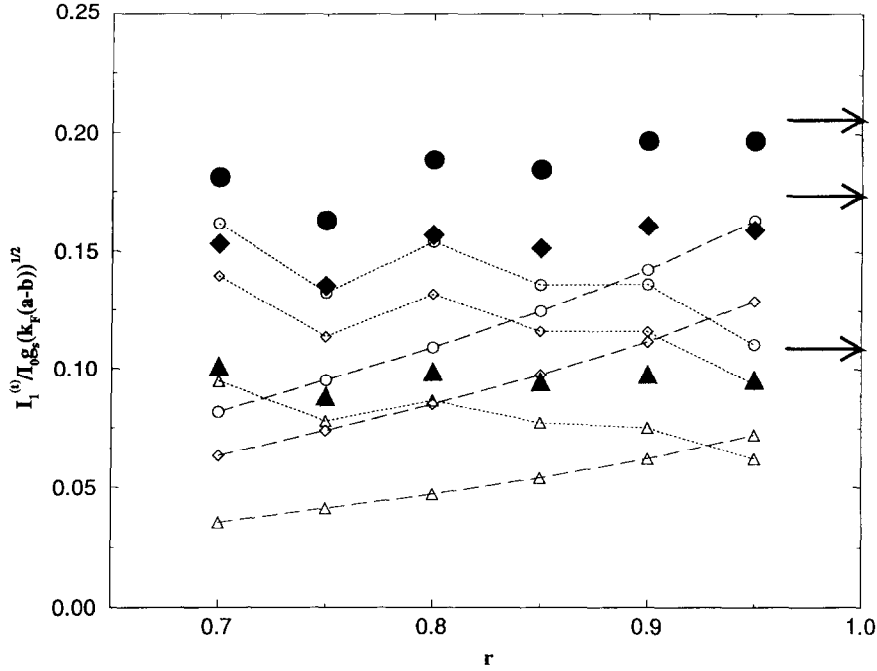


Fig. 5. First harmonic of the typical persistent current in rings of different thickness ($r = b/a$) for various cutoff lengths $L_c = 30a$ (circles), $6a$ (diamonds) and $3a$ (triangles) according to Eq. (4.29). Filled symbols correspond to the total persistent current and lay approximately on a horizontal line for each L_c , consistent with the asymptotic behavior of Eq. (4.39) indicated by arrows on the extreme right of the plot. Unfilled symbols represent the contributions from both types of trajectories and are joined by dotted lines (type-I) and dashed lines (type-II). This guide to the eye exhibits the approximate behavior of Eqs. (4.38) and shows how the r characteristic of the switching from one type of trajectories to the other increases with temperature.

type) survive the averaging for large enough $\Delta(k_F a)$. Therefore

$$\begin{aligned} \frac{I^{(1)}}{I_0} \simeq g_s(k_F a)^{1/2} \sum_{M_1, M_2 \geq \tilde{M}_2} \left[\left(\mathcal{J}_{M,I}^{(1)} \right)^2 \sin^2 \left(\frac{eH}{\hbar c} \mathcal{A}_M \right) R_T^2(L_M) \right. \\ \left. + \left(\mathcal{J}_{M,II}^{(1)} \right)^2 \sin^2 \left(\frac{eH}{\hbar c} \tilde{\mathcal{A}}_M \right) R_T^2(\tilde{L}_M) \right]^{1/2}, \end{aligned} \quad (4.30)$$

where $(\mathcal{J}_{M,I}^{(1)})^2$ and $(\mathcal{J}_{M,II}^{(1)})^2$ are obtained from Eqs. (4.28) simply by replacing the average of $\cos^2(k_F L_M + \pi/4 - 3M_2\pi/2)$ and $\sin^2(k_F \tilde{L}_M + \pi/4)$ by $\frac{1}{2}$.

In Fig. 5 we present the typical persistent current and its two contributions for various ratios $r = b/a$ and cutoff lengths L_c for the first harmonic ($M_1 = 1$). The contribution $\mathcal{J}_{M,I}^{(1)}$ of type-I trajectories dominates for small r (where the inner circle is not important and we recover the magnetic response of the circular billiard) while type-II trajectories take over for narrow rings. The cross-over r depends on temperature through L_c due to the different dependence of the trajectory length on M (Eqs. (4.13) and (4.24)) for both types of trajectories.

As in the case of $\chi^{(1)}$ for the circular billiard, $I^{(1)}$ gives a vanishing contribution to the persistent current of an ensemble of rings with different sizes or electron fillings as soon as the dispersion in

$k_F a$ is of the order of 2π . We therefore need to go to the term $\Delta F^{(2)}$ in the free-energy expansion, which is obtained (see Eq. (2.20c)) from

$$N^{\text{osc}}(\bar{\mu}) = \sum_{M_1, M_2 \geq \hat{M}_2} \{N_{M, \text{I}}(\bar{\mu}) + N_{M, \text{II}}(\bar{\mu})\}, \quad (4.31)$$

where $N_{M, \text{I}}(\bar{\mu})$ and $N_{M, \text{II}}(\bar{\mu})$ are given in terms of the respective contributions to the field-dependent density of states through Eq. (2.15b). For an ensemble with a large dispersion of sizes only diagonal terms survive the average and we have (with $\bar{D} = \mathbf{g}_s m A (1 - r^2) / (2\pi \hbar^2)$)

$$\frac{\overline{I^{(2)}}}{I_0} = \mathbf{g}_s \sum_{M_1, M_2 \geq \hat{M}_2} \left\{ \overline{\mathcal{F}_{M, \text{I}}^{(2)}} \sin\left(\frac{2eH}{\hbar c} \mathcal{A}_M\right) R_{\text{T}}^2(L_M) + \overline{\mathcal{F}_{M, \text{II}}^{(2)}} \sin\left(\frac{2eH}{\hbar c} \tilde{\mathcal{A}}_M\right) R_{\text{T}}^2(\tilde{L}_M) \right\}, \quad (4.32)$$

$$\overline{\mathcal{F}_{M, \text{I}}^{(2)}} = \frac{2}{\pi} \frac{1}{M_2^4} \left(\frac{L_M}{a}\right) \left(\frac{\mathcal{A}_M}{a^2}\right) \frac{1}{1 - r^2}, \quad (4.33a)$$

$$\overline{\mathcal{F}_{M, \text{II}}^{(2)}} = \frac{32}{\pi} \frac{\left(\tilde{\mathcal{A}}_M/a^2\right)}{\left(\tilde{L}_M/a\right)^3} \frac{(1 - r \cos \delta)(r \cos \delta - r^2)}{1 - r^2}. \quad (4.33b)$$

The k_F dependence of the average persistent current is linear (through I_0), similarly to the case of the average susceptibility of an ensemble of circular billiards.

4.3.1. Thin rings

In the case of thin rings ($a \simeq b$, $r \simeq 1$) further approximations can be performed on Eqs. (4.28) and (4.33) using $(1 - r)$ as a small parameter, giving more compact and meaningful expressions for the typical and average persistent currents. Since in addition this is the configuration used in the experiment of Ref. [26], we shall consider more closely this limiting case. First, we note that $\hat{\delta} = \arccos r \simeq \sqrt{2(1 - r)} \ll 1$. Thus

$$\hat{M}_2 = \text{Int} \left[\pi M_1 / \hat{\delta} \right] \simeq (\pi / \sqrt{2}) (M_1 / \sqrt{1 - r}) \gg M_1, \quad (4.34)$$

and for $M_2 \geq \hat{M}_2$, the area and length of contributing orbits can be approximated by

$$\mathcal{A}_M \simeq \tilde{\mathcal{A}}_M \simeq M_1 A = M_1 \pi a^2; \quad L_M \simeq M_1 L = M_1 2\pi a. \quad (4.35)$$

For the length of type-II trajectories we have $\tilde{L}_M \simeq M_1 L$ for $M_2 \simeq \hat{M}_2$, and $\tilde{L}_M \simeq 2M_2(a - b)$ when $M_2 \gg \hat{M}_2$. All trajectories with winding number M_1 enclose approximately the same flux $M_1 \Phi$, and the field-dependent terms in Eq. (4.27) may be replaced by $\sin(2\pi M_1 \Phi / \Phi_0)$. There is therefore no difference between the case that we study (where a uniform magnetic field H is applied) and the ideal case of a flux line Φ through the inner circle of the ring. The length-dependent factors R_{T}^2 can also be taken outside the sum over M_2 since the main contribution of type-II trajectories comes from $M_2 \simeq \pi M_1 / [5^{1/6}(1 - r)^{2/3}]$. Even if these M_2 's are much larger than \hat{M}_2 , their associated \tilde{L}_M are still of the order of $M_1 L$ to leading order in $1 - r$.

Turning now to the typical and ensemble average currents, it should be stressed that for narrow rings it is necessary to go to fairly large energies before an average on a scale being quantum mechanically large but classically small is possible. Indeed, one has for both types of trajectories

$k_F(L_{\hat{M}_2+1} - L_{\hat{M}_2}) \simeq k_F(\tilde{L}_{\hat{M}_2+1} - \tilde{L}_{\hat{M}_2}) \simeq (4\sqrt{2}/3)\pi\mathcal{N}\sqrt{1-r}$, where $\mathcal{N} = k_F(a-b)/\pi$ is the number of transverse occupied channels. Therefore, \mathcal{N} should be much larger than $(1-r)^{-1/2}$ if one wants to assume $\Delta(k_F a)$ sufficiently large to average out all nondiagonal terms without violating the condition $\Delta(k_F a) \ll k_F a$. Supposing the previous condition is met, and introducing the typical amplitudes $\mathcal{J}_{M_1, I}^{(t)}$ and $\mathcal{J}_{M_1, II}^{(t)}$ of each harmonic, we write

$$\frac{I^{(t)}}{I_0} = \mathbf{g}_s \left[\sum_{M_1} \left\{ \left(\mathcal{J}_{M_1, I}^{(t)} \right)^2 + \left(\mathcal{J}_{M_1, II}^{(t)} \right)^2 \right\} \sin^2 \left(2\pi M_1 \frac{\Phi}{\Phi_0} \right) R_T^2(M_1 L) \right]^{1/2}, \quad (4.36)$$

$$\left(\mathcal{J}_{M_1, I}^{(t)} \right)^2 = k_F a \sum_{M_2 \geq \hat{M}_2} \left(\mathcal{J}_{M, I}^{(t)} \right)^2 = 2k_F a M_1 \left[\sum_{M_2 \geq \hat{M}_2} \frac{1}{M_2^4} \right], \quad (4.37a)$$

$$\left(\mathcal{J}_{M_1, II}^{(t)} \right)^2 = k_F a \sum_{M_2 \geq \hat{M}_2} \left(\mathcal{J}_{M, II}^{(t)} \right)^2 = 2\pi k_F a M_1^2 \left[\sum_{M_2 \geq \hat{M}_2} \frac{(1-r)^2 - \delta^4/4}{M_2^5 ((1-r)^2 + \delta^2)^{5/2}} \right]. \quad (4.37b)$$

Since $\hat{M}_2 \gg 1$ we can convert the previous sums into integrals and obtain

$$\left(\mathcal{J}_{M_1, I}^{(t)} \right)^2 \simeq \frac{4\sqrt{2}}{3(\pi M_1)^2} \mathcal{N} (1-r)^{1/2}. \quad (4.38a)$$

$$\left(\mathcal{J}_{M_1, II}^{(t)} \right)^2 \simeq \frac{4}{3(\pi M_1)^2} \mathcal{N} \left(1 - \sqrt{2}(1-r)^{1/2} \right). \quad (4.38b)$$

In leading order in $1-r$ the persistent current is dominated by type-II trajectories (independent of the temperature) and given by

$$\frac{I^{(t)}}{I_0} = \frac{2}{\pi\sqrt{3}} \mathbf{g}_s \sqrt{\mathcal{N}} \left[\sum_{M_1} \frac{1}{M_1^2} \sin^2 \left(2\pi M_1 \frac{\Phi}{\Phi_0} \right) R_T^2(M_1 L) \right]^{1/2}, \quad (4.39)$$

consistent with the result of Ref. [32]. For the next-order term the contribution from type-I trajectories is cancelled by that of type-II resulting in the relatively flat character of the curves for $I^{(t)}$ in Fig. 5.

For the current of an ensemble of thin rings, the calculations are similar to those of Eqs. (4.38), and in leading order in $1-r$ we obtain:

$$\frac{\overline{I^{(2)}}}{I_0} = \mathbf{g}_s \sum_{M_1} \left\{ \overline{\mathcal{J}_{M_1, I}^{(2)}} + \overline{\mathcal{J}_{M_1, II}^{(2)}} \right\} \sin \left(4\pi M_1 \frac{\Phi}{\Phi_0} \right) R_T^2(M_1 L), \quad (4.40)$$

$$\overline{\mathcal{J}_{M_1, I}^{(2)}} = \sum_{M_2 \geq \hat{M}_2} \overline{\mathcal{J}_{M, I}^{(2)}} = \frac{4\sqrt{2}}{3\pi^2} \sqrt{1-r} \frac{1}{M_1}, \quad (4.41a)$$

$$\overline{\mathcal{J}_{M_1, II}^{(2)}} = \sum_{M_2 \geq \hat{M}_2} \overline{\mathcal{J}_{M, II}^{(2)}} = \frac{2}{\pi^2} \left(1 - \frac{2\sqrt{2}}{3} \sqrt{1-r} \right) \frac{1}{M_1}. \quad (4.41b)$$

Type-II trajectories once again dominate the average magnetic response of thin rings and the amplitude for the first harmonic is $\overline{I_1^{(2)}}/I_0 \simeq (2\mathbf{g}_s/\pi^2) \sin(4\pi\Phi/\Phi_0) R_T^2(L)$, independently of the number of transverse channels \mathcal{N} . The average persistent current shows the halving of the flux period with

respect to $I^{(1)}$ characteristic for ensemble results (as found in the disordered case and consistently with the results for averages in the following sections).

4.3.2. Comparison with experiment

Persistent currents have been measured by Mailly et al. [26] in a thin semiconductor ring (with effective outer and inner radii $a = 1.43 \mu\text{m}$ and $b = 1.27 \mu\text{m}$) in the ballistic and phase-coherent regime ($l = 11 \mu\text{m}$ and $L_\phi = 25 \mu\text{m}$). The Fermi velocity is $v_F = 2.6 \times 10^7 \text{ cm/s}$ and therefore the number of occupied channels is $\mathcal{N} \simeq 4$. The quoted temperature of $T = 15 \text{ mK}$ makes the temperature factor irrelevant for the first harmonic ($L_c \simeq 30a$, $R_T(L) \simeq 1$). The magnetic response exhibits an hc/e flux periodicity and changes from diamagnetic to paramagnetic by changing the microscopic configuration, consistently with Eqs. (4.27)–(4.28). Unfortunately, the sensitivity is not high enough in order to test the signal averaging with these microscopic changes. The typical persistent current was found to be 4 nA , while Eq. (4.39) and Ref. [32] would yield 7 nA . The difference between the theoretical and measured values is not significant given the experimental uncertainties as discussed in Refs. [26, 30]. Moreover, as we stressed above, a very large $k_F a$ interval is needed for the average of $(I^{(1)})^2$ in order to recover $I^{(1)}$; otherwise we expect large statistical fluctuations. As in the case of the susceptibility of squares that we analyze in the next section, residual disorder (reducing the magnetic response without altering the physical picture) and interactions may be necessary in order to attempt a detailed comparison with the experiment. Clearly, new experiments on individual rings of various thickness and on ensembles of ballistic rings would be helpful in order to test the ideas of the present section.

5. Simple regular geometries: the square

The circular and annular billiards studied in Section 4 have the remarkable property that, due to their rotational symmetry, they remain integrable under the application of a magnetic field. However, for a generic integrable system (a *regular* geometry) any perturbation breaks the integrability of the dynamics. Moreover, the periodic orbits which are playing the central role in the semiclassical trace formulas are most strongly affected by the perturbation. Indeed, the Poincaré–Birkhoff theorem [65] states that as soon as the magnetic field is turned on, all resonant tori (i.e. all families of periodic orbits) are instantaneously broken, leaving only two isolated periodic orbits (one stable and one unstable). It is therefore no longer possible to use the Berry–Tabor semiclassical trace formula to calculate the oscillating part of the density of states for finite field since it is based on a sum over resonant tori, which do not exist any further. One has therefore to devise a semiclassical technique allowing to calculate $d^{\text{osc}}(E)$ for nearly, but not completely, integrable systems.

To achieve this, it is necessary to go back to the basic equations from which the standard semiclassical trace formulae of Gutzwiller [51], Balian-Bloch [54] and Berry-Tabor [53] are derived. The density of states $d(E)$, Eq. (1.4), is related to the trace of the energy-dependent Green function $G(\mathbf{q}, \mathbf{q}'; E)$ by

$$d(E) = -\frac{\mathbf{g}_s}{\pi} \text{Im } \mathcal{G}(E), \quad \mathcal{G}(E) = \int d\mathbf{q} G(\mathbf{q}, \mathbf{q}; E), \quad (5.1)$$

where again the factor $\mathbf{g}_s = 2$ comes from the spin degeneracy. $G(\mathbf{q}, \mathbf{q}'; E)$ has a singularity (logarithmic in two dimensions) when $\mathbf{r} \rightarrow \mathbf{r}'$ which just gives the smooth (Weyl) part $\bar{d}(E)$ of the

density of states in a leading order semiclassical expansion. However, in order to consider only the oscillating part of $d(E)$ one can use the semiclassical approximation of the Green function [21]

$$G_E^{\text{sc}}(\mathbf{q}, \mathbf{q}'; E) = \frac{1}{i\hbar} \frac{1}{\sqrt{2i\pi\hbar}} \sum_t D_t \exp \left[\frac{i}{\hbar} S_t - i\eta_t \frac{\pi}{2} \right] \quad (5.2)$$

where the sum runs over all classical trajectories t joining \mathbf{q} and \mathbf{q}' at energy E . S_t is the action along the trajectory t , D_t a determinant involving second derivatives of the action (the general expression of which is given in Appendix D) and η_t is the Maslov index of the trajectory, i.e. the number of focal points encountered when traveling from \mathbf{q} to \mathbf{q}' . As in Section 4, we shall also take into account in η_t the phase π acquired at each reflection at the wall of a billiard with Dirichlet boundary conditions.

By taking the trace (5.1) the sum in Eq. (5.2) becomes a sum over all orbits closed in configuration (i.e. \mathbf{q}) space, to which we will refer in the following as *recurrent* orbits. The standard route to obtain d^{osc} is to evaluate this integral by stationary-phase approximation. This selects the trajectories which are not only closed in configuration space ($\mathbf{r}' = \mathbf{r}$), but also closed in phase space ($\mathbf{p}' = \mathbf{p}$), i.e. *periodic* orbits. When these latter are (well) isolated the Gutzwiller Trace Formula [51] is obtained. For integrable systems, all recurrent orbits are in fact periodic since the action variables are constants of motion.

Periodic orbits appear in continuous families associated with resonant tori. All orbits of a family have the same action and period, and one can calculate the density of states using the Berry–Tabor formula as described in the previous section. For systems such as the square billiard, the physical effect which generates the susceptibility comes along with the breaking of the rational tori, so that just ignoring this, i.e. using the Berry–Tabor Formula, is certainly inadequate. On the other hand, for $H \rightarrow 0$ the remaining orbits are not sufficiently well isolated to apply the Gutzwiller Trace Formula. Therefore, as stated before, we need a uniform treatment of the perturbing field, in which not only the orbits being closed in phase space are taken in account, but also the orbits closed in configuration space which can be traced back to a periodic orbit when $H \rightarrow 0$.

In this section we show how this can be performed in the particular case of a square billiard. Because of the simplicity of its geometry, the integrals involved in the trace Eq. (5.1) can be performed exactly for weak magnetic fields. Moreover, the square geometry deserves special interest since it was the first microstructure experimentally realized to measure the magnetic response in the ballistic regime. We present here a semiclassical approach addressing the physical explanation of the experimental findings of Ref. [25], which have pointed the way for the ongoing research. In order to obtain semiclassical expressions for the susceptibility of individual and ensembles of squares we will proceed as outlined in Section 2: We will calculate the density of states and use the decomposition of the susceptibility according to Eq. (2.19) into contributions corresponding to $\Delta F^{(1)}$ and $\Delta F^{(2)}$. In Section 6 we present the theory for a generic integrable system perturbed by a magnetic field, generalizing the results of this section.

5.1. Oscillating density of states for weak field

To start with, we consider a square billiard (of side a) in the absence of a field. Each family of periodic orbits can be labeled by the topology $\mathbf{M} = (M_x, M_y)$ where M_x and M_y are the number of

bounces occurring on the bottom and left side of the billiard (see Fig. 6). The length of the periodic orbits for all members of a family is

$$L_M = 2a\sqrt{M_x^2 + M_y^2}. \quad (5.3)$$

The unperturbed action along the trajectory is, as for any billiard system, $S_M^0/\hbar = kL_M$ where k is the wave number. The Maslov indices are $\eta_M = 4(M_x + M_y)$, and we will omit them from now on since they only yield a dephasing of a multiple of 2π . Finally the unperturbed determinant reduces to

$$D_M = m/\sqrt{\hbar k L_M}. \quad (5.4)$$

One way to obtain this result is to use the method of images (see Fig. 7) and express the exact Green function $G(\mathbf{q}, \mathbf{q}'; E)$ in terms of the free Green function $G^0(\mathbf{q}, \mathbf{q}'; E)$ as [54, 51]

$$G(\mathbf{q}, \mathbf{q}'; E) = G^0(\mathbf{q}, \mathbf{q}'; E) + \sum_{\mathbf{q}_i} \varepsilon_i G^0(\mathbf{q}_i, \mathbf{q}'), \quad (5.5)$$

where the \mathbf{q}_i represent all the mirror images of \mathbf{q} by any combination of symmetry across a side of the square, and $\varepsilon_i = +1$ or -1 depending on whether one needs an even or odd number of symmetries to map \mathbf{q} on \mathbf{q}_i . $G^0(\mathbf{q}, \mathbf{q}'; E)$ gives the above-mentioned logarithmic singularity of G when $\mathbf{q}' \rightarrow \mathbf{q}$, but the long-range asymptotic behavior of the two-dimensional free Green function

$$G^0(\mathbf{q}_i, \mathbf{q}') \simeq \frac{1}{i\hbar} \frac{m}{\sqrt{2i\pi\hbar}} \frac{\exp(ik|\mathbf{q}' - \mathbf{q}_i|)}{\sqrt{\hbar k}|\mathbf{q}' - \mathbf{q}_i|} \quad (5.6)$$

can be used for all other terms (images).

For sufficiently weak magnetic fields, one may follow the same approach as in the previous section, keeping in Eq. (5.2) the zeroth-order approximation for the prefactor D_M , and using the first-order correction δS to the action which, as expressed by Eq. (4.7), is proportional to the area enclosed by the unperturbed trajectory. Here however, as is the generic case (and contrary to circular or annular geometries) the area enclosed by an orbit varies within a family.

Let us consider the contribution to the density of states of the family of recurrent trajectories which for $H \rightarrow 0$ tends to the family of shortest periodic orbits with nonzero enclosed area, that plays a crucial role in determining the magnetic response, as already recognized in Ref. [25]. For $H = 0$, this family consists in the set of orbits which, say, start with an angle of 45° with respect to the boundary on the bottom side of the billiard at a distance x_0 ($0 \leq x_0 \leq a$) from its left corner, bounce once on each side of the square before returning to their initial position (family $\mathbf{M} = (1, 1)$, see Fig. 6(a)). It is convenient to use as configuration space coordinates x_0 which labels the trajectory, the distance s along the trajectory, and the index $\varepsilon = \pm 1$ which specifies the direction in which the trajectory is traversed. In this way, each point \mathbf{q} is counted four times corresponding to the four sheets of the invariant torus. The enclosed area $\mathcal{A}_\varepsilon(x_0, s)$ obviously does not depend on s and is given by

$$\mathcal{A}_\varepsilon(x_0) = \varepsilon 2 x_0 (a - x_0). \quad (5.7)$$

Periodic orbits are those paths for which the action is extremal ($\nabla S = \mathbf{p}' - \mathbf{p} = 0$). Therefore Eqs. (4.7) and (5.7) illustrate the contents of the Poincaré–Birkhoff theorem, that for any nonzero

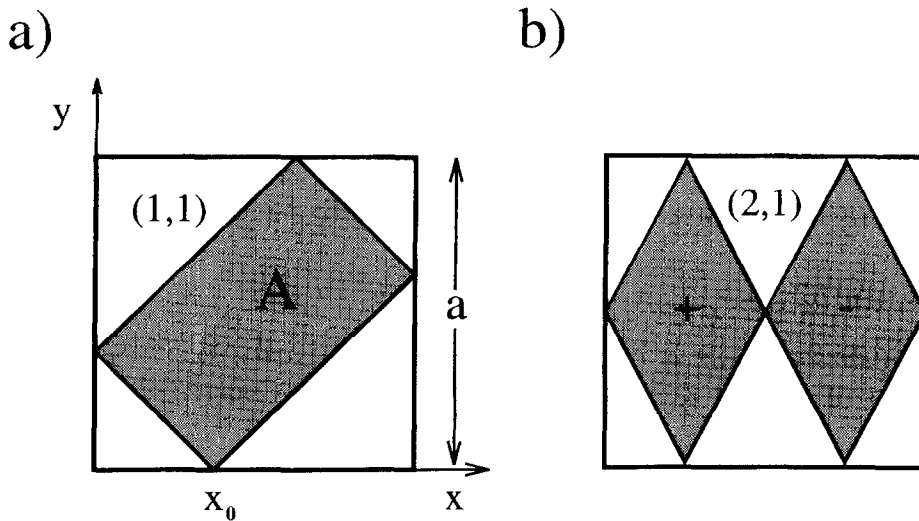


Fig. 6. (a) Trajectory from the family (1,1) of the square billiard. The abscissa x_0 of the intersection of the trajectory with the lower side of the square, together with the label $\varepsilon = \pm 1$ precisig the sense of the motion, label the trajectories inside the family. (b) Trajectory from the family (2,1) of the square billiard, illustrating the flux cancelation occurring for other periodic trajectories than those in the (1,1) family (or their repetitions).

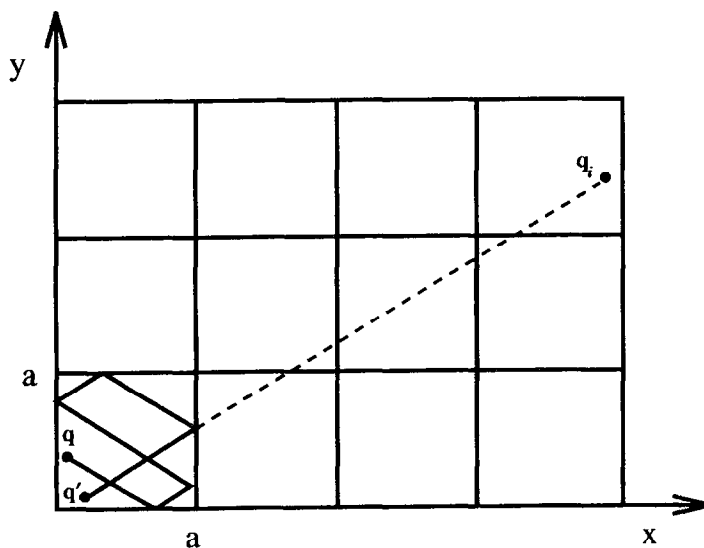


Fig. 7. The method of images: The Green function $G(q, q')$ is constructed from the free Green function G^0 by placing a source point at each mirror image q_i of the actual source q . To each of the resulting contribution $G^0(q_i, q')$ is associated a classical trajectory (solid line). This latter is obtained from the straight line joining q_i to q' (dash line) by mapping all its intersected images back onto the original billiard.

field only the two trajectories corresponding to $x_0 = a/2$ remain periodic (one stable, one unstable according to the two possible directions of traversal). The contribution of the family (1,1) to $d^{\text{osc}}(E)$ is $d_{11}(E) = -(\mathbf{g}_s/\pi) \text{Im } \mathcal{G}_{11}(E)$. Inserting Eqs. (5.7) and (4.7) into the integral of Eq. (5.1) we have

$$\mathcal{G}_{11}(H) = \frac{1}{i\hbar} \frac{1}{\sqrt{2i\pi\hbar}} \int_0^{L_{11}} ds \left(\frac{dy}{ds} \right) \int_0^a dx_0 \sum_{\varepsilon=\pm 1} D_{11} \exp \left[ikL_{11} + i \frac{2e\varepsilon}{\hbar c} Hx_0(a - x_0) \right]. \quad (5.8)$$

The contribution to the density of states of the family (1,1) factorizes into an unperturbed (Berry–Tabor-like) term and a field-dependent factor

$$d_{11}(E, H) = d_{11}^0(E) \mathcal{C}(H) \quad (5.9)$$

with

$$d_{11}^0 \equiv d_{11}(H=0) = \frac{4\mathbf{g}_s}{\pi} \frac{ma^2}{\hbar^2(2\pi kL_{11})^{1/2}} \sin \left(kL_{11} + \frac{\pi}{4} \right), \quad (5.10)$$

and

$$\mathcal{C}(H) = \frac{1}{a} \int_0^a dx_0 \cos \left(\frac{2e}{\hbar c} Hx_0(a - x_0) \right) = \frac{1}{\sqrt{2\varphi}} [\cos(\pi\varphi)C(\sqrt{\pi\varphi}) + \sin(\pi\varphi)S(\sqrt{\pi\varphi})]. \quad (5.11)$$

C and S respectively denote the cosine and sine Fresnel integrals [68], and

$$\varphi = Ha^2/\Phi_0 \quad (5.12)$$

is the total flux through the square measured in units of the flux quantum ($\Phi_0 = hc/e$). For the circular and annular geometries, the field dependence of the density of states, and therefore the susceptibility, was related to the dephasing between time-reversal families of orbits. Here, Eq. (5.11) expresses that the dependence of d^{osc} on the field is also determined by the field induced decoherence of different orbits *within* a given family.

As soon as φ reaches a value close to one, the Fresnel integrals can be replaced by their asymptotic value $\frac{1}{2}$, which amounts to evaluate $\mathcal{C}(\varphi)$ by stationary phase, i.e.

$$\mathcal{C}^S(\varphi) = \cos(\pi\varphi - \pi/4)/\sqrt{4\varphi}. \quad (5.13)$$

This means that for $\varphi > 1$ the dominant contribution to $\mathcal{C}(\varphi)$ comes from the neighborhood of the two surviving periodic orbits ($x_0 = a/2, \varepsilon = \pm 1$), and the oscillations of $\mathcal{C}(\varphi)$ are related to the successive dephasing and rephasing of these orbits. In fact, one would have obtained just $d_{11}^S = d_{11}^0 \mathcal{C}^S(\varphi)$ by evaluating the contribution to the density of states of the two surviving periodic orbits using the Gutzwiller trace formula with a first-order classical perturbative evaluation of the actions and stability matrices. $\mathcal{C}^S(\varphi)$ however diverges when $H \rightarrow 0$, while the full expression Eq. (5.11) simply gives $\mathcal{C}(0) = 1$.

To compute the contribution d_M of longer trajectories, it is worthwhile to write (M_x, M_y) as (ru_x, ru_y) , where u_x and u_y are coprime integers labeling the primitive orbits and r is the number of repetitions. As illustrated in Fig. 6(b), for any orbit of the family the square can be decomposed into $u_x \times u_y$ cells, such that the algebraic area enclosed by the trajectory inside two adjacent cells

exactly compensate. Therefore, keeping x_0 as a label of the orbit (with $x_0 \in [0, a/u_x]$ to avoid double counting), the total area enclosed by the trajectory (ru_x, ru_y) is

$$\mathcal{A}_M = \begin{cases} 0 & u_x \text{ or } u_y \text{ even,} \\ r \frac{\mathcal{A}_v(u_x x_0)}{u_x u_y} & u_x \text{ and } u_y \text{ odd,} \end{cases} \quad (5.14)$$

where $\mathcal{A}_v(x_0)$ is given by Eq. (5.7). From the above equation, and proceeding in the same way as for the orbit (1, 1) Eq. (5.9) can be generalized to

$$d_M(E, H) = \begin{cases} d_M^0(E) & u_x \text{ or } u_y \text{ even,} \\ d_M^0(E) \mathcal{C} \left(\frac{r\varphi}{u_x u_y} \right) & u_x \text{ and } u_y \text{ odd,} \end{cases} \quad (5.15)$$

where $\mathcal{C}(\varphi)$ is given by Eq. (5.11) and $d_M^0 \equiv d_M(H=0)$ is the zero-field contribution of the family M

$$d_M^0 = \frac{4g_s}{\pi} \frac{ma^2}{\hbar^2 (2\pi k L_M)^{1/2}} \sin \left(k L_M + \frac{\pi}{4} \right). \quad (5.16)$$

5.2. The susceptibility: individual samples versus ensemble averages

For clarity of the presentation we will calculate in a first stage the susceptibility contribution of the family (1, 1) of the shortest flux enclosing orbits only. This corresponds to the temperature regime of the experiment Ref. [25] where the characteristic length L_c given by Eq. (A5) is of the order of L_{11} , the length of the shortest orbits, and contributions of all longer orbits are eliminated due to temperature damping. In the next subsection we will state the results valid at arbitrary temperature by taking into account the contribution of longer orbits.

From the expressions (5.9) and (5.10) of the contributions of the family (1, 1) to $d^{\text{osc}}(E, H)$ one obtains the corresponding contribution to $\Delta F^{(1)}$ (Eqs. (2.15c) and (2.20b)) as

$$\Delta F_{11}^{(1)}(H) = \frac{g_s \hbar^2}{m} \left(\frac{2^3 a}{\pi^3 L_{11}^5} \right)^{1/2} (k_F a)^{3/2} \sin \left(k_F L_{11} + \frac{\pi}{4} \right) \mathcal{C}(H) R_T(L_{11}). \quad (5.17)$$

$R_T(L_{11})$ is the temperature-dependent reduction factor Eq. (A5), valid for billiard systems. The field-dependent factor $\mathcal{C}(\varphi)$ is given by Eq. (5.11). Taking the derivatives with respect to the magnetic field, we have [for $L_c \simeq L_{11}$]

$$\frac{\chi^{(1)}}{\chi_L} = -\frac{3}{(\sqrt{2\pi})^{5/2}} (k_F a)^{3/2} \sin \left(k_F L_{11} + \frac{\pi}{4} \right) \frac{d^2 \mathcal{C}}{d\varphi^2} R_T(L_{11}). \quad (5.18)$$

The susceptibility of a given square oscillates as a function of the Fermi energy and can be paramagnetic or diamagnetic (see Fig. 8(a)). Since we are considering only one kind of trajectory the typical susceptibility $\chi^{(1)}$ (with the definition (4.18)) is simply proportional to the prefactor of $\chi^{(1)}$. Therefore, it is of the order of $(k_F a)^{3/2}$, which is much larger than the Landau susceptibility χ_L . As shown in Fig. 8(b) (solid line) $\chi^{(1)}$ exhibits also (by means of $\partial^2 \mathcal{C} / \partial \varphi^2$) oscillations as a function

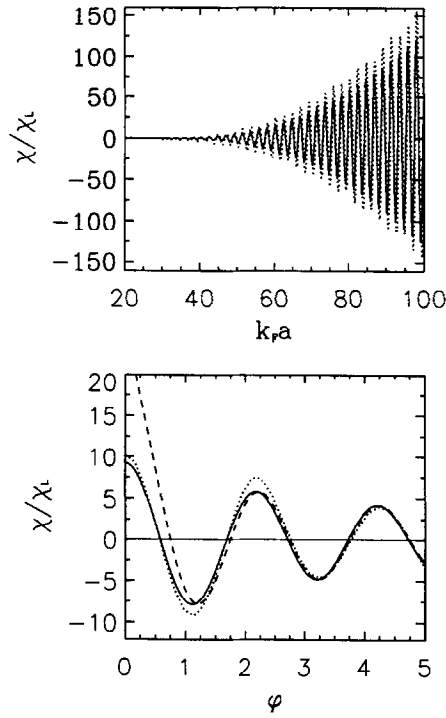


Fig. 8. (a) Magnetic susceptibility of a square as a function of $k_F a$ from numerical calculations (dotted line) at zero field and at a temperature equal to 10 level-spacings. The number of electrons is $N = g_s(k_F a)^2/(4\pi)$. The full line shows our semiclassical approximation (Eq. (5.18)) taking into account only the family (11) of shortest orbits with the temperature correction factor $R_T(L_{11})$. The period $\pi/\sqrt{2}$ of the quantum result indicates the dominance of the shortest periodic orbits enclosing nonzero area with length $L_{11} = 2\sqrt{2}a$. (b) Susceptibility χ as a function of the normalized flux through the sample (at a Fermi energy corresponding to ~ 400 enclosed electrons) from Eq. (5.18) (solid) and numerics (dotted). The susceptibility arising from the stationary-phase integration \mathcal{C}^S (Eq. (5.13)) shown as the dashed line diverges at $\varphi \rightarrow 0$.

of the flux at a given number of electrons in the square. The divergent susceptibility obtained from \mathcal{C}^S (dashed line) provides a good description of $\chi^{(1)}$ for $\varphi \gtrsim 1$.

For a measurement made on an ensemble of squares of different sizes a , $\chi^{(1)}$ vanishes under averaging if the dispersion of $k_F L_{11}$ across the ensemble is larger than 2π . In that case the average susceptibility is given by the contribution to $\Delta F^{(2)}$ arising from the (1,1) family (Eq. (2.20c)). Proceeding in a similar way as for the first-order term, the contribution of the family (1,1) to the integrated density N^{osc} is given by Eq. (2.15b) as

$$N_{11}(\bar{\mu}, H) = -g_s \left(\frac{2^3 a^3}{\pi^3 L_{11}^3} \right)^{1/2} (k_F a)^{1/2} \cos \left(k_F L_{11} + \frac{\pi}{4} \right) \mathcal{C}(H) R_T(L_{11}). \quad (5.19)$$

To calculate $\chi^{(2)}$ we have to consider $\Delta F^{(2)} = (N^{\text{osc}})^2/2\bar{D}$ (with $\bar{D} = (g_s m a^2)/(2\pi\hbar^2)$), and in particular the term

$$\frac{(N_{11}(\bar{\mu}, H))^2}{2\bar{D}} = \frac{g_s \hbar^2}{(\sqrt{2})^3 \pi^2 m a^2} k_F a \cos^2 \left(k_F L_{11} + \frac{\pi}{4} \right) \mathcal{C}^2(\varphi) R_T^2(L_{11}). \quad (5.20)$$

This contribution is of lower order in $k_F a$ than that of $\Delta F_{11}^{(1)}$, but its sign does not change as a function of the phase $k_F L_{11}$. Therefore the squared cosine survives the ensemble average⁹ and we obtain, performing the derivatives with respect to φ (still in the regime $L_c \simeq L_{11}$),

$$\frac{\overline{\chi^{(2)}}}{\chi_L} = -\frac{3}{(\sqrt{2}\pi)^3} k_F a \frac{d^2 \mathcal{C}^2}{d\varphi^2} R_T^2(L_{11}). \quad (5.21)$$

The total averaged susceptibility is therefore

$$\bar{\chi} = -\chi_L + \overline{\chi^{(2)}},$$

since, as seen in Section 3, one has also to include the diamagnetic (bulk) “Landau term” $-\chi_L$ arising from \hbar corrections to F^0 . In the regime $L \simeq L_c$ we are considering here, χ_L is negligible with respect to $\overline{\chi^{(2)}}$ as $\hbar \rightarrow 0$, and one can use $\bar{\chi} \simeq \overline{\chi^{(2)}}$. Note however that when $L_c \ll L$, Eqs. (5.18) and (5.21) remain valid but $\chi^{(1)}$ as well as $\chi^{(2)}$ is exponentially suppressed. In this “trivial” regime χ (and thus $\bar{\chi}$) reduces to the Landau susceptibility, and becomes independent of the underlying classical dynamics. The linear dependence of the average susceptibility on k_F is shown in Fig. 9(a).

Since \mathcal{C} has its absolute maximum at $\varphi = 0$, the average zero-field susceptibility is paramagnetic and attains a maximum value of [57, 59]

$$\overline{\chi^{(2)}}(H=0) = \frac{4\sqrt{2}}{5\pi} k_F a \chi_L R_T^2(L_{11}). \quad (5.22)$$

For small fields the average susceptibility (thin solid line, Fig. 9(b)) has an overall decay as $1/\varphi$ and oscillates in sign on the scale of one flux quantum through the sample. As in the disordered case [34] the period of the field oscillations of the average is half of that of the individual systems (see Fig. 8(b)). In our case the difference can be traced to the \mathcal{C}^2 dependence that appears in Eq. (5.21) in contrast to the simple \mathcal{C} dependence of Eq. (5.18).

For an ensemble with a wide distribution of lengths (as in Ref. [25]) an average $\langle \dots \rangle$ on a classical scale (i.e. $\Delta a/a \ll 1$) rather than on a quantum scale ($\Delta(k_F a) \simeq 2\pi$) needs to be performed, and the dependence of \mathcal{C} on a (through φ) has to be considered. Since the scale of variation of \mathcal{C} with a is much slower than that of $\sin^2(k_F L_{11})$ we can effectively separate the two averages and obtain the total mean by averaging the local mean:

$$\langle \chi \rangle = \int da \bar{\chi} P(a), \quad (5.23)$$

where the quantum average $\bar{\chi}$ is given by Eq. (5.21) and $P(a)$ is the probability distribution of sizes a . Taking for $P(a)$ a Gaussian distribution with a 30% dispersion we obtain the thick solid line of Fig. 9(b). The low-field oscillations with respect to φ are suppressed under the second average, while the zero-field behavior remains unchanged.

⁹ Beside the orbits (1,1) the orbits (1,0) and (0,1) which are even shorter contribute to $\Delta F^{(1)}$ in the limit $L_c \sim L_{11}$. Since they do not enclose any flux the second derivative of $\Delta F_{10}^{(1)}$ with respect to H , i.e. $\chi_{10}^{(1)}$ can be neglected for small fields. However, they enter into $\chi^{(2)}$ by means of the cross-products $(N_{10} + N_{01})N_{11}$ in $(N^{\text{osc}})^2$. Nevertheless, they play no role for the averaged $\overline{\chi^{(2)}}$ because N_{10} and N_{11} do not oscillate with the same frequency and therefore their product averages out.

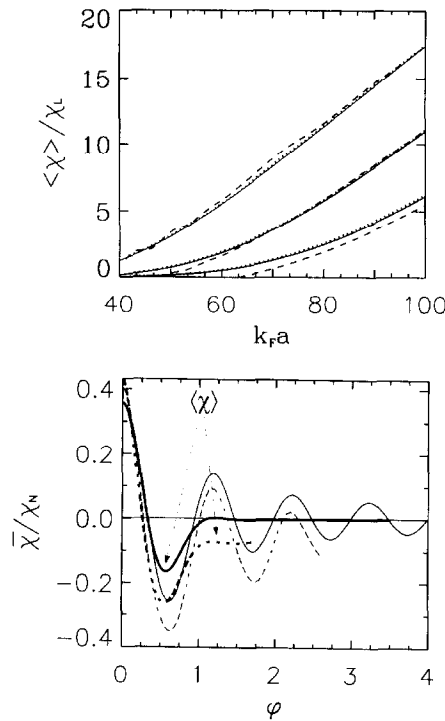


Fig. 9. (a) Average magnetic susceptibility of an ensemble of squares differing in size as a function of $k_F a$ for various temperatures (8, 6 and 4 level spacings for the three triplets of curves from below) and a flux $\varphi = 0.15$. Solid line: average of the semiclassical approximation to $\chi^{(2)}$ according to the analytical result of Eq. (5.21). Dotted line: average of $\chi^{(2)}$ obtained by using Eq. (2.20c) and exact diagonalization. Dashed curve: average of the canonical susceptibility calculated directly from Eq. (5.33) after the exact diagonalization. The considerable agreement between the solid and dotted curves illustrates the precision of the semiclassical approximation, while the agreement between the dotted and dashed lines shows the applicability of the thermodynamical expansion Eq. (2.20). (b) Flux dependence of the averaged susceptibility normalized to $\chi_N = \chi_L k_F a R_+^2(L_{11})$ at $k_F a \simeq 70$ from the semiclassical expression Eq. (5.21) (solid) and numerical calculations (dashed). The thick solid (dashed) curve denotes an average of the semiclassical (numerical) result over an ensemble with a large dispersion of sizes which is denoted by $\langle \chi \rangle$ (see text). The shift of the numerical with respect to the semiclassical results reflects the Landau susceptibility (due to F^0 in Eq. (2.19)) and effects from bouncing-ball orbits (see Section 7.1) not included in the semiclassical trace.

The expected value for the susceptibility measured in an ensemble of n squares is $n \langle \chi \rangle \propto n k_F a$, with a *large* statistical dispersion of $\sqrt{n} \chi^{(1)} \propto \sqrt{n} (k_F a)^{3/2}$. However, for experiments like the one of Ref. [25] where $n \simeq 10^5 \gg k_F a \simeq 10^2$, it is not possible to obtain a diamagnetic response by a statistical fluctuation.

5.3. Contribution of longer orbits

In the zero-temperature limit¹⁰ or more generally if one is interested in results valid at any temperature, it is necessary to take also into account the contribution of longer trajectories. This can be done following exactly the same lines as for the contribution of the family (1,1). From

¹⁰It should be kept in mind however that the expansion in Eq. (2.19) is a priori not valid when $T \rightarrow 0$.

Eqs. (5.15) and (5.16) one obtains the contribution of the family $\mathbf{M} = (M_x, M_y) = (ru_x, ru_y)$, (where u_x and u_y are coprime) to $\Delta F^{(1)}$

$$\Delta F_M^{(1)}(H) = \frac{g_s \hbar^2}{m} \left(\frac{2^3 a}{\pi^3 L_M^5} \right)^{1/2} (k_F a)^{3/2} \sin \left(k_F L_M + \frac{\pi}{4} \right) \mathcal{C}_M(\varphi) R_T(L_M), \quad (5.24)$$

where

$$\mathcal{C}_M(\varphi) = \begin{cases} 1 & u_x \text{ or } u_y \text{ even,} \\ \mathcal{C} \left(\frac{r\varphi}{u_x u_y} \right) & u_x \text{ and } u_y \text{ odd.} \end{cases} \quad (5.25)$$

L_M and the function $\mathcal{C}(\varphi)$ are given respectively by Eqs. (5.3) and (5.11). In order to get $\chi^{(1)}$ we have to take the second derivative of \mathcal{C}_M with respect to the magnetic field. This yields zero if either u_x or u_y is even and a factor $r^2/(u_x u_y)^2$, if both are odd. We therefore obtain

$$\begin{aligned} \frac{\chi^{(1)}}{\chi_L} &= -\frac{3}{\pi^{5/2}} (k_F a)^{3/2} \sum_r \sum_{\substack{u_x, u_y \\ \text{odd}}} \frac{1}{r^{1/2} (u_x^2 + u_y^2)^{5/4} (u_x u_y)^2} \sin \left(k_F L_M + \frac{\pi}{4} \right) \\ &\times \mathcal{C}'' \left(\frac{r\varphi}{u_x u_y} \right) R_T(L_M), \end{aligned} \quad (5.26)$$

valid at any temperature.

The low temperature result for $\chi^{(2)}$ follows in essentially the same way, but taking the average is made rather intricate in the case of a square (as compared for instance to a rectangle) because of the degeneracies in the lengths of the particular orbits of this system. Indeed, there are infinitely many integers which can be decomposed in at least two different ways into sums of two squares. For instance, $11^2 + 7^2 = 13^2 + 1^2 = 170$. As a consequence, $L_{11,7} = L_{13,1}$, and $\overline{N_{11,7} N_{13,1}} \neq 0$. An explicit formula for $\chi^{(2)}$ therefore requires to handle correctly all the non-diagonal terms containing orbits of degenerated lengths which do not average to zero. This leads to a number theoretical problem (i.e. characterizing all numbers which decomposition as the sum of two squares is not unique), with which we do not deal and which moreover will be seen to be of no practical relevance. Therefore, instead of considering a square, we will give the expression for $\chi^{(2)}$ for a rectangle of area a^2 and of horizontal and vertical lengths $a \cdot e$ and $a \cdot e^{-1}$. In that case, all the formulae given in Section 5.1 remain valid. As the only difference one has now

$$L_M = 2a \sqrt{(M_x/e)^2 + (M_y e)^2}$$

instead of Eq. (5.3), which does not give rise to length degeneracies if, as we will suppose, e^4 is irrational. Noting that the prefactor of N_M^2 depends as L_M^{-3} on the length of the orbit (instead of $L_M^{-5/2}$ for $\Delta F_M^{(1)}$), one obtains for the canonical correction to the susceptibility

$$\frac{\chi^{(2)}}{\chi_L} = -\frac{3}{\pi^3} k_F a \sum_r \sum_{\substack{u_x, u_y \\ \text{odd}}} \frac{1}{r ((u_x/e)^2 + (u_y e)^2)^{3/2} (u_x u_y)^2} (\mathcal{C}^2)'' \left(\frac{r\varphi}{u_x u_y} \right) R_T^2(L_M). \quad (5.27)$$

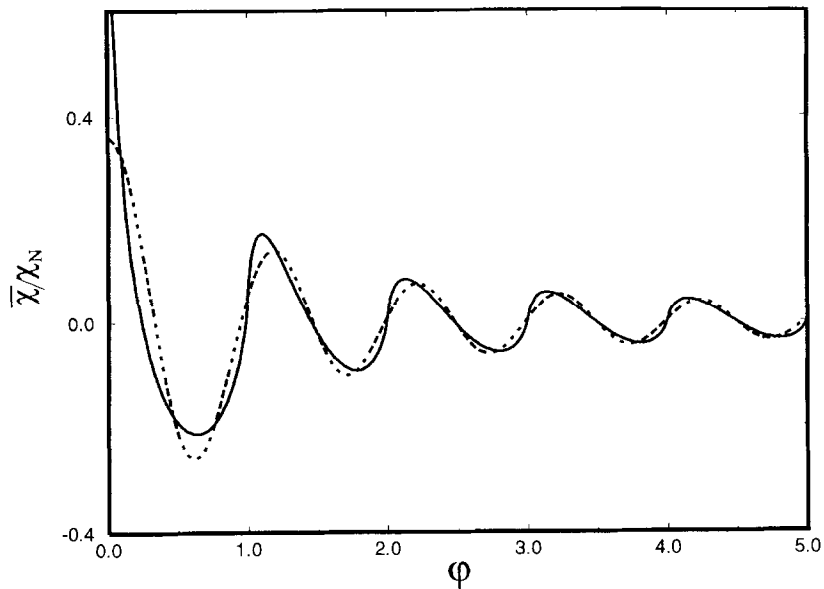


Fig. 10. Solid: low temperature limit of the average susceptibility $\bar{\chi}^{(2)}$ of an ensemble of squares, as given by Eq. (5.27) and normalized by χ_N as defined in the previous figure caption. Dashed: contribution of the family (1,1) to this result. Even in the very low temperature regime the magnetic response is dominated by the (1,1) family except for the singularity which develops at zero magnetic field.

Eqs. (5.26) and (5.27) show that even at zero temperature the strong flux cancellation typical for the square (or rectangular) geometry generates a very small prefactor $1/(r^{1/2}(u_x^2 + u_y^2)^{5/4}(u_x u_y)^2)$ for $\chi^{(1)}$ (square geometry) and $1/(r((u_x/e)^2 + (u_y/e)^2)^{3/2}(u_x u_y)^2)$ for $\chi^{(2)}$ (rectangular geometry). For the second shortest contributing primitive orbit, $\mathbf{M} = (1, 3)$, this yields for instance for $\chi^{(1)}$ a damping of $1/(9 \times 10^{5/4}) \simeq 0.0062$. For $\chi^{(2)}$ the multiplicative factor is even smaller. In practice only the repetitions (r, r) of the family (1,1) will contribute significantly to the susceptibility, and one can use Eqs. (5.26) and (5.27) keeping only the term $u_x = u_y = 1$ of the second summation. As a consequence, all the complications due to the degeneracies in the length of the orbits for the square are of no practical importance (Eq. (5.27) restricted to $u_x = u_y = 1$ can be used for the square with $e = 1$), showing why their detailed treatment was not necessary. As illustrated in Fig. 10 for $\bar{\chi}^{(2)}$, the repetitions of the orbit (1,1) are yielding a diverging susceptibility at zero field when the temperature goes to zero, but barely affect the result even as $T \rightarrow 0$ for finite H , where the contributions of the repetitions do no longer add coherently.

5.4. Numerical calculations

As a check of our semiclassical results we calculated quantum mechanically the orbital susceptibility of spinless particles in a square potential well $[-a/2, a/2]$ in an homogeneous magnetic field. Within the symmetric gauge $\mathbf{A} = H(-y/2, x/2, 0)$ the corresponding Hamiltonian in scaled units

$\tilde{x} = x/a$ and $\tilde{E} = (ma^2/\hbar^2)E$ reads

$$\tilde{\mathcal{H}} = -\frac{1}{2} \left(\frac{\partial^2}{\partial \tilde{x}^2} + \frac{\partial^2}{\partial \tilde{y}^2} \right) - i\pi \varphi \left(\tilde{y} \frac{\partial}{\partial \tilde{x}} - \tilde{x} \frac{\partial}{\partial \tilde{y}} \right) + \frac{\pi^2}{2} \varphi^2 (\tilde{x}^2 + \tilde{y}^2), \quad (5.28)$$

with the normalized flux φ defined as in Eq. (5.12). Taking into account the invariance of the Hamiltonian (5.28) with respect to rotations by $\pi, \pi/2$ we use linear combinations of plane-waves which are eigenfunctions of the parity operators $\mathbf{P}_\pi, \mathbf{P}_{\pi/2}$, respectively. Omitting the tilde in order to simplify the notation, they read

$$\sqrt{2}[S_n(x)C_m(y) \pm iC_m(x)S_n(y)]; \quad (P_\pi = -1), \quad (5.29)$$

$$\begin{aligned} \sqrt{2}[C_n(x)C_m(y) \pm C_m(x)C_n(y)], \\ \sqrt{2}i[S_n(x)S_m(y) \pm S_m(x)S_n(y)], \end{aligned} \quad (P_\pi = +1) \quad (5.30)$$

with $S_n(u) = \sin(n\pi u)$, n even, and $C_m(u) = \cos(m\pi u)$, m odd, obeying Dirichlet boundary conditions. In this representation the resulting matrix equation is real symmetric and decomposes into four blocks representing the different symmetry classes. By diagonalization we calculated the first 3000 eigenenergies taking into account up to 2500 basis functions for each symmetry class. A typical energy level diagram of the symmetry class $(P_\pi, P_{\pi/2}) = (1, 1)$ as a function of the magnetic field is shown in Fig. 1(a). In between the two separable limiting cases $\varphi = 0$ and $\varphi \rightarrow \infty$ the spectrum exhibits a complex structure typical for a nonintegrable system which classical dynamics is at least partly chaotic.

We calculate numerically the *grand-canonical* susceptibility (Eq. (1.2), Fig. 1(b)) from

$$\chi^{\text{GC}}(\mu) = -\frac{\mathbf{g}_s}{a^2} \frac{\partial^2}{\partial H^2} \sum_{i=1}^{\infty} \frac{\varepsilon_i}{1 + \exp[\beta(\varepsilon_i - \mu)]} \quad (5.31)$$

where \mathbf{g}_s accounts for the spin degeneracy and ε_i denotes the single particle energies.

However, in order to address the experiment of Ref. [25] and to compare with the semiclassical approach of the preceding subsection we have to work in the canonical ensemble. At $T = 0$ the free energy F reduces to the total energy and the canonical susceptibility (Eq. (2.2)) is given as the sum

$$\chi(T = 0) = -\frac{\mathbf{g}_s}{a^2} \sum_{i=1}^N \frac{\partial^2 \varepsilon_i}{\partial H^2} \quad (5.32)$$

over the curvatures of the N single-particle energies ε_i . The susceptibility is therefore dominated by large paramagnetic singularities each time the highest occupied state undergoes a level crossing with a state of a different symmetry class or a narrow avoided crossing with a state of the same symmetry. This makes $T = 0$ susceptibility spectra of quasi-integrable billiards (with nearly exact level crossings) or systems with spectra composed of energy levels from different symmetry classes (as it is the case for the square) looking much more erratic than those of chaotic systems with stronger level repulsion [27].

The $T = 0$ peaks are compensated once the next higher state at a (quasi) crossing is considered, and therefore disappear at finite temperature when the occupation of nearly degenerated states be-

comes almost the same. Thus finite temperature regularizes the singular behavior of χ at $T = 0$ and of course describes the physical situation. We obtain the canonical susceptibility at finite T from

$$\chi = \frac{g_s}{a^2 \beta} \frac{\partial^2}{\partial H^2} \ln Z_N(\beta). \quad (5.33)$$

The canonical partition function $Z_N(\beta)$ is given by

$$Z_N(\beta) = \sum_{\{\alpha\}} \exp[-\beta E_\alpha(N)] \quad (5.34)$$

with

$$E_\alpha(N) = \sum_{i=1}^{\infty} \varepsilon_i n_i^\alpha, \quad N = \sum_{i=1}^{\infty} n_i^\alpha. \quad (5.35)$$

The $n_i^\alpha \in \{0, 1\}$ describe the occupation of the single-particle energy levels. A direct numerical computation of the canonical partition function becomes extremely time consuming at finite temperature. We approximate the sum in Eq. (5.34) which runs over all (infinitely many) occupation distributions $\{\alpha\}$ for N electrons by a finite sum $Z_N(M; \beta)$ over all possibilities to distribute N particles over the first M levels with $M \geq N$ sufficiently large. Following Brack et al. [69] we calculate $Z_N(M; \beta)$ recursively using

$$Z_N(M; \beta) = Z_N(M-1; \beta) + Z_{N-1}(M-1; \beta) \exp(-\beta \varepsilon_M) \quad (5.36)$$

with initial conditions

$$Z_0(M; \beta) \equiv 1, \quad Z_N(N-1; \beta) \equiv 0 \quad (5.37)$$

and increase M until convergence of $Z_N(M, \beta)$, i.e. the difference between $Z_N(M; \beta)$ and $Z_N(M-1; \beta)$ is negligible. This recursive algorithm reduces the number of algebraic operations to calculate Z_N drastically and is fast and accurate even if $k_B T$ is of the order of 10 or 20 times the mean level spacing, i.e. in a regime where a direct calculation of Z_N is not feasible.

5.5. Comparison between numerical and semiclassical results

Our numerical results for the susceptibility of individual and ensembles of squares are displayed as the dashed lines in Figs. 8 and 9 and are in excellent agreement with the semiclassical predictions of Section 5.2. Fig. 8(a) shows the numerical result for the canonical susceptibility and the semiclassical leading order contribution $\chi_{11}^{(1)}$ at zero field as a function of $k_F a$ ($\sqrt{4\pi N/g_s}$ in terms of the number of electrons). The temperature $k_B T$ is equal to five times the mean level spacing Δ of the single-particle spectrum. The quantum result oscillates with a period $\pi/\sqrt{2}$ as semiclassically expected (Eq. (5.18)) indicating the dominant effect of the fundamental orbits of length $L_{11} = 2\sqrt{2}a$. The semiclassical amplitudes (solid line) are slightly smaller than the numerics because only the shortest orbits are included.

Fig. 8(b) shows the flux dependence of χ for a fixed number of electrons $N \approx 1100g_s$. The semiclassical prediction (Eq. (5.18), solid curve) is again in considerable agreement with the quantum

result while the analytical result (Eq. (5.13), dashed line) from stationary phase integration yields an (unphysical) divergence for $\varphi \rightarrow 0$ as discussed in Section 5.2.

For the numerical calculations we can perform the ensemble average directly and we obtain the averages on the quantum scale (thin dashed line, Fig. 9(b)) or classical scale (thick dashed line) by taking a Gaussian distribution of sizes with respectively a small or large $\Delta a/a$ dispersion. Fig. 9(a) depicts the $k_F a$ dependence of $\bar{\chi}$ assuming a Gaussian distribution of lengths a with a standard deviation $\Delta a/a \approx 0.1$ for each of the three temperatures $k_B T/\Delta = 2, 3, 5$. The dashed curves are the ensemble averages of the quantum mechanically calculated *entire* canonical susceptibility $\bar{\chi}$. The dotted lines are the *exact* (numerical) results for the averaged term $\overline{\chi_{\text{qm}}^{(2)}} = (\overline{N_{\text{qm}}^{\text{osc}}})^2/2\Delta$. They are nearly indistinguishable (on the scale of the figure) from the *semiclassical* approximation of Eq. (5.21) (solid line). Although a small flux $\varphi \approx 0.15$ has been chosen (here the contribution from the next longer orbits (2,2) nearly vanishes) the precision of the semiclassical approximation based on the fundamental orbits (1,1) is striking. The difference between the results for $\bar{\chi}$ and $\overline{\chi^{(2)}}$ gives an estimate for the precision of the thermodynamic expansion Eq. (2.19). The convoluted semiclassical result has been shifted additionally by $-\chi_L$ to account for the diamagnetic Landau contribution and is again in close agreement with the numerical result of the averaged susceptibility $\bar{\chi}$.

5.6. Comparison with the experiment

In a recent experiment, Lévy et al. [25] measured the magnetic response of an *ensemble* of 10^5 microscopic billiards of square geometry lithographically defined on a high mobility GaAs heterojunction. The size of the squares is on average $a = 4.5 \mu\text{m}$, but has a large variation (estimated between 10% and 30%) between the center and the border of the array. Each square can be considered as phase-coherent and ballistic since the phase-coherence length and elastic mean free path are estimated, respectively, to be between 15 and 40 μm and between 5 and 10 μm .

Therefore, it is worthwhile to compare the observed magnetic response with the prediction of our clean model of noninteracting electrons, to see whether this simple picture contains the main physical input to understand the experimental observations, although one should control in addition that the residual impurities do not alter fundamentally the magnetic response of the system. This is the subject of a forthcoming article [43]. Ongoing calculations including (weak) disorder indeed indicate that the underlying physical picture remains correct.

At a qualitative level, a large paramagnetic peak at zero field has been observed in Ref. [25], two orders of magnitude larger than the Landau susceptibility, decreasing on a scale of approximately one flux quantum through each square. Since there is a large dispersion of sizes we do not observe the field oscillations of the quantum average (5.21), but the comparison has to be established with the classical average results Eq. (5.23). The corresponding results from our semiclassical calculations (Eqs. (5.21) and (5.23)) and the full quantum calculations are shown in Fig. 9(b) as the thick full, respectively dashed, lines (denoted by $\langle\chi\rangle$ in the figure). The offset in the semiclassical curve with respect to the quantum mechanical curve is due to the Landau susceptibility χ_L and additional effects from bouncing-ball orbits (see Section 7.1) not included in the semiclassical trace. Our theoretical results for the flux dependence of the average $\langle\chi\rangle$ with respect to a wide distribution in the size of the squares agree on the whole with the experiment. However, the diamagnetic response for $\langle\chi\rangle$ that we obtain for $\varphi \approx 0.5$ is not observed experimentally, indicating that there may be a more

important size dispersion than estimated. As will be discussed in more detail in Section 6, a very large distribution of lengths enhances the effect of the breaking of time reversal invariance due to the magnetic field, yielding a vanishing average response at *finite field* and a paramagnetic susceptibility at *zero field* decaying on a field scale Φ_0 by the dephasing of the contribution of time-reversal symmetric orbits to the density of states.

More quantitatively, the experiment of Ref. [25] yielded a paramagnetic susceptibility at $H = 0$ with a value of approximately 100 (with an uncertainty of a factor of 4) in units of χ_L . The two electron densities considered in the experiment are 10^{11} and 3×10^{11} corresponding to approximately 10^4 occupied levels per square. Therefore our semiclassical approximation is well justified. For a temperature of 40 mK the factor $4\sqrt{2}/(5\pi)k_F a R_7^2(L_{11})$ from Eq. (5.22) gives zero-field susceptibility values of 60 and 170, respectively, in reasonable agreement with the measurements. In order to attempt a more detailed comparison with the measurements we need to incorporate the suppression of the clean susceptibility by the residual disorder, which depends on the strength and correlation length of the impurity potential [43]. The field scale for the decrease of $\langle \chi(\varphi) \rangle$ is of the order of one flux quantum through each square, in agreement with our theoretical findings. The temperature dependence experimentally observed seems however less drastic than the theoretical prediction.

6. Generic integrable and chaotic systems

In Sections 4 and 5 we have studied in detail specific geometries of conceptual as well as experimental relevance. In particular, we have demonstrated the degree of accuracy of our semiclassical approach by a careful comparison with exact quantum results. The aim of the present section is to take a broader point of view and to give more general semiclassical implications concerning the magnetic properties of ballistic quantum dots. We shall first consider the weak-field behavior of generic integrable systems, generalizing the results of the previous section. We focus on weak fields because only this regime is affected by the integrability of the dynamics at zero field. The case of systems which remain integrable at arbitrary field strength was discussed in Section 4. In the second stage we shall turn to chaotic systems (at weak as well as finite fields) and finally finish the section by discussing the similarity and differences of the magnetic response for the various cases of classical stability.

6.1. Generic integrable systems

We consider the generic magnetic response of two-dimensional integrable systems perturbed by a weak magnetic field breaking the integrability. Eqs. (2.15) and (2.20), which relate the thermodynamic functions $\Delta F^{(1)}$ and $\Delta F^{(2)}$ to the oscillating part $d^{\text{osc}}(E)$ of the density of states, are general relations which apply in particular here. The main difficulty is therefore to obtain semiclassical uniform approximations for $d^{\text{osc}}(E)$ interpolating between the zero-field regime, for which the Berry–Tabor Formula [52,53] (suitable for integrable systems) applies, and higher fields (still classically perturbative however), for which the periodic orbits which have survived under the perturbation are sufficiently well isolated in order to use the Gutzwiller trace formula [51]. This problem of computing for a generic system the oscillating part of the density of states in the nearly but not exactly integrable regime has been addressed by Ozorio de Almeida [55,56]. We are going to follow this

approach for the case of a perturbation by a magnetic field. However, for the sake of completeness and in order to define their regime of validity, we will give a brief derivation of the basic results needed. This is the subject of Section 6.1.1. In Section 6.1.2 we then deduce the grand-canonical and canonical contributions to the susceptibility.

6.1.1. Perturbation theory for magnetic fields

Let $\hat{\mathcal{H}}(\hat{\mathbf{p}}, \hat{\mathbf{q}})$ be a quantum Hamiltonian which classical analog can be expressed as

$$\mathcal{H}(\mathbf{p}, \mathbf{q}) = \mathcal{H}^0 \left(\mathbf{p} - \frac{e}{c} \mathbf{A}, \mathbf{q} \right). \quad (6.1)$$

$\mathcal{H}^0(\mathbf{p}, \mathbf{q})$ is the Hamiltonian describing the motion in the absence of a magnetic field and \mathbf{A} is the vector potential generating a uniform magnetic field H . \mathcal{H}^0 is supposed to be integrable which permits to define action-angle coordinates $(\mathbf{I}, \boldsymbol{\varphi})$, $\varphi_1, \varphi_2 \in [0, 2\pi]$ such that at zero field the Hamiltonian $\mathcal{H}^0(I_1, I_2)$ depends only on the actions.

To compute $d^{\text{osc}}(E)$ we start from the same basic equations as for the square geometry. In the weak-field regime which we are considering, the only recurrent trajectories of the sum Eq. (5.2) which contribute noticeably to the trace Eq. (5.1) are those which merge into periodic orbits of the unperturbed Hamiltonian as $H \rightarrow 0$. Considering only these contributions, which we can label by the topology \mathbf{M} of the unperturbed periodic orbits, and dropping the Weyl part of the trace $\mathcal{G}(E)$ of the Green function we can write

$$\mathcal{G}(E) \simeq \sum_{\mathbf{M}} \mathcal{G}_{\mathbf{M}}, \quad \mathcal{G}_{\mathbf{M}}(E) = \frac{1}{i\hbar} \frac{1}{\sqrt{2i\pi\hbar}} \int dq_1 dq_2 D_{\mathbf{M}} \exp \left[\frac{i}{\hbar} S_{\mathbf{M}} - i\eta_{\mathbf{M}} \frac{\pi}{2} \right]. \quad (6.2)$$

Let us now focus on the contribution $\mathcal{G}_{\mathbf{M}}$ of the family of closed orbits \mathbf{M} . For sufficiently low fields we will employ (as in Sections 4 and 5) that the change in the semiclassical Green function by changing H is essentially given by the modification of the phase, $S_{\mathbf{M}}/\hbar$ being large in the semiclassical limit. The variation in the determinant $D_{\mathbf{M}}$ can usually be neglected. Therefore, in the evaluation of the integral in Eq. (6.2) one should keep the (unperturbed) zeroth order approximation for $D_{\mathbf{M}}$ and evaluate the action up to the first-order correction. For the action this yields

$$S_{\mathbf{M}}(\mathbf{q}, \mathbf{q}) = S_{\mathbf{M}}^0 + \delta S_{\mathbf{M}}(\mathbf{q}, \mathbf{q}) \quad (6.3)$$

with

$$S_{\mathbf{M}}^0 = \oint_{\text{orbit}} \mathbf{p} \cdot d\mathbf{q} = \oint_{\text{orbit}} \mathbf{I} \cdot d\boldsymbol{\varphi} = 2\pi \mathbf{I}_{\mathbf{M}} \cdot \mathbf{M}, \quad (6.4)$$

noting $\mathbf{I}_{\mathbf{M}}$ the action coordinates of the periodic orbit family \mathbf{M} at $H = 0$. The contribution $\delta S_{\mathbf{M}}$ is expressed in terms of the area enclosed by the *unperturbed* orbit by means of Eq. (4.7). $S_{\mathbf{M}}^0$ is constant for all members of the family, but δS generically depends on the trajectory on which the point \mathbf{q} lies. However, the area enclosed by the orbit and thus $\delta S_{\mathbf{M}}$ does not change when varying \mathbf{q} along the orbits. It is therefore convenient to use a coordinate system such that one coordinate is constant along the unperturbed trajectory. Writing $\mathbf{M} = (ru_1, ru_2)$ where u_1 and u_2 are coprime integers, this is provided explicitly by the standard canonical transformation $(\mathbf{I}, \boldsymbol{\varphi}) \rightarrow (\mathbf{J}, \boldsymbol{\theta})$ generated

by $F_2(\mathbf{J}, \boldsymbol{\varphi}) = (u_2\varphi_1 - u_1\varphi_2)J_1 + \varphi_2J_2$:

$$\begin{aligned} \theta_1 &= u_2\varphi_1 - u_1\varphi_2, & J_1 &= I_1/u_2, \\ \theta_2 &= \varphi_2, & J_2 &= I_2 + (u_1/u_2)I_1, \end{aligned} \quad (6.5)$$

for which θ_1 is constant along a trajectory on the torus \mathbf{I}_M . Then θ_1 specifies the trajectory and θ_2 the position on the trajectory. For a square geometry, θ_1 and θ_2 are up to a dilatation, respectively, the variables x_0 and s introduced in Section 5. θ_2 should be taken in the range $[0, 2\pi u_2]$ (rather than $[0, 2\pi]$) to ensure that the transformation Eq. (6.5) constitutes a one to one correspondence.

After substituting \mathbf{q} by $\boldsymbol{\theta}$ in the integral of Eq. (6.2), δS depends only on θ_1 , but no longer on θ_2 . One can moreover show (see Appendix D) the following relation for the zero field approximation of the determinant D_M :

$$D_M \cdot \left| \left(\frac{\partial \mathbf{q}}{\partial \boldsymbol{\theta}} \right) \right| = \frac{1}{\theta_2} \frac{1}{|2\pi r u_2^3 g_E''|^{1/2}}, \quad (6.6)$$

where $I_2 = g_E(I_1)$ is the function introduced in Section 4 to describe the energy surface E . From Eq. (6.2) and (6.6) one gets

$$\mathcal{G}_M(E) = \frac{1}{i\hbar} \frac{1}{\sqrt{2i\pi\hbar}} \frac{1}{|2\pi r u_2^3 g_E''|^{1/2}} \exp \left[\frac{i}{\hbar} S_M^0 - i\eta_M \frac{\pi}{2} \right] \int_0^{2\pi u_2} \frac{d\theta_2}{\theta_2} \int_0^{2\pi} d\theta_1 \exp \left[\frac{i}{\hbar} \delta S(\theta_1) \right]. \quad (6.7)$$

The integral over θ_2 is the period τ_M/r of the primitive periodic orbit. In the absence of a field the integral over θ_1 is simply 2π which gives

$$\mathcal{G}_M^0(E) = -\frac{i\tau_M}{\hbar^{3/2} M_2^{3/2} |g_E''|^{1/2}} \exp i \left[\frac{S_M^0}{\hbar} - \eta_M \frac{\pi}{2} - \frac{\pi}{4} \right]. \quad (6.8)$$

$d_M^0(E)$, the zero-field contribution of the orbits of topology \mathbf{M} to the oscillating part of the density of states, is obtained from Eq. (6.8) as $d_M^0(E) = -(\mathbf{g}_s/\pi) \text{Im} \mathcal{G}_M^0(E)$. Therefore, except for the evaluation of the Maslov indices that we have disregarded here, one recovers in this way for the integrable limit the Berry–Tabor formula Eq. (4.3) of a two-dimensional system (as we have used in Section 4).

Inspection of Eq. (6.7) for weak magnetic fields shows that, upon perturbation, \mathcal{G}_M is just given by the product of the unperturbed result \mathcal{G}_M^0 and a factor

$$\tilde{\mathcal{C}}_M(H) = \frac{1}{2\pi} \int_0^{2\pi} d\theta_1 \exp [2i\pi H \mathcal{A}_M(\theta_1)/\Phi_0]. \quad (6.9)$$

This accounts for the small dephasing between different closed (in configuration space) orbits of topology \mathbf{M} due to the fact that the resonant torus on which they are living is slightly broken by the perturbation. (An orbit of topology \mathbf{M} closed in configuration space is then generally not periodic, i.e. closed in phase space.) Supposing the unperturbed motion to be time reversal invariant, it can be seen moreover that only the real part of $\tilde{\mathcal{C}}_M(H)$ has to be considered: The function $\mathcal{A}_M(\theta_1)$ is defined for the unperturbed system. Therefore, the time reversed of a trajectory labeled by θ_1 is a periodic orbit of the unperturbed system which encloses an area $-\mathcal{A}_M(\theta_1)$. Its contribution cancels

the imaginary part of $\exp[2i\pi H \mathcal{A}_M(\theta_1)/\Phi_0]$, and one can use

$$\mathcal{C}_M(H) = \frac{1}{2\pi} \int_0^{2\pi} d\theta_1 \cos[2\pi H \mathcal{A}_M(\theta_1)/\Phi_0] \quad (6.10)$$

instead of $\tilde{\mathcal{C}}_M(H)$. Since $\mathcal{C}_M(H)$ is real, one obtains from Eq. (5.1)

$$d^{\text{osc}}(E) = \sum_{M \neq 0} \mathcal{C}_M(H) d_M^0(E), \quad (6.11)$$

where $d_M^0(E)$ is the zero-field contribution given by the Berry–Tabor expression of Eq. (4.3). At zero field we obviously have $\mathcal{C}_M(0) = 1$. At sufficiently large field, the integral (6.9) can be evaluated using stationary phase approximation.¹¹ \mathcal{C}_M can be expressed as a sum over all extrema of $\mathcal{A}_M(\theta_1)$ (i.e. of δS). These are all the periodic orbits which survive under the perturbation. It can be seen [70] that, in this approximation, Eq. (6.11) yields exactly the Gutzwiller trace formula for which the actions, periods and stabilities of the periodic orbits are evaluated using classical perturbation theory. Eq. (6.11) thus provides an interpolation between the Berry–Tabor and Gutzwiller formulae.

The functions $\mathcal{A}_M(\theta_1)$, and therefore $\mathcal{C}_M(H)$, are system and trajectory dependent. One can, however, gain some further understanding of the perturbative regime by following again Ozorio de Almeida and writing $\mathcal{A}_M(\theta_1)$ in term of its Fourier series

$$\mathcal{A}_M = \sum_{n=0}^{\infty} \mathcal{A}_M^{(n)} \sin(n\theta_1 - \gamma^{(n)}). \quad (6.12)$$

If \mathcal{A}_M is a smooth function of θ_1 , the coefficients $\mathcal{A}_M^{(n)}$ are usually rapidly decaying functions of n . For systems where one can neglect all harmonics higher than the first one, the integral Eq. (6.10) can be performed, and it is possible to distinguish two types of functions $\mathcal{C}_M(H)$, depending on the symmetry properties of the unperturbed family of orbits under time reversal.

Indeed, one may encounter two different situations depending on whether the torus I_M is time-reversal invariant (e.g. square geometry) or has a distinct partner I_M^* in phase space which is its counterpart under time reversal (e.g. circular geometry). In the former case, the origin of the angles θ_1 can be chosen such that $\mathcal{A}_M(\theta_1)$ is an antisymmetric function, while in the latter case it can be in principle any real function of θ_1 .¹²

If I_M is time-reversal invariant, $\mathcal{A}_M(-\theta_1) = -\mathcal{A}_M(\theta_1)$ implies that $\mathcal{A}_M^{(0)} = 0$ (as well as all the phases $\gamma^{(n)}$). In this case

$$\mathcal{C}(H) \simeq J_0(2\pi H \mathcal{A}_M^{(1)}/\Phi_0). \quad (6.13)$$

It is interesting to compare the approximation of $\mathcal{C}(H)$ given by the above Bessel function with the exact integral Eq. (5.11) obtained in Section 5 for the shortest family ($M = (1, 1)$) of the square

¹¹ To be precise the ratio HA/Φ_0 rather than the field must be large. Formally, one has to consider not the $H \rightarrow \infty$ limit, which is incompatible with the classical perturbation scheme, but an \hbar (i.e. Φ_0) $\rightarrow 0$ limiting process, which does not change the classical mechanics. In practice this means that the fluxes considered are large on a quantum scale, but still small on the classical scale. This is achieved at high enough energies.

¹² Note in the former case $\tilde{\mathcal{C}}_M = \mathcal{C}_M$, while in the latter $\tilde{\mathcal{C}}_M \neq \mathcal{C}_M$ but $\mathcal{G}_M + \mathcal{G}_{M^*} = \mathcal{G}_M^0 \mathcal{C}_M(H) + \mathcal{G}_{M^*}^0 \mathcal{C}_{M^*}(H)$.

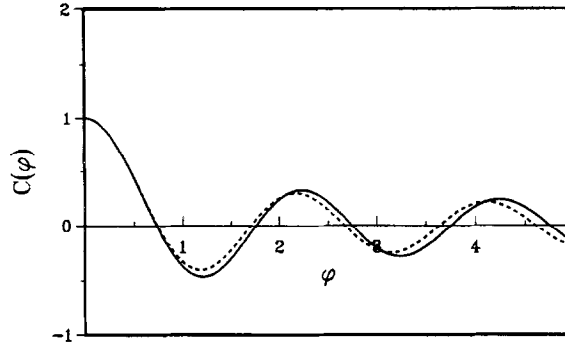


Fig. 11. Solid: exact (Fresnel) function $\mathcal{C}(\varphi)$ as given by Eq. (5.11). Dashed: approximation of $\mathcal{C}(\varphi)$ by the Bessel function $J_0(32\varphi/\pi^2)$ (see text).

geometry. Noting that $\theta_1 = \varepsilon\pi x_0/a$ and using Eq. (5.7), the Fourier coefficients $\mathcal{A}_{11}^{(n)}$ of $\mathcal{A}_{11}(\theta_1)$ are given by

$$\mathcal{A}_{11}^{(n)} = \begin{cases} \frac{16}{(n\pi)^3} a^2 & n \text{ odd}, \\ 0 & n \text{ even}. \end{cases} \quad (6.14)$$

Keeping only the first harmonic of $\mathcal{A}_{11}(\theta_1)$ amounts to approximate the function $\mathcal{C}(\varphi)$ of Eq. (5.11) by $J_0(32\varphi/\pi^2)$ which, as seen in Fig. 11, is an excellent approximation.

If the torus I_M is not its own time reversal, $\mathcal{A}_M(\theta_1)$ is not constrained to be an antisymmetric function, and in particular $\mathcal{A}_M^{(0)}$ is usually nonzero. Neglecting, as above, all harmonics of $\mathcal{A}_M(\theta_1)$ except the first gives

$$\mathcal{C}_M(H) = \cos\left(2\pi \frac{H \mathcal{A}_M^{(0)}}{\Phi_0}\right) J_0\left(2\pi \frac{H \mathcal{A}_M^{(1)}}{\Phi_0}\right). \quad (6.15)$$

If moreover $\mathcal{A}_M^{(1)} \ll \mathcal{A}_M^{(0)}$, then the field oscillation frequency is essentially given by the mean area $\mathcal{A}_M^{(0)}$ enclosed by the orbits of the family while the overall decrease is determined by the first harmonic coefficient $\mathcal{A}_M^{(1)}$. The circular billiard can be regarded as a particular case where $\mathcal{A}_M^{(0)}$ is nonzero while $\mathcal{A}_M^{(1)}$ as well as all other coefficients vanish.

6.1.2. Magnetic susceptibility for a generic integrable system

From the expression (6.11) of the oscillating part of the density of states the contributions $\chi^{(1)}$ and $\chi^{(2)}$ to the susceptibility are obtained by the application of Eqs. (2.15a) and (2.20a), which express $\Delta F^{(1)}$ and $\Delta F^{(2)}$ in terms of $d^{\text{osc}}(E, H)$. Taking twice the field derivative according to Eq. (2.2) and introducing the dimensionless quantities

$$\mathcal{C}_M''(H) \equiv \left(\frac{\Phi_0}{2\pi A}\right)^2 \frac{d^2 \mathcal{C}_M}{dH^2}; \quad (\mathcal{C}^2)_M''(H) \equiv \left(\frac{\Phi_0}{2\pi A}\right)^2 \frac{d^2 \mathcal{C}_M^2}{dH^2},$$

(A is the total area of the system) one obtains for the grand canonical contribution to the susceptibility

$$\frac{\chi^{(1)}}{\chi_L} = -24\pi mA \sum_M \frac{R_T(\tau_M)}{\tau_M^2} \frac{d_M^0(\mu)}{g_s} \mathcal{C}_M''(H). \quad (6.16)$$

If one assumes moreover that there are no degeneracies in the length of the orbits, one has for the averaged canonical correction

$$\begin{aligned} \overline{\chi^{(2)}}_{\chi L} &= -24\pi^2 \hbar^2 \sum_M \frac{R_T^2(\tau_M)}{\tau_M^2} \frac{\overline{(d_M^0(E))^2}}{\mathbf{g}_s^2} (\mathcal{C}^2)''_M(H) \\ &= -\frac{12}{\hbar} \sum_M \frac{R_T^2(\tau_M)}{M_2^3 |g''_{\mu}(\mathbf{I}_M)|} (\mathcal{C}^2)''_M(H). \end{aligned} \quad (6.17)$$

The field-dependent component of $\overline{\chi^{(2)}}$ for weak fields is given by

$$(\mathcal{C}^2)''_M(H=0) = -\frac{1}{2\pi A^2} \int_0^{2\pi} d\theta_1 A_M^2(\theta_1),$$

which is always negative. Therefore, for an ensemble of integrable structures the magnetic response is always paramagnetic at zero field. We shall come back to this point in the last part of this section.

6.2. Generic chaotic systems

Let us now consider generic chaotic systems, more generally, systems where all the periodic orbits are sufficiently isolated that the trace of the semiclassical Green function Eq. (5.1) can be evaluated within stationary phase approximation. In this case the Gutzwiller trace formula provides the appropriate path to calculate the oscillating part of the density of states (with or without magnetic field). The Gutzwiller trace formula expresses the oscillating part of the density of states as a sum over all (here isolated) periodic orbits t as [21]

$$d^{\text{osc}}(E, H) = \sum_t d_t; \quad d_t(E, H) = \frac{1}{\pi \hbar} \frac{\tau_t}{r_t |\det(M_t - I)|^{1/2}} \cos\left(\frac{S_t}{\hbar} - \sigma_t \frac{\pi}{2}\right). \quad (6.18)$$

S_t is the action along the orbit t , τ_t the period of the orbit, M_t the stability matrix, σ_t its Maslov index, and r_t the number of repetitions of the full trajectory along the primitive orbit. All these classical quantities generally depend on energy and magnetic field. If, as considered above for the integrable case, one is interested in the magnetic response to weak field, one can express $d_t(E, H)$ in terms of the characteristics of the orbits at zero field by taking into account the field dependence only in the actions. Proceeding in exactly the same way as in Section 4.1, i.e. grouping together the contributions of time-reverse symmetrical orbits, one obtains the same relation as Eq. (4.9) [50, 61]:

$$d_t(E, H) = d_t^0 \cos[2\pi(H \mathcal{A}_t^0 / \Phi_0)]. \quad (6.19)$$

d_t^0 is the zero-field contribution of the orbit, obtained from Eq. (6.18) at $H = 0$, and \mathcal{A}_t^0 is the enclosed area of the *unperturbed* orbit. In the case of a generic integrable system, the zero-field regime played a peculiar role: except for the circular and annular geometries which remain integrable at all fields, a generic integrable system loses its integrability under the effect of a perturbing magnetic field. For chaotic geometries on the contrary, the zero field behavior is not substantially different from that at finite fields (as far as the stability of the dynamics is concerned). Since we are discussing the general semiclassical formalism of chaotic systems without referring to specific examples we do not need to restrict ourselves to weak fields. Within this generic framework

the chaotic geometries have the same conceptual simplicity as the systems which remain integrable at arbitrary field studied in Section 6. Namely Eq. (6.18) applies independently of the field, and for derivatives with respect to the field one can use

$$\frac{\partial S_t(H)}{\partial H} = \frac{e}{c} \mathcal{A}_t(H), \tag{6.20}$$

where $\mathcal{A}_t(H)$ is the area enclosed by the trajectory t at the considered field. Therefore the computation of the contribution $\chi^{(1)}$ and $\chi^{(2)}$ to the susceptibility follows essentially along the same lines as described in Section 4: $\Delta F^{(1)}$ and $\Delta F^{(2)}$ are given by Eqs. (2.15a) and (2.20a), and to leading order in \hbar the derivatives with respect to the field should be applied only to the rapidly varying term. As a consequence, taking twice the derivative of the contribution of the orbit t to $\Delta F^{(1)}$ merely amounts to a multiplication by a factor $(e\mathcal{A}_t)^2/(c\hbar)^2$, yielding

$$\frac{\chi^{(1)}}{\chi_L} = 24\pi mA \sum_t \frac{R_T(\tau_t)}{\tau_t^2} \left(\frac{\mathcal{A}_t}{A}\right)^2 \frac{d_t(\mu)}{\mathbf{g}_s}, \tag{6.21}$$

where d_t is given by Eq. (6.18). Note that Eq. (6.21) applies also to systems which remain integrable at all fields provided the Berry–Tabor formula Eq. (4.3) is used instead of the Gutzwiller one. For chaotic as well as for integrable systems, $\chi^{(1)}$ can be paramagnetic or diamagnetic with equal probability. The response of an ensemble of structures is given by $\Delta F^{(2)}$, which can be calculated as a double sum over all pairs of orbits

$$\begin{aligned} \frac{\chi^{(2)}}{\chi_L} = 24 \sum_{t,t'} \frac{R_T(\tau_t)R_T(\tau_{t'})}{r_t r_{t'} |\det(M_t - I) \det(M_{t'} - I)|^{1/2}} & \left[\left(\frac{\mathcal{A}_t - \mathcal{A}_{t'}}{A}\right)^2 \cos\left(\frac{S_t - S_{t'}}{\hbar} - (\sigma_t - \sigma_{t'})\frac{\pi}{2}\right) \right. \\ & \left. - \left(\frac{\mathcal{A}_t + \mathcal{A}_{t'}}{A}\right)^2 \cos\left(\frac{S_t + S_{t'}}{\hbar} - (\sigma_t + \sigma_{t'})\frac{\pi}{2}\right) \right]. \end{aligned} \tag{6.22}$$

Here some remarks are in order. Due to the exponential proliferation of closed orbits in chaotic systems off-diagonal terms should be considered at low temperatures since near-degeneracies in the actions of long orbits may appear, so that their contributions do not average out. However, at sufficiently high temperatures where only short periodic orbits are relevant, off-diagonal terms (of orbits not related by time-reversal symmetry) are eliminated upon averaging. At finite field where time-reversal symmetry is broken (more precisely, when no anti-unitary symmetry is preserved) only the terms with $t' = t$ survive the averaging process, and (at the order of \hbar considered) $\overline{\chi^{(2)}}$ vanishes since then $\mathcal{A}_t = \mathcal{A}_{t'}$. The origin of the weak-field response for an ensemble is a consequence of time-reversal symmetry since nondiagonal terms involving an orbit and its time reversal have an action sufficiently close to survive the average process but an area of opposite sign. Indeed, assuming (in the weak-field regime) an ensemble average such that only diagonal and time reversal related terms are not affected, Eq. (6.22) reduces to

$$\overline{\chi^{(2)}}_D = 24 \sum_t \frac{R_T^2(\tau_t^0)}{r_t^2 |\det(M_t^0 - I)|} \left(\frac{2\mathcal{A}_t^0}{A}\right)^2 \cos\left(\frac{4\pi A_t^0 H}{\Phi_0}\right). \tag{6.23}$$

At zero field the cosine of the surviving terms in Eq. (6.23) is one and their prefactors positive. This merely reflects that the dephasing of time-reversal orbits due to the perturbing magnetic field

necessarily induces on average a decrease of the amplitude of N^{osc} , and therefore by means of Eq. (2.20c) a *paramagnetic* susceptibility. For extremely large distributions in systems size, such as those discussed in Section 5.6, even the oscillating patterns of Eq. (6.23) due to the subsequent rephasing and dephasing of the time-reversal orbits contributions vanish upon smoothing. In this case, only the paramagnetic response related to the original dephasing is observed, and the average susceptibility reaches zero as soon as $4\pi A_1^0 H / \Phi_0$ is of the order of 2π for all trajectories.

6.2.1. Magnetization line-shape for chaotic systems

The expressions we have obtained up to now in this subsection do not require the system to be actually chaotic, but only that periodic orbits are isolated. They should therefore be valid also for the contribution of isolated orbits in mixed systems, where the phase space contains both regular and chaotic regions. This includes for instance the contributions of elliptic, i.e. stable orbits, provided they are not close to any bifurcation and the surrounding island of stability is large enough.

For geometries being actually chaotic it is however possible to proceed further and to derive a general expression for the line-shape of the field-dependent susceptibility, if the temperature is low enough. For temperatures such that the cutoff time τ_c of the damping factor $R_T(\tau_i)$ is of the order of the period of the fundamental periodic orbits, the average susceptibility will be dominated by the shortest orbits, whose characteristics are largely system dependent. However, for higher τ_c a large number of trajectories will contribute to $\overline{\chi_D^{(2)}}$, and a statistical treatment of the sum on the r.h.s. of Eq. (6.23) is possible, yielding an *universal* line-shape for the average susceptibility. For sake of clarity, we discuss here only the case of billiard-like structures, but the following developments can be generalized in a straightforward way to any kind of potentials.

Two basic ingredients are required here in addition to Eq. (6.23) to obtain the magnetization peak line-shape. The first one is the semiclassical sum rule derived by Hannay and Ozorio de Almeida [71], which states that in sums like Eq. (6.23) the two effects of an exponential decrease in the prefactors on the one hand and the exponential proliferation of orbits on the other hand cancel each other yielding

$$\sum_i \frac{\delta(\tau_i - \tau)}{|\det(M_i - I)|} = \frac{1}{\tau}. \quad (6.24)$$

(Note, that in the above sum the contributions of orbits with number of repetitions $r_i > 1$ are neglected.) To be valid, this equation requires that the periodic orbits are uniformly distributed in phase space which will only be achieved for sufficiently large τ . For billiards the periods are given, up to a multiplication by the Fermi speed, by the length of the orbits and the periods τ in Eq. (6.24) can be replaced by the lengths L . We call L_1^* the characteristic length for which periodic orbits can be taken as uniformly distributed in phase space. Typically, L_1^* is not much larger than the shortest period of the system.

The second ingredient is the distribution of area enclosed by the trajectories. For chaotic systems, this distribution has a generic form [24, 72]. Namely the probability $P_N(\Theta)$ for a trajectory to enclose an algebraic area Θ after N bounces on the boundaries of the billiard is given by

$$P_N(\Theta) = \frac{1}{\sqrt{2\pi N\sigma_N}} \exp\left(-\frac{\Theta^2}{2N\sigma_N}\right). \quad (6.25)$$

This result actually follows from a general argument [72] which in our case can be stated as follows: With a proper choice of the origin, the area swept by the ray vector for a given bounce is characterized by a distribution, with zero mean value and a width σ_N which define the parameter of the distribution Eq. (6.25). For a strongly chaotic system, successive bounces can be taken as independent events, which by means of the central limit theorem yield the distribution Eq. (6.25). Denoting \bar{L} the average distance between two successive reflections and $\sigma_L = \sigma_N/\bar{L}$, this is equivalent to

$$P_L(\Theta) = \frac{1}{\sqrt{2\pi L\sigma_L}} \exp\left(-\frac{\Theta^2}{2L\sigma_L}\right). \quad (6.26)$$

Now $P_L(\Theta)$ is the distribution of enclosed areas for trajectories of length L , and the above equation is valid for L larger than a characteristic value L_2^* , which again is of the order of the shortest closed orbit's length.

For temperature sufficiently low so that $L_c > L_1^*, L_2^*$, Eqs. (6.24) and (6.26) can be used to replace the sum over periodic orbits Eq. (6.23) by the integral

$$\frac{\overline{\chi_D^{(2)}}}{\chi_L} = 24 \int_0^\infty \frac{dL}{L} \int_{-\infty}^{+\infty} d\Theta P_L(\Theta) R_T^2(L) \left(\frac{4\Theta^2}{A^2}\right) \cos\left(\frac{4\pi\Theta H}{\Phi_0}\right). \quad (6.27)$$

Performing the Gaussian integral over Θ , and introducing the dimensionless factor $\xi = 2\pi H \sqrt{\sigma_L L_c}/\Phi_0$, one obtains the average susceptibility as

$$\frac{\overline{\chi_D^{(2)}}}{\chi_L} = 96 \left(\frac{\sigma_L L_c}{A^2}\right) F(\xi) \quad (6.28)$$

where the function $F(\xi)$ is defined as

$$F(\xi) = \int_0^\infty \left(\frac{x}{\sinh x}\right)^2 (1 - 4\xi^2 x) \exp(-2\xi^2 x) dx; \quad x = L/L_c. \quad (6.29)$$

The quadrature cannot be performed analytically (in a closed expression) for arbitrary ξ ¹³, but it can easily be calculated numerically. As seen in Fig. 12, $F(\xi)$ has a maximum at $\xi = 0$ with a half-width $\Delta\xi \simeq 0.317$. Expansion of $F(\xi)$ for small ξ yields $F(\xi) \approx \pi^2/6 - 9\xi(3)\xi^2$ (where $\zeta(x)$ is the Zeta function). Denoting $A = \sigma_L L_c/A^2$, the susceptibility at zero field is thus given by

$$\frac{\overline{\chi_D^{(2)}}}{\chi_L}(H=0) = 16\pi^2 A, \quad (6.30)$$

and the value half-width $\Delta\Phi$ by

$$\frac{\Delta\Phi}{\Phi_0} = \frac{\Delta\xi}{2\pi} A^{-1/2}. \quad (6.31)$$

¹³ Using for $R_T(L)$ the asymptotic expression $R_T(L) = 2(L/L_c) \exp(-L/L_c)$, valid for $L > L_c = \hbar\beta v_F/\pi$, yields $F(\xi) = (1 - 5\xi^2)/(1 + \xi^2)^4$, but the contribution of the range $L \leq L_c$ is of the same order.

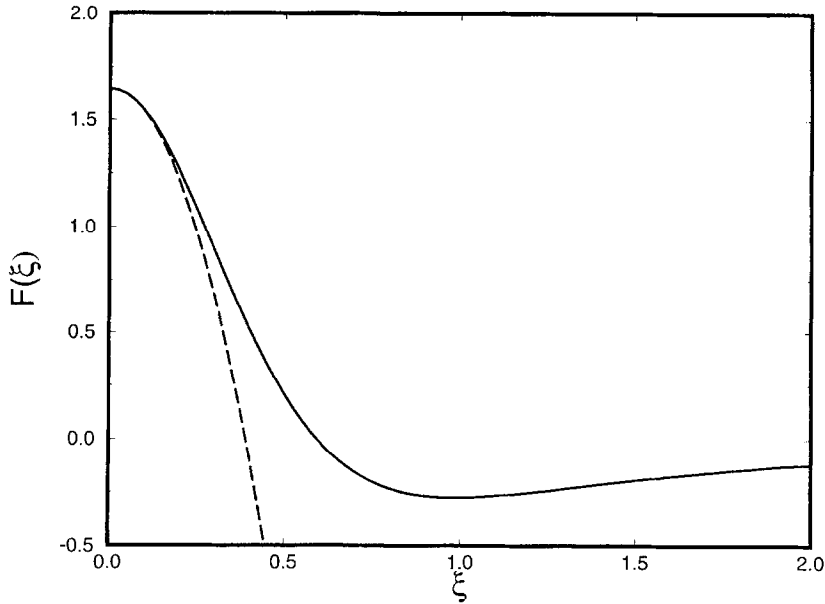


Fig. 12. Solid: function $F(\xi)$ (see Eq. (6.29)) describing the magnetic field dependence of the average susceptibility for an ensemble of chaotic microstructures. Dashed: quadratic approximation $\pi^2/6 - 9\zeta(3)\xi^2$ of $F(\xi)$.

The experimental observation of Eq. (6.28) would be a very stringent confirmation for the applicability of the whole semiclassical picture developed here. However, two remarks are in order:

(i) it is experimentally usually rather difficult to make a clear cut distinction between the function $F(\xi)$ we obtained and, say, a Lorentzian shape. Therefore, the temperature dependence (through L_c) of both the height and, more surprisingly, the width of the magnetization peak should be observable rather than the precise functional form of Eq. (6.28).

The physical picture underlying these results is that at a given temperature, the cutoff length L_c determines the length of the orbits providing the main contribution to the susceptibility. The smaller the temperature, the larger L_c and the longer the contributing orbits. The typical areas enclosed by these orbits thus increase, making them more sensitive to the magnetic field and yielding a larger susceptibility at zero field and a smaller width since time reversal invariance is more rapidly destroyed. The precise temperature dependence of the height and the width (and their relationship, which might be useful when σ_L is unknown) is given by Eqs. (6.30) and (6.31).

(ii) It should be borne in mind that Eq. (6.28) gives only the contribution of the diagonal part of $\chi^{(2)}$, but does not take into account the contribution of pairs of orbits which are not related by time-reversal symmetry. Moreover, the statistical approach used implies that fairly long orbits are contributing to the susceptibility, which because of the exponential proliferation of such orbits should yield an increasing number of quasidegeneracies in their length. Therefore, to smooth out these nondiagonal term, one should a priori require that the smoothing is taken on a very large range of $(k_F a)$. In practice however, and as will be discussed in more detail in [43], the smooth disorder characteristic of the GaAs/AlGaAs heterostructures for which this kind of experiments are done will actually be responsible for the cancelation of the nondiagonal terms *without affecting* (for

small enough disorder) *the contribution we have calculated*.¹⁴ The effects of nondiagonal terms should therefore be noticeably less important in actual systems that it might appear in a clean model.

6.3. Integrable versus chaotic geometries

The magnetic responses of chaotic and integrable systems have similarities and differences with respect to their treatment as well as to the resulting susceptibility. The most remarkable similarity is the paramagnetic character of the average susceptibility, while the magnitude of this response greatly differs for both types of geometries. Concerning their treatment the differences arise from the lack of structural stability of integrable systems under a perturbing magnetic field. Indeed, for nongeneric integrable systems such as the ring or circular billiards which remain integrable at all fields, the structure of the obtained equations are, except for the use of the Berry–Tabor trace formula instead of the Gutzwiller trace formula, the same as those for the chaotic systems. For generic integrable systems however, the breaking of invariant tori requires a more careful treatment yielding slightly less transparent, though essentially similar expressions.

6.3.1. Paramagnetic character of the average susceptibility

Because of this formal similarity, the qualitative behavior of the magnetic response is also quite the same for generic chaotic and integrable systems. The susceptibility of a single structure can be paramagnetic or diamagnetic and changes sign with a periodicity in $k_F a$ of the order of 2π . On the other hand, the average susceptibility for an ensemble of microstructure is, as expressed by Eqs. (6.17) and (6.23), paramagnetic at zero field independent of the kind of dynamics considered. Indeed Eq. (2.20c) states that $\overline{\Delta F^{(2)}}$ is, up to a multiplicative factor, the variance of the (temperature smoothed) number of states for a given chemical potential μ . In integrable and chaotic systems the basic mechanism involved is that the magnetic field reduces the degree of symmetry of the system, which as a general result lowers this variance. Therefore the $\overline{\Delta F^{(2)}}$ necessarily decreases when the magnetic field is applied and the average susceptibility is paramagnetic at zero field.

There are some differences worth being considered. First, for chaotic systems the only symmetry existing at zero field is the time-reversal invariance, while for integrable systems the breaking of time-reversal invariance *and* the breaking of invariant tori together reduces the amplitude of $N^{\text{osc}}(E)$. For chaotic systems *the paramagnetic character of the ensemble susceptibility arises as naturally as the negative sign of the magnetoresistance in coherent microstructures*. The situation is similar to a random matrix point of view, where the ensembles modeling the fluctuations of time-reversal invariant systems are known to be less rigid (in the sense that the fluctuation of the number of states in any given stretch of energy is larger) compared to the case where time-reversal invariance is broken. The transition from one symmetry class to the other can be understood by the introduction of generalized ensembles whose validity can be justified semiclassically [67]. It is however

¹⁴ Without entering into any details, the reason for this is the following. For smooth disorder, one should distinguish between an “elastic mean free path” l , and a transport mean free path l_T which is much larger than l . For small disorder, l_T can be assumed infinite, but long orbits will usually be longer than l . As a consequence, the action of each orbit is going to acquire a random phase from sample to sample, which is decorrelated for different orbits, but is the same for time-reversal symmetric orbits. Thus the diagonal contribution we have calculated will not be affected, but nondiagonal terms will be strongly suppressed.

important to recognize that even for the chaotic case we do not have the standard GOE-GUE transition [22] since (2.20c) involves the integration over a large energy interval. We are therefore not in the universal, but in the “saturation” regime where $(N^{\text{osc}}(E))^2$ is given by the shortest periodic orbits.

Secondly, for chaotic systems and for temperatures sufficiently low that a large number of orbits contribute to the susceptibility, it is possible – similar as in the weak localization effect in electric transport [24] – to derive a universal shape of the magnetization peak. This is not possible for integrable systems, which do not naturally lend themselves to a statistical treatment.

6.3.2. Typical magnitude of the magnetic susceptibility

Even if there are some analogies between the magnetic response of chaotic and integrable systems (especially when the latter remain integrable at finite fields), the *magnitude* of the susceptibility exhibits significant differences. The contribution of an orbit to the Gutzwiller formula for two-dimensional systems is half an order in \hbar smaller than a term in the Berry–Tabor formula for the integrable case. More generally, in the case of f degrees of freedom, the \hbar dependence of the Berry–Tabor formula is $\hbar^{-(1+f)/2}$ being the same as in the semiclassical Green function. The Gutzwiller formula is obtained by performing the trace integral of the Green function by stationary phase in $f - 1$ directions, each of which yielding a factor $\hbar^{1/2}$. This results in an entire \hbar^{-1} behavior independent of f for a chaotic system. Important consequences therefore arise for the case of two-dimensional billiards of typical size a at temperatures such that only the first few shortest orbits are significantly contributing to the free energy, and gives rise to a different parametrical $k_F a$ characteristic of integrable and chaotic systems. The $k_F a$ behavior of the density of states and susceptibility for individual systems as well as ensemble averages is displayed in Table 1. While the magnetic response of chaotic systems results from *isolated* periodic orbits, it is the existence of *families* of flux enclosing orbits in quasi-integrable or partly integrable systems which is reflected in a parametrically different dependence of their magnetization and susceptibility on $k_F a$ (or \sqrt{N} in terms of the number of electrons). The difference is especially drastic for ensemble averages where we expect a $k_F a$ independent response $\bar{\chi}$ for a chaotic system while the averaged susceptibility for integrable systems, e.g. the ensemble of square potential wells in the experiment discussed in Section 5, increases linearly in $k_F a$. Under the conditions of that measurement [25] the enhancement should be of the order of 100 compared to an ensemble of chaotic quantum dots. We therefore suggested [57] to use the different parametrical behavior of the magnetic response as a tool in order to unambiguously distinguish (experimentally) chaotic and integrable dynamics in quantum dots. We stress that this criterion is not based on the long-time behavior of the chaotic dynamics but on short time properties, namely the existence of families of orbits contributing in phase to the trace of the Green function of integrable systems.

7. Non-perturbative fields: bouncing-ball- and de Haas–van Alphen-oscillations

Up to now we have essentially focused on mesoscopic effects in the weak magnetic field regime where the classical cyclotron radius r_c is large compared to the typical size a of the system, i.e.

$$r_c/a = c\hbar k/eH a \gg 1. \quad (7.1)$$

Table 1

$(k_F a)$ dependence of the oscillating part of the density of states and of the magnetic response depending on the absence (chaotic case) or the presence (regular case) of continuous families of periodic orbits for two-dimensional billiard-like microstructures. ($\bar{D} = (g_s mA)/(2\pi\hbar^2)$ is independent of the nature of the dynamics)

	$D^{\text{osc}}(E)/\bar{D}$	χ/χ_L	$\bar{\chi}/\chi_L$
Chaotic	$(k_F a)^{-1}$	$(k_F a)$	$(k_F a)^0$
Regular	$(k_F a)^{-1/2}$	$(k_F a)^{3/2}$	$(k_F a)$

Then, electron trajectories can be considered as straight lines between bounces and the dominant effect of the magnetic field enters as a semiclassical phase in terms of the enclosed flux. Nevertheless, as shown in Fig. 1 in the introduction (for the case of a square) the low-field oscillations of χ are accurately described by *classical* perturbation theory in terms of the family (11) of unperturbed orbits (left inset in Fig. 1(b)). They persist up to field strengths $\varphi \approx 10$ which is by orders of magnitude larger than the typical flux scale which describes the breakdown of first-order *quantum* perturbation theory, i.e. magnetic fluxes where the first avoided level crossings appear. Due to condition (7.1) the relevant classical “small” parameter is H/k_F . The semiclassical “weak-field” regime increases with increasing Fermi energy.

In this section we will go beyond this (classically) perturbative regime and discuss microstructures under larger fields, where the magnetic response reflects the interplay between the scale of the confining energy and the scale of the magnetic field energy $\hbar\omega_c$ on the quantum level. Classically, nonperturbative fields affect the motion not only through a change of the actions (by means of the enclosed flux), but additionally due to the bending of the trajectories. A priori, the semiclassical approach we used for weak magnetic fields applies also to this case without any difference: Oscillating components of the single-particle density of states can be related to periodic (or nearly periodic) orbits by taking the trace of the semiclassical Green function. The magnetic response is then obtained from integration over the energy and taking the derivatives with respect to the magnetic field. These operations correspond to the multiplication by the inverse of the period of the orbit, by the damping factor R_T and by the area enclosed by the orbit. Three field regimes (weak ($a \ll r_c$), intermediate ($a \simeq r_c$), and high ($a \geq 2r_c$) fields) can be clearly distinguished as is illustrated in Fig. 1(b) for the square geometry. The distinction of the three regimes appears not because they deserve a fundamentally different semiclassical treatment, but simply because of some salient features of the classical dynamics associated to each of these regimes.

In the high-field regime, most of the orbits simply follow a cyclotron motion. In that case, the system behaves essentially as an infinite system, and one recovers the well known de Haas–van Alphen oscillations for $\chi^{(1)}$. We shall moreover see below that within our semiclassical approach, the destruction of some of the cyclotronic orbits due to reflections at the boundaries can be taken into account, allowing to handle correctly the cross-over regime where $a \geq 2r_c$ but r_c is not yet negligible with respect to a .

While the high-field ($a \gg r_c$) classical dynamics is generally (quasi-) integrable the dynamics in the intermediate-field regime is always mixed (in the sense that chaotic and regular motion coexists in phase space) except for particular cases of systems with rotational symmetry which remain integrable independent of the magnetic field. In contrast to that, systems in the small field regime can exhibit any degree of chaoticity *in the zero field limit*. Indeed, there is a large variety of geometries for which the motion of the electrons in the absence of a magnetic field is either integrable, or completely

chaotic. Therefore, increasing the field starting from an integrable (respectively chaotic) configuration at $H = 0$, the intermediate-field regime will be characterized by an increase (respectively a decrease) of the degree of chaos of the classical dynamics, which will noticeably affect the magnetic response of the system. However, if the zero-field configuration already shows a mixed dynamics (which is generically the case), the only noticeable difference between the weak and intermediate field regime will consist in the complete lost of time-reversal symmetry and naturally its consequences on $\overline{\chi^{(2)}}$ as discussed in Section 6.

In addition, for some particular geometries, namely those for which the boundary contains some pieces of parallel straight lines, the intermediate field susceptibility will be characterized by the dominating influence of *bouncing-ball orbits*, periodic electron motion due to reflection between opposite boundaries. Fig. 1(b) depicts a whole scan of the magnetic susceptibility of a square from zero flux up to flux $\varphi = 55$ ($3r_c \approx a$). We can see there, and we will discuss in detail below, that there are – besides the small-field oscillations due to orbits (11) – two well separated regimes of susceptibility oscillations: The intermediate field regime ($2r_c > a$) reflects quantized *bouncing-ball periodic orbits* (second inset) and the oscillations in the strong field regime ($2r_c < a$) which, as mentioned above, are related to *cyclotron orbits* (right inset). Although the results to be reported are of quite general nature we will discuss them quantitatively for the case of square microstructures. We study individual squares and perform our analysis within the grand canonical formalism.

7.1. Intermediate fields: Bouncing-ball magnetism

The full line in Fig. 13(a) shows the quantum mechanically calculated (see Section 5.4) grand canonical susceptibility for small and intermediate fluxes at a Fermi energy corresponding to ~ 2100 enclosed electrons in a square at a temperature such that $k_B T/\Delta = 8$. The semiclassical result $\chi_{(11)}^{(1)}$ from the family (11) (Eq. (5.18)) shown as the dashed-dotted line (with negative offset) in Fig. 13(a) exhibits the onset of deviations from the quantum result with respect to phase and amplitude starting at $\varphi \approx 8$ ($r_c \approx 2a$) indicating the breakdown of the family (11) of straight line orbits. With increasing flux we enter into a regime where the nonintegrability of the system manifests itself in a complex structured energy level diagram (see Fig. 1(a)) on the quantum level and in a mixed classical phase space [73] of co-existing regular and chaotic motion. However, besides the variety of isolated stable and unstable periodic orbits there remains a family of orbits with specular reflections only on opposite sides of the square. We will denote these periodic orbits shown in Fig. 14 which are known as “bouncing-ball” orbits in billiards without magnetic field by $(M_x, 0)$ and $(0, M_y)$ according to the labeling introduced in Section 5.1. (M_x and M_y are the number of bounces at the bottom and left side of the square.) These orbits form families which can be parameterized, e.g. for the case $(M_x, 0)$ in terms of the point of reflection x_0 at the bottom of the square. We thus expect – as in the case of the families (M_x, M_y) in Section 5 – in the semiclassical limit a parametrical dependence on $k_F a$ of the related susceptibilities which should strongly dominate the contributions of the co-existing isolated periodic orbits.

We present our semiclassical calculation of the susceptibility contribution related to bouncing-ball orbits for the primitive periodic orbits, i.e. $(M_x, 0) = (1, 0)$ and generalize our results at the end to the case of arbitrary repetitions. We proceed as in Section 5 for the derivation of $\chi_{11}^{(1)}$. However, while those calculations were performed in the limit of a small magnetic field (assuming H -independent classical amplitudes and shapes of the trajectories (11)) we now have to consider explicitly the field

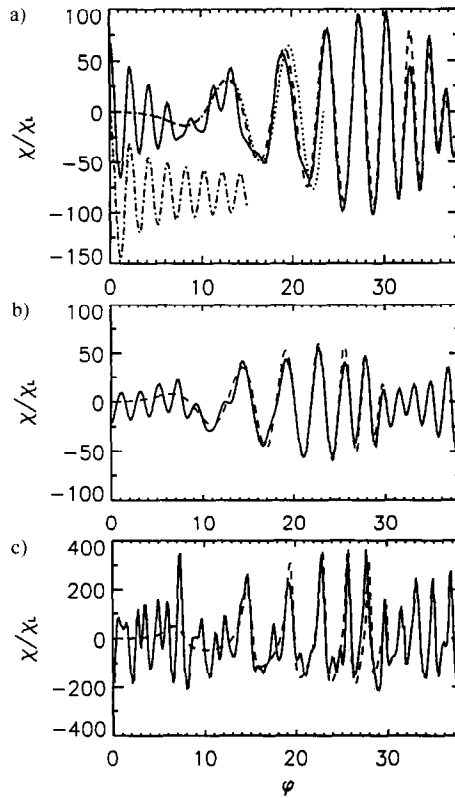


Fig. 13. Grand-canonical susceptibility of a square potential well as a function of magnetic flux $\varphi = Ha^2/\Phi_0$. The full lines always denote the quantum mechanical results. Panel (a): χ/χ_L calculated at a Fermi energy of 2140 enclosed electrons at a temperature $kT/\Delta = 8$. Dashed (dotted) line: Semiclassical result due to bouncing-ball orbits from Eq. (7.11) with action S_{10} according to the exact expression of Eq. (7.3), (quadratic approximation Eq. (7.12)). Dashed-dotted line: Susceptibility contribution from family (11) from Eq. (5.18) with offset of -80 for reasons of representation. (b) Dashed line: Semiclassical contribution (Eq. (7.13)) from bouncing-ball orbits for 1440 electrons and $kT/\Delta = 7$. The lower value of k_F makes it necessary to describe the actions by Eq. (7.3). (c) same as in (b) but for a low temperature $kT/\Delta = 2$ for which repetitions are important and the use of Eq. (7.13) is necessary to approach the quantum results.

dependence of the classical motion. The contribution to the diagonal part of the Green function of a recurring path starting at a point \mathbf{q} on a bouncing-ball orbit reads

$$\mathcal{G}_{10}(\mathbf{q}, \mathbf{q}' = \mathbf{q}; E, H) = \frac{1}{i\hbar\sqrt{2\pi i\hbar}} D_{10} \exp \left[i \left(\frac{S_{10}}{\hbar} - \eta_{10} \frac{\pi}{2} \right) \right]. \quad (7.2)$$

Simple geometry yields for its length, enclosed area, and action

$$L_{10}(H) = \frac{2a\zeta}{\sin \zeta}; \quad A_{10}(H) = -(2\zeta - \sin 2\zeta)r_c^2; \quad \frac{S_{10}}{\hbar} = k \left(L_{10} + \frac{A_{10}(H)}{r_c(H)} \right); \quad (7.3)$$

where ζ , the angle between the tangent to a bouncing-ball trajectory at the point of reflection and the normal to the side, is given by (see Fig. 14)

$$\sin \zeta = a/2r_c. \quad (7.4)$$

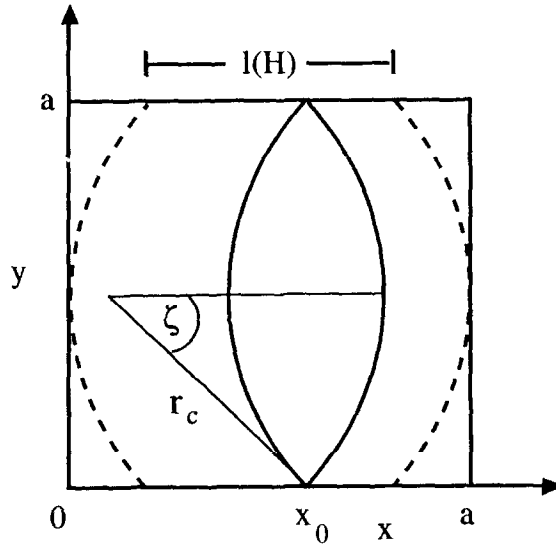


Fig. 14. Schematic representation of a typical flux-enclosing bouncing-ball orbit with cyclotron radius r_c . The dashed lines denote the limits of the H -dependent range of bouncing-ball orbits.

The Maslov index η_{10} is four and will be therefore omitted from now on.

As in Section 5, we will use as configuration space coordinates the couple $\mathbf{q} = (x_0, s)$, where x_0 labels the abscissa of the last intersection of the trajectory with the lower side of the square (see Fig. 14) and s is the distance along the trajectory. This choice has the advantage that $D_{10}(x_0, s)$ is constant, and therefore taking the trace of the Green function merely amounts to a multiplication by the size of the integration domain. As discussed in more detail in Appendix D, the semiclassical amplitude D_{10} is given by [21]

$$D_{10}(\mathbf{q}, \mathbf{q}' = \mathbf{q}) = \frac{1}{|\dot{s}|} \left| \frac{\partial x'_0}{\partial p_{x_0}} \right|_{x_0' = x_0}^{-1/2}, \quad (7.5)$$

where $(x_0, p_{x_0}) \rightarrow (x'_0, p'_{x_0})$ is the Poincaré map between two successive reflections on the lower side of the billiard. Noting $u_{x_0} = (p_{x_0} - eA_x/c)/(\hbar k)$ (u_{x_0} is the projection of the unit vector parallel to the initial velocity on the x axis) one obtains from simple geometrical considerations

$$\begin{aligned} p'_{x_0} &= p_{x_0} \\ x'_0 &= x_0 + 2r_c \left(\sqrt{1 - (u_{x_0} - a/r_c)^2} - \sqrt{1 - (u_{x_0})^2} \right). \end{aligned} \quad (7.6)$$

For the periodic orbits, $x'_0 = x_0$ implies that $u_{x_0} = a/2r_c = \sin \zeta$, and therefore

$$D_{10}(\mathbf{q}, \mathbf{q}' = \mathbf{q}) = \frac{1}{|\dot{s}|} \sqrt{\frac{\hbar k \cos \zeta}{2a}} \quad (7.7)$$

which reduces to Eq. (5.4) in the limit $H = 0$ ($\zeta = 0$). For the contribution of the whole family (1,0) we must perform the trace integral Eq. (5.1). The integral over s gives as usual a multiplication

by the period

$$\tau_{10} = \frac{L_{10}}{\hbar k/m}$$

of the orbit. Moreover, since neither the actions S_{10} , nor the amplitude D_{10} depend on x_0 , the x_0 -component of the trace integral simply yields a length factor

$$l(H) = a \left(1 - \tan \frac{\zeta}{2} \right) \quad (7.8)$$

(see Fig. 14) which describes the magnetic field dependent effective range for the lower reflection points of bouncing-ball trajectories (1,0). $l(H)$ vanishes for magnetic fields corresponding to $2r_c = a$. We therefore obtain for the bouncing-ball contribution $d_{10} = -(\mathbf{g}_s/\pi)\text{Im } \mathcal{G}_{10}$ to the density of states

$$d_{10}(E, H) = -\frac{2\mathbf{g}_s}{(2\pi\hbar)^{3/2}} l(H) L_{10} D_{10} \sin \left(\frac{S_{10}}{\hbar} + \frac{\pi}{4} \right). \quad (7.9)$$

In order to compute the contribution $\chi_{10}^{(1)}$ to the (grand canonical) susceptibility we first have to calculate $\Delta F_{10}^{(1)}$ by performing the energy integral Eq. (2.15c), and then to take twice the derivative with respect to the magnetic field. In a leading \hbar calculation, integrals and derivative should again be applied only on the rapidly oscillating part of d_{10} . Noting moreover that Eq. (4.7) is not restricted to perturbation around $H = 0$, i.e. that at any field

$$\frac{\partial S_{10}}{\partial H} = \frac{e}{c} A_{10},$$

we therefore obtain in the same way as we did for Eq. (6.21)

$$\chi_{10}^{(1)} = \frac{1}{a^2} \left(\frac{eA_{10}}{c\tau_{10}} \right)^2 d_{10}(\mu, H) R_T(L_{10}). \quad (7.10)$$

Inserting the expressions Eqs. (7.3), (7.8) and (7.7) into Eqs. (7.9) and (7.10), we finally have $\chi_{10}^{(1)}$ explicitly in terms of ζ as

$$\begin{aligned} \frac{\chi_{10}^{(1)}}{\chi_L} &= \frac{3}{8\pi^{1/2}} (k_F a)^{3/2} \frac{\sqrt{\cos \zeta} (\sin \zeta + \cos \zeta - 1)}{\zeta} \frac{(2\zeta - \sin(2\zeta))^2}{\sin^4 \zeta} \\ &\times \sin \left(\frac{S_{10}}{\hbar} + \frac{\pi}{4} \right) R_T(L_{10}). \end{aligned} \quad (7.11)$$

The entire bouncing-ball susceptibility $(\chi_{10}^{(1)} + \chi_{01}^{(1)})/\chi_L = 2\chi_{10}^{(1)}/\chi_L$ according to Eq. (7.11) is shown in Fig. 13(a) as the dashed line. At fluxes up to $\varphi \approx 15$ it just explains the low frequency shift in the oscillations of the quantum result indicating that the overall small field susceptibility is well approximated by $\chi_{11} + \chi_{10} + \chi_{01}$. For fluxes between $\varphi \approx 15$ ($r_c = 1.2a$) up to $\varphi \approx 37$ (the limit where $r_c = a/2$, i.e. the last bouncing-ball orbits vanish) the magnetic response is entirely governed by bouncing-ball periodic motion and the agreement between the semiclassical prediction and the full quantum result is excellent.

The flux dependence of the actions S_{10} (see Eq. (7.3)) is rather complicated. However, an expansion for $a/r_c = 2\pi\varphi/(k_F a) \ll 1$ yields a quadratic dependence on φ

$$\frac{S_{10}}{\hbar} \simeq 2k_F a \left[1 - \frac{1}{24} \left(\frac{2\pi\varphi}{k_F a} \right)^2 \right]. \quad (7.12)$$

The susceptibility from Eq. (7.11) with S_{10} according to Eq. (7.12) is shown as dotted curve in Fig. 13(a). It agrees well at moderate fields and runs out of phase at a flux corresponding to $a/r_c > 1$. While the period of the χ_{11} small field oscillations is nearly constant with respect to φ we find a quadratic φ characteristic for the oscillations in the intermediate regime which turns into a $1/\varphi$ behavior in the strong field regime (see next subsection).

To show that the agreement between the semiclassical (dashed) curve and the quantum result is not an artefact of the particular number of electrons chosen, Fig. 13(b) depicts semiclassical and quantum bouncing-ball oscillations for $k_B T/\Delta = 7$ and at a different Fermi energy corresponding to ~ 1400 electrons. With decreasing Fermi energy the upper limit $r_c = a/2$ (or $k_F a/(2\pi\varphi) = \frac{1}{2}$) of the bouncing-ball oscillations is shifted towards smaller fluxes ($\varphi \approx 30$ in Fig. 13(b)) and the number of oscillations shrinks. The oscillations for $\varphi > 30$ belong already to the strong field regime discussed in the next subsection.

Up to now we discussed the magnetic response of the family of primitive orbits (1,0) and (0,1) which completely describes the intermediate-field regime at rather high temperatures corresponding to a temperature cutoff length in the order of the system size. At low temperatures we have to include contributions from higher repetitions ($r, 0$), $(0, r)$ along bouncing-ball paths. L_{r0} and A_{r0} have a linear r -dependence, and from the Poincaré map Eq. (7.6), one obtains that $D_{r0} = r^{-1/2} D_{10}$. Therefore

$$\begin{aligned} \frac{\chi^{(1)}}{\chi_L} &= \frac{1}{\chi_L} \sum_{r=1}^{\infty} (\chi_{r0}^{(1)} + \chi_{0r}^{(1)}) \\ &= \frac{3}{4\pi^{1/2}} (k_F a)^{3/2} \frac{\sqrt{\cos \zeta} (\sin \zeta + \cos \zeta - 1) (2\zeta - \sin(2\zeta))^2}{\zeta \sin^4 \zeta} \\ &\quad \times \sum_{r=1}^{\infty} r^{-1/2} \sin \left(r \frac{S_{10}}{\hbar} + \frac{\pi}{4} \right) R_T(r L_{10}). \end{aligned} \quad (7.13)$$

Fig. 13(c) shows the susceptibility at the same Fermi energy as in Fig. 13(b) but at a significantly lower temperature $k_B T/\Delta = 2$. The bouncing-ball peaks are much higher and new peaks related to long periodic orbits differing from the bouncing-ball ones appear. However, the bouncing-ball peak heights and even their shape (which is no longer sinusoidal and symmetrical with respect to $\chi = 0$) is well reproduced by the analytical sum Eq. (7.13) showing the correct temperature characteristic of the semiclassical theory.

The $k_F a$ behavior of the bouncing-ball susceptibility at a fixed flux is not as simple as in the case of the weak-field oscillations (where $\chi_{11}^{(1)} \sim (k_F a)^{3/2}$) since the angle ζ occurring in the prefactor in Eq. (7.11) depends on $k_F a$ and the action is nonlinear in $k_F a$. Nevertheless, the overall oscillatory behavior is similar as for example in Fig. 8(a). However, at a given nonzero magnetic field the classically relevant parameter Eq. (7.1) changes with energy. Therefore, by increasing the Fermi energy beginning at the ground state one generally passes from the strong field regime (at small energies or high field strengths, see next section) to the bouncing-ball regime and will finally reach

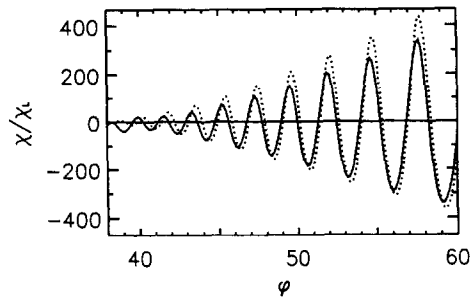


Fig. 15. De Haas–van Alphen like oscillations of the susceptibility of a square at magnetic fluxes corresponding to $r_c < a/2$ for 2140 electrons at $kT/\Delta = 8$. Full line: quantum calculations; dashed line: analytical semiclassical result from cyclotron orbits according to Eq. (7.19).

the regime of oscillations related to the family (11). A unique behavior of periodic orbit oscillations is only expected by changing magnetic field and Fermi energy simultaneously in order to keep the classical parameter Eq. (7.1) which determines the classical phase space of the microstructure constant. Such a technique is known as *scaled energy spectroscopy* in the context of atomic spectra [74].

Bouncing-ball oscillations are expected to exist in general in microstructures with parts of their opposite boundaries being parallel and in spherical symmetrical microstructures as the disk discussed in Section 4. (In the latter case the oscillations should be even stronger than in the square since the effective length $l(H)$ (Eq. (7.8)) is not reduced with increasing magnetic field.) An investigation of rectangular billiards for instance shows a splitting of the frequencies of oscillations related to orbits $(M_x, 0)$ and $(0, M_y)$ due to the different lengths of the orbits in x and y direction.

7.2. Strong field regime

At large magnetic field strengths or small energy the spectrum of a square potential well exhibits the Landau fan corresponding to bulk-like Landau states being almost unaffected by the system boundaries, while surface affected states fill the gaps between the Landau levels and condensate successively into the Landau channels with increasing magnetic field (see, e.g., Fig. 1(a)). This spectral characteristic corresponds to susceptibility oscillations which emerge with increasing amplitude for fluxes corresponding to $r_c < a/2$, for instance for $\varphi > 40$ in Fig. 1(b). They are shown in more detail in Fig. 15 where the full line depicts the numerical quantum result. These susceptibility oscillations exhibit the same period $\sim 1/H$ as de Haas–van Alphen bulk oscillations but differ in amplitude, because here the cyclotron radius is not negligible compared to the system size.

For the bulk or in the extreme high field regime $r_c \ll a$, where quantum mechanically the influence of the boundaries of the microstructure on the position of the quantum levels can be neglected, an expression for the susceptibility is most easily obtained by Poisson summation of the quantum density of states as was briefly sketched in the introduction following standard textbooks [2]. One then obtains the bulk magnetism as given by Eq. (1.11). It may be interesting to note however that a semiclassical interpretation of this equation follows naturally from an analysis similar to the one we followed throughout this paper. In this case only one type of primitive periodic orbits exists, the

cyclotron orbits with length, enclosed area, and action given by

$$L_0(H) = 2\pi r_c; \quad A_0(H) = -\pi r_c^2; \quad \frac{S_0}{\hbar} = kL_0 + \frac{e}{c\hbar}HA_0 = k\pi r_c. \quad (7.14)$$

Moreover, the trajectory passes through a focal point after each half traversal along the cyclotron orbit. Therefore, using $\eta_n = 2n$ for the Maslov indices and omitting the Weyl part of G , one obtains from Eq. (5.2) a semiclassical expression for the diagonal part of the Green function

$$G(\mathbf{r}, \mathbf{r}' = \mathbf{r}) = \frac{1}{i\hbar\sqrt{2\pi i\hbar}} \sum_n (-1)^n D_n \exp(in\pi k r_c), \quad (7.15)$$

in which the main structure of Eq. (1.11) is already apparent. A direct evaluation of the amplitude D_n in configuration space is however complicated here by the fact that all trajectories starting at some point \mathbf{r} refocus precisely at \mathbf{r} (focal point). Therefore, an expression like Eq. (7.5) for D_n is divergent and cannot be used. A method to overcome this problem by working with a Green function $\tilde{G}(x, y; p'_x, y')$ in momentum representation for the x' direction instead of $G(x, y; x', y')$ is described in Appendix E. It yields (see Eq. (E12))

$$D_n/i\hbar\sqrt{2\pi i\hbar} = m/i\hbar^2. \quad (7.16)$$

Inserting this expression in Eq. (7.15) we obtain the oscillating part of density of states

$$d^{\text{osc}}(E; H) = \sum_n d_n(E, H) = \frac{g_s A m}{\pi \hbar^2} \sum_n (-1)^n \cos(n\pi k r_c), \quad (7.17)$$

from which the de Haas–van Alphen susceptibility Eq. (1.11) is obtained by using

$$\chi^{(1)} = \frac{1}{A} \left(\frac{eA_0}{c\tau_0} \right)^2 \sum_n d_n(\mu, H) R_{\uparrow}(nL_0). \quad (7.18)$$

(with $\tau_0 = L_0/v_F$) which applies for the same reasons as Eq. (7.10).

For an infinite system, this direct semiclassical approach to the susceptibility therefore yields the same result as the Poisson summation. For billiard systems, it allows moreover to take correctly into account the fact that the trajectories too close to the boundary do not follow a cyclotron motion. Indeed, as seen in Appendix E, the contribution of cyclotron orbits to the susceptibility Eq. (1.11) has to be modified when r_c is not negligible compared to a by the introduction of a multiplicative factor $s(H)$. It accounts for the effect that the family of periodic cyclotron orbits (not affected by the boundaries) which can be parameterized by the positions of the orbit centers is diminished with decreasing field since the minimal distance between orbit center and boundary must be at least r_c . One therefore obtains for a billiard-like quantum dot

$$\frac{\chi_{\text{cyc}}^{\text{GC}}}{\chi_{\text{L}}} = -6s(H)(k_F r_c)^2 \sum_{n=1}^{\infty} (-1)^n R_{\uparrow}(2\pi n r_c) \cos(n\pi k_F r_c), \quad (7.19)$$

where $s(H)$ is given by Eq. (E15). In the case of the square we find for the area reduction factor

$$s(H) = \left(1 - 2\frac{r_c}{a}\right)^2 \Theta\left(1 - 2\frac{r_c}{a}\right), \quad (7.20)$$

Θ being the Heavyside step function. The last cyclotron orbit disappears at a field where $r_c = a/2$, i.e. $s(\varphi) = 0$ which happens near $\varphi \approx 38$ in Fig. 15. There the dashed line showing the semiclassical expression (7.19) is in good agreement with our numerical results and reproduces the decrease in the amplitudes of the de Haas–van Alphen oscillations when approaching $\varphi(r_c = a/2)$ from the strong field limit. This behavior is specific for quantum dots and does not occur in the two-dimensional bulk. Corresponding bulk de Haas–van Alphen oscillations under the same conditions as for the curves in Fig. 15 have (nearly constant) amplitudes in the order of $\chi/\chi_L \approx 3000$.

The semiclassical curve which only reflects the contribution from unperturbed cyclotron orbits agrees with the numerical curve (representing the complete system) even in spectral regions which show a complex variety of levels between the Landau manifolds (see Fig. 1). Due to temperature cutoff and since angular momentum is not conserved in the square the corresponding edge or whispering gallery orbits are mostly chaotic and do not show up in the magnetic response. The strong de Haas–van Alphen-like oscillations manifest the dominant influence of the family of cyclotron orbits. In related work on the magnetization of a (angular momentum conserving) circular disk in the quantum Hall effect regime Sivan and Imry [46] observed additional high frequency oscillations related to whispering gallery orbits superimposed on the de Haas–van Alphen oscillations.

8. Conclusion

In this work we have studied orbital magnetism and persistent currents of small mesoscopic samples in the ballistic regime. Within a model of noninteracting electrons we have provided a comprehensive semiclassical description of these phenomena based on the semiclassical trace formalism initiated by Gutzwiller, Balian, and Bloch. We have moreover treated in detail a few examples of experimental relevance such as the square, circle and ring geometries.

The global picture that emerges from our study can be summarized as follows. The magnetic response is obtained from the variation of the thermodynamic potential (or the free energy) under an applied magnetic field and therefore, in a noninteracting model, from the knowledge of the single-particle density of states. The semiclassical formalism naturally leads to a separate treatment of the smooth (in energy) component of the density of states (or its integrated versions) and of its rapidly oscillating part. The former is related to the local properties of the energy manifold, while the latter is associated with the dynamical properties of the system, more precisely to its periodic (or nearly periodic) orbits. For the smooth component we have shown that, despite the leading (Weyl) term in an \hbar expansion is independent of the field, higher-order terms can be computed and give rise to the standard Landau diamagnetism for any confined electron system at arbitrary magnetic fields. In the high-temperature regime, where the rapidly oscillating component of the density of states is suppressed by the rounding of the Fermi surface, the magnetic response reduces to the Landau diamagnetism. On the other hand, for the temperatures of experimental relevance the contribution coming from the oscillating part of the density of states is much larger than the Landau term and dominates the magnetic response. Similarly to the case of diffusive systems, the susceptibility of a ballistic sample in contact with a particle reservoir with chemical potential μ can be paramagnetic or diamagnetic (depending on μ) with equal probability. The fact that the samples are isolated (with respect to electron transfer) forces us to work in the canonical ensemble. Because of the breaking of time-reversal invariance occurring when the field is turned on, this results,

for essentially the same reason as in the diffusive regime, in a small paramagnetic asymmetry for the probability distribution of the susceptibility of a given sample. For generic integrable systems, this effect is reinforced by the breaking of invariant tori, which acts concurrently with the lost of time-reversal invariance. The asymmetry disappears for a flux $\Delta\Phi$ inside the system which is of the order of the quantum flux Φ_0 at a temperature selecting only the first few shortest orbits contributions, but may be smaller for lower temperature. Measuring the magnetic response of an ensemble of structures with a large dispersion in the size or the number of electrons magnifies this asymmetry and yields a total response (per structure) which is paramagnetic and much smaller than the typical susceptibility for a flux smaller than $\Delta\Phi$, and zero for larger flux. For ensembles with only microscopic differences between the individual structures (i.e. $\Delta(k_F a) \geq 2\pi$, but still $\Delta a/a \ll 1$ and $\Delta N/N \ll 1$) further oscillating patterns in the average susceptibility should be observed for larger fields.

Since the oscillating part of the density of states is semiclassically related to the classical periodic orbits, the nature of the classical dynamics quite naturally plays a major role in the determination of the amplitude of the magnetic response. Indeed, for a system in which continuous families of periodic orbits are present, these orbits contribute in phase to the density of states, yielding much larger fluctuations of the density of states than for systems possessing only isolated orbits, and therefore much larger magnetic response. Families of periodic orbits are characteristic for integrable systems, while for chaotic systems the periodic orbits are usually isolated. This different behavior can therefore be referred to as the hallmark for the distinction between integrable and chaotic systems. It should be borne in mind however that this difference is due to short-time properties, namely the existence or absence of families of orbits, rather than to long-time properties such as exponential divergence of orbits. In this respect, some atypical chaotic systems, such as the Sinai billiard for instance, may show a magnetic response typical for an integrable system because of the existence of marginally stable families of orbits.

The importance of classical mechanics can be illustrated in the (experimentally relevant) case of two-dimensional billiard-like quantum dots in the weak-field regime. If the system is chaotic, more precisely if the periodic trajectories are isolated, the typical susceptibility scales as $(k_F a)\chi_L$, where k_F is the Fermi wave number and a the typical size of the dot. By comparison, the typical susceptibility of an integrable system scales with $(k_F a)^{3/2}\chi_L$. This characteristic behavior of integrable systems is found in the generic case (like the square) where the magnetic field breaks the integrability as well as in the nongeneric case (like the disk) where the system remains integrable at finite fields. The difference due to the nature of the classical mechanics is even stronger for measurements on ensembles of structures since one obtains a $(k_F a)\chi_L$ dependence for integrable systems and no dependence on $(k_F a)$ for the chaotic ones. The same parametric dependences are obtained for the persistent currents in integrable and chaotic multiply connected geometries. Therefore, the nature of the dynamics yields an order of magnitude difference in the magnetic response of integrable and chaotic systems, which should be easy to observe experimentally (especially for ensemble measurements). Finally, for systems with mixed dynamics, for which the phase space is characterized by the coexistence of regular and chaotic motion, the magnetic response should be dominated by the nearly integrable regions of phase space. This gives rise to a $(k_F a)^{3/2}\chi_L$ dependence for the typical susceptibility as long as some families of periodic orbits remain sufficiently unperturbed. The precise calculation of the prefactor may however present some complications that we have not considered here (the general semiclassical treatment of mixed

systems remains an open problem) and should depend on the fraction of phase space being integrable.

The semiclassical approach we are using not only allows a global understanding of the magnetic response of ballistic devices, but also provides precise predictions when specific systems are considered. The detailed comparison between exact quantum calculations and semiclassical results for the square geometry demonstrates indeed that the semiclassical predictions are extremely accurate. This has been shown in Section 5 for weak fields, such that the trajectories are essentially unaffected by the magnetic field, and also in Section 7 for fields large enough to yield a cyclotron radius of the order of the typical size of the structure (where the bending of the classical trajectories has to be taken into account). For intermediate fields we have identified a new regime where the magnetic susceptibility is dominated by bouncing-ball trajectories that alternate between opposite sides of the structure (enclosing flux due to their bending). For high fields the electrons move on cyclotron orbits and we have recovered the de Haas–van Alphen oscillations (with finite-size corrections that we calculated semiclassically).

In order to understand the success of the semiclassical approach, it should be kept in mind that the lack of translational invariance characteristic for the ballistic regime, where the shape of the device plays an important role, complicates the application of other approximation schemes as e.g. diagrammatic expansions. Therefore, except for very specific cases where exact quantum calculations are possible, and unless one is satisfied by direct numerical calculations, some semiclassical ideas have to be implemented to deal with such problems. Moreover, from a more practical point of view, the semiclassical trace formalism we have used appears perfectly adapted to deal with thermodynamic quantities such as the grand potential $\Omega(\mu)$ or its first and second derivatives $N(\mu)$ and $D(\mu)$. Indeed, the beauty of this approach is that the oscillating part of the density of states is directly expressed in terms of Fourier-like components, each of which is associated with a periodic (or nearly periodic) orbit. The thermodynamic properties are obtained from their purely quantal (or zero temperature) analogs ω , n and d by temperature smoothing, which merely amounts to multiply each oscillating component by a temperature-dependent damping factor. For all fields (high, intermediate, or weak), this factor depends only on the ratio of the *period* τ of the corresponding orbit and the temperature-dependent cutoff time $\tau_c = \beta\hbar/\pi$ and suppresses exponentially the contribution of orbits with period longer than τ_c . As a consequence, not only the effect of temperature is taken into account in an intuitive transparent way, but in addition only the shortest periodic orbits have to be considered in the semiclassical expansion. All the problems concerning the convergence of trace formulae and the validity of semiclassical propagation of the wave function for very long times are of no importance here. One therefore avoids most of the problems which plague the field of quantum chaos when semiclassical trace formulae are used to resolve the spectrum on a mean-spacing scale. Mesoscopic physics is usually concerned with the properties of the spectrum on an energy scale large compared to the mean spacing. In the spirit of the work of Balian and Bloch [54], this is the situation for which the semiclassical trace formalism is especially appropriate.

Having stressed the success of the semiclassical approach in dealing with our model of noninteracting electrons evolving in a clean medium, it is worthwhile to consider in more detail how the above picture should be modified when going closer to the real world, and incorporating the effects of residual disorder, electron–electron or electron–phonon interactions. As stressed in the introduction, the first of these points is relatively harmless because of finite temperature smoothing.

The restriction to short periodic orbits actually justifies an approach to the ballistic regime using a model for clean systems since long diffusive trajectories do not contribute to the finite-temperature susceptibility. Indeed, careful numerical and semiclassical studies of the effect of small residual disorder [43] show that, except for a possible reduction of the magnetic response, the above description of the orbital magnetism of ballistic systems remains essentially unaltered. In particular, the mechanism proposed by Gefen et al. [60] is not borne out by the numerical simulations at the temperatures of experimental relevance. For smooth disorder, such as presumably prevails in the systems of Refs. [25, 26], the magnetic response is decreased by the dephasing of nearby trajectories in a way that depends on its strength and the ratio between the correlation length and the size of the structure [43], but diffusive trajectories can be seen to be absolutely irrelevant if the elastic mean free path is larger than the size of the structure. The precise knowledge of this reduction is however needed in order to make a decisive comparison with the experimental results of Ref. [25].

At the low temperatures of the experiments the inelastic mean free path of the electrons is much larger than the system size since electron–phonon interactions are suppressed. On the other hand, the effect of electron–electron interactions on the magnetic response is a much more controversial point. In particular, it has been invoked to be the necessary mechanism to obtain the measured values [75] for the problem of persistent currents in disorder metals. In a first approximation to the experimental conditions that we investigated in this work we would infer that electron–electron interactions are not crucial since the screening length is much smaller than the size of the samples and since the 2-d renormalization of the effective mass at these electron densities is only about 11% [76]. Clearly the two previous criteria will not be satisfied in smaller structures, and the possibility that electron–electron interactions express themselves through a mechanism for which these estimates are not relevant remains open even in the experimental realizations we consider.

Contrarily to the effect of disorder, which can be implemented within a semiclassical framework without essential difficulties, a semiclassical treatment of the electron–electron interaction still remains an open problem. However, the genuine effects that we have found within our semiclassical approach for the clean model of noninteracting electrons should prevail in more sophisticated theories. We think that the rich variety of possible experimental configurations for ballistic devices (the shape and the size can nowadays be chosen at will) provides an ideal testing ground for these more complete approaches. We hope that the work presented here will stimulate experimental and theoretical activity addressing the magnetic response of ballistic microstructures.

Acknowledgements

We acknowledge helpful discussions with H. Baranger, O. Bohigas, Y. Gefen, M. Gutzwiller, L. Lévy, F. von Oppen, N. Pavloff, B. Shapiro and H. Weidenmüller. We are particularly indebted to H. Baranger for continuous support and a careful reading of the manuscript, and to O. Bohigas for forcing us not to stop until getting to the bones of the problem. We thank B. Mehlis for communicating us Ref. [61]. KR and RAJ acknowledge support from the “Coopération CNRS/DFG” (EB/EUR-94/41). KR thanks the A. von Humboldt foundation for financial support. The Division de Physique Théorique is “Unité de recherche des Universités Paris 11 et Paris 6 associée au C.N.R.S.”

Appendix A. Convolution of a rapidly oscillating function with the derivative of the Fermi function

When considering thermodynamic quantities related to the oscillating part of the density of states at finite temperature T , one has to evaluate integrals of the form

$$I(T) = \int_0^\infty dE A(E) \exp\left[\frac{i}{\hbar}S(E)\right] f'(E - \mu), \quad (\text{A1})$$

where $f'(E - \mu)$ is the derivative of the Fermi function

$$f(E - \mu) = 1/[1 + \exp \beta(E - \mu)],$$

and $\beta = 1/k_B T$. The rapidly oscillating function $A(E) \exp[(i/\hbar)S(E)]$ usually originates from the contribution of a classical orbit (or a family of orbits) to the oscillating part of the density of states. In this case $S(E)$ is the action integral along the orbit, and its derivative $dS/dE \equiv \tau(E)$ is the period of the orbit.

At zero temperature $f' = -\delta(E - \mu)$ giving for $I_0 \equiv I(T=0)$

$$I_0 = -A(\mu) \exp[(i/\hbar)S(\mu)]. \quad (\text{A2})$$

In this appendix we show that, to leading order in \hbar and in β^{-1} (but without making any assumption concerning their relative value), the integral of Eq. (A1) is given by

$$I(T) = I_0 R_T(\tau) \quad (\text{A3})$$

with the temperature dependence

$$R_T(\tau) = \frac{\tau(\mu)/\tau_c}{\sinh(\tau(\mu)/\tau_c)} \quad \tau_c = \frac{\beta\hbar}{\pi}. \quad (\text{A4})$$

For systems without potential, i.e. free particles confined in a box (billiards), the period of the trajectory is related to its length L by $\tau(\mu) = L/v_F$, where $v_F = \hbar k_F/m$ is the Fermi velocity. R_T can then be written as

$$R_T(L) = \frac{L/L_c}{\sinh(L/L_c)}; \quad L_c = \frac{\hbar v_F \beta}{\pi}. \quad (\text{A5})$$

In the case of unconfined free particles, the formulae (A4) and (A5) are equivalent to the usual form of the temperature dependence of the de Haas–van Alphen effect Eq. (1.10) given in the introduction. Below we present a slight variation of a standard calculation (see e.g. [2]) of the temperature dependence of the de Haas–van Alphen effect, which generalizes it to any type of dynamics, once we cast it in the form of Eq. (A4).

Performing the integral (A1) along the contour shown in Fig. 16 and noting that the singularities of the derivative of the Fermi function are double poles located at $E_k = \mu + i(2k + 1)\pi/\beta$ ($k = 0,$

$\pm 1, \pm 2, \dots$) with a coefficient $1/\beta$, one finds the following relation

$$\begin{aligned} & \int_0^\infty dE A(E) \exp[(i/\hbar)S(E)] f'(E - \mu) - \int_{0+i2\pi/\beta}^{\infty+i2\pi/\beta} dE A(E) \exp[(i/\hbar)S(E)] f'(E - \mu) \\ &= \frac{2i\pi}{\beta} \frac{i\tau(E_1)}{\hbar} A(E_1) \exp[(i/\hbar)S(E_1)] . \end{aligned} \quad (\text{A6})$$

At low temperatures, the function $f'(E - \mu)$ is essentially zero everywhere in the complex plane, except for a narrow band of width β^{-1} near the line $\text{Re}(E) = \mu$, therefore the vertical portions of the contour ($E = 0$ and $E \gg \mu$) give negligible contributions. Noticing that $f'(E - \mu)$ has a periodicity of $2i\pi/\beta$ we can ignore the complex part of E in the factor f' of the second integral. Finally, since $\text{Im}(E_1) = \pi/\beta$ and $\text{Im}(E) = 2\pi/\beta$ along the upper portion, we can evaluate the prefactors at μ and expand the actions (which are multiplied by $1/\hbar$) as $S(E) = S(\mu) + \tau(\mu)(E - \mu)$ in leading order in β^{-1} and \hbar , obtaining

$$I(T) \left(1 - \exp \left[-\frac{2\pi\tau(\mu)}{\beta\hbar} \right] \right) = -\frac{2\pi\tau(\mu)}{\beta\hbar} A(\mu) \exp \left[\frac{i}{\hbar} S(\mu) - \frac{\pi\tau(\mu)}{\beta\hbar} \right] .$$

That is,

$$I(T) \left(1 - \exp \left[-\frac{2\tau(\mu)}{\tau_c} \right] \right) = I_0 \frac{2\tau(\mu)}{\tau_c} \exp \left[-\frac{\tau(\mu)}{\tau_c} \right] ,$$

from which one readily obtains the result of Eq. (A3).

A.1. Further comments

We would like to use the above calculation to motivate some choices made in Section 2 which might have appeared rather arbitrary. Concerning for instance the grand potential $\Omega(\mu)$ two equivalent expressions have been introduced: The usual Eq. (1.3) and Eq. (2.6c) which is obtained from integration by parts. On the other hand, we have used only

$$\Omega^{\text{osc}}(\mu) = - \int_0^\infty dE \omega^{\text{osc}}(E) f'(E - \mu) \quad (\text{A7})$$

as the “operational” definition of the oscillating part Ω^{osc} of Ω , and one might wonder whether an integral analogue to the one of Eq. (1.3) like

$$- \int d^{\text{osc}}(E) f^{(-1)}(E - \mu) dE , \quad (\text{A8})$$

(where $f^{(-1)}(E - \mu) = \ln(1 + \exp[\beta(\mu - E)])/\beta$ is the primitive of the Fermi function) could not be used as well. This is not the case for the two following reasons:

(i) First, the oscillating functions d^{osc} or ω^{osc} are usually obtained in a semiclassical approach and are therefore valid only for large energies. If the chemical potential μ is in the semiclassical regime and $\beta^{-1} \ll \mu$, which is always the case for the problems we consider, only the neighborhood of μ in which ω^{osc} can be used safely, contributes significantly to the integrals of Eq. (A7). On the contrary, the integral (A8) involves energies close to zero. Therefore there is no reason that d^{osc} is accurate, being quite often a diverging function.

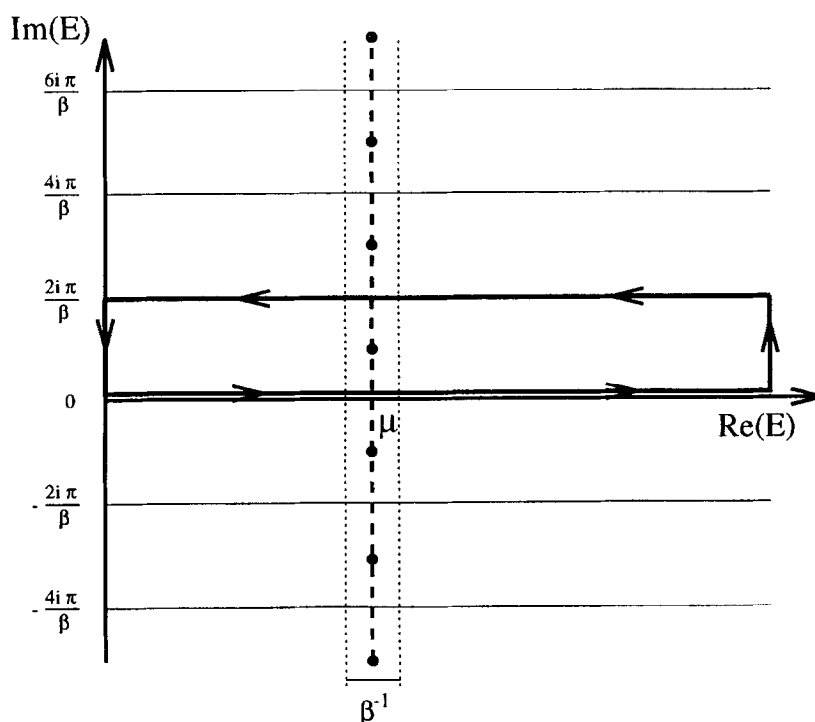


Fig. 16. Contour of integration in the complex energy plane used to evaluate the integral Eq. (A1). The derivative $f'(E-\mu)$ of the Fermi function has a periodicity of $2i\pi/\beta$ and double poles located at $E_n = \mu + i(2n+1)\pi/\beta$ (n being a positive or negative integer). Moreover, at low temperature, $f'(E-\mu)$ is essentially zero except for a narrow band of width β^{-1} near the line $\text{Re}(E) = \mu$. With this contour of integration, the integrand of Eq. (A1) has to be evaluated only in the small domain $[\mu - \beta^{-1}, \mu + \beta^{-1}] \times [0, 2i\pi\beta^{-1}]$ where a linearized approximation of the action is accurate.

(ii) In addition, even if one has at hand an equation as (1.6) which is a non-semiclassically exact expression, the integrals of Eqs. (A7) and (A8) are, strictly speaking, not equivalent. The latter form contains some boundary terms not present in the former, which obviously have to be removed from Ω^{osc} since they do not average to zero under a local smoothing.

In a semiclassical treatment the derivative f' of the Fermi function is superior to any of its integrated versions since it is significant only at energies where semiclassical approximations can be used safely.

Appendix B. Semiclassical expansion of the mean density of states

In this appendix we calculate the first two terms in an \hbar expansion of the smooth part of the density of states $\bar{d}(E)$. We follow the standard approach introduced by Wigner [63] using the notion of the Wigner transform of an operator. The Wigner transform of a quantum operator \hat{O} is defined by

$$[\mathcal{O}]_{\text{W}}(\mathbf{q}, \mathbf{p}) = \int d\mathbf{x} e^{-i\mathbf{p}\cdot\mathbf{x}/\hbar} \left\langle \mathbf{q} + \frac{\mathbf{x}}{2} \left| \hat{O} \left| \mathbf{q} - \frac{\mathbf{x}}{2} \right. \right. \right\rangle. \quad (\text{B1})$$

Among different properties of the Wigner transform we will essentially make use of the following two: First, the trace of an operator is related to the integral over phase space of its transform by means of

$$\text{Tr}(\hat{C}) = \frac{1}{(2\pi\hbar)^d} \int d\mathbf{q} d\mathbf{p} [\mathcal{C}]_w(\mathbf{q}, \mathbf{p}). \quad (\text{B2})$$

(We stress that this is an exact, not semiclassical, relation.) Secondly, for any operator function of the position and momentum quantum operators $\mathcal{F}(\hat{\mathbf{q}}, \hat{\mathbf{p}})$ (with some specified ordering), the semiclassical leading-order approximation to its Wigner transform is just the related classical function, that is

$$[\mathcal{F}(\hat{\mathbf{q}}, \hat{\mathbf{p}})]_w = \mathcal{F}(\mathbf{q}, \mathbf{p}) + O(\hbar). \quad (\text{B3})$$

When \mathcal{F} depends only on $\hat{\mathbf{q}}$ or $\hat{\mathbf{p}}$, the relation between the Wigner transform and the classical function is exact (no corrective terms in \hbar), as can be directly checked from Eq. (B1).

We will follow closely the presentation of Ref. [77] to which the reader is referred to for further details. The first step in the calculation of $\bar{d}(E)$ is to consider the Laplace transform of the level density, Eq. (3.2), which due to the property (B2) can be written as

$$Z(\lambda) = \frac{\mathbf{g}_s}{(2\pi\hbar)^d} \int d\mathbf{q} d\mathbf{p} [e^{-\lambda\mathcal{H}}]_w(\mathbf{q}, \mathbf{p}) \quad (\text{B4})$$

($\mathbf{g}_s = 2$ is the spin degeneracy factor). Using Eq. (B3), the leading order (Weyl) term in \hbar , Z_w , is obtained by replacing $[e^{-\lambda\mathcal{H}}]_w(\mathbf{q}, \mathbf{p})$ by $e^{-\lambda\mathcal{H}(\mathbf{q}, \mathbf{p})}$, where

$$\mathcal{H} = \frac{1}{2m} \left(\mathbf{p} - \frac{e}{c} \mathbf{A} \right)^2 + V(\mathbf{q}) \quad (\text{B5})$$

is the classical Hamiltonian. At this level of approximation $Z(\lambda)$ is given by

$$Z_w(\lambda) = \frac{\mathbf{g}_s}{(2\pi\hbar)^d} \int d\mathbf{q} d\mathbf{p} \exp \left(-\lambda \left[\frac{(\mathbf{p} - \frac{e}{c} \mathbf{A})^2}{2m} + V(\mathbf{q}) \right] \right). \quad (\text{B6})$$

Since this term is field independent (see the change of variable (3.5) in the text) we need to go to the next order in λ in order to obtain nonvanishing contributions to the magnetic susceptibility. Therefore we consider the asymptotic semiclassical expansion

$$[e^{-\lambda\mathcal{H}}]_w(\mathbf{q}, \mathbf{p}) = e^{-\lambda[\mathcal{H}]_w(\mathbf{q}, \mathbf{p})} \sum_{n=0}^{\infty} \left(\frac{-\hbar^2}{4} \right)^n \frac{C_n(\mathbf{q}, \mathbf{p}, \lambda)}{(2n)!}. \quad (\text{B7})$$

We have already seen that $C_0 = 1$. The following coefficients C_n can be obtained recursively by grouping terms according to their power in \hbar . In particular, the first coefficient is given by [63, 77]

$$\frac{\partial C_1}{\partial \lambda} = -e^{\lambda[\mathcal{H}]_w} \left([\hat{\mathcal{H}}]_w \overleftarrow{\Lambda}^2 e^{-\lambda[\mathcal{H}]_w} \right), \quad (\text{B8})$$

where $\overleftarrow{\Lambda} = \sum_{i=1}^d \overleftarrow{\partial} q_i \overleftarrow{\partial} p_i - \overleftarrow{\partial} p_i \overleftarrow{\partial} q_i$ is the Moyal bracket.

Inserting the classical Hamiltonian (B5) at the place of $[\hat{\mathcal{H}}]_w$ we obtain C_1 as the sum of three terms

$$C_1 = (C_1^0) + (C_1^a) + (C_1^s),$$

where

$$(C_1^0) = \frac{1}{m} \left[\lambda^2 \nabla^2 V(\mathbf{q}) - \frac{\lambda^3}{3m} \left(m \nabla V(\mathbf{q}) \cdot \nabla V(\mathbf{q}) + ((\mathbf{p} - (e/c)\mathbf{A}) \cdot \nabla)^2 V(\mathbf{q}) \right) \right] \quad (\text{B9})$$

is, up to the change of variable Eq. (3.5) in the integration over the phase space, the first-order correction without magnetic field $C_{1(H=0)}$ given in [63]. (C_1^a) is given by terms being antisymmetric in \mathbf{p} that vanish when taking the trace over phase space. Finally,

$$\begin{aligned} (C_1^s) = & \frac{e^2}{c^2} \sum_{i,k=1}^d \left\{ \frac{\lambda^2}{m^2} [(\partial q_i A_k)(\partial q_i A_k) - (\partial q_i A_k)(\partial q_k A_i)] \right. \\ & + \frac{2\lambda^3}{3m^3} [(\partial q_i A_k)(\partial q_k A_i)(p_i - (e/c)A_i)^2 - (\partial q_i A_k)(\partial q_i A_k) \\ & \left. \times \frac{(p_k - (e/c)A_k)^2 + (p_i - (e/c)A_i)^2}{2} \right\}. \end{aligned} \quad (\text{B10})$$

The first correction to the Laplace transform of the density of states is given by

$$Z_1(\lambda) = \frac{-g_s}{(2\pi\hbar)^d} \int d\mathbf{q} d\mathbf{p} \left[\lambda^2 \frac{\mu_B^2 H^2}{6} + \frac{\hbar^2}{8} C_1^0 \right] e^{-i\lambda \mathcal{H}} \quad (\text{B11})$$

($\mu_B = (e\hbar)/(2mc)$ is the Bohr magneton). Eqs. (B11) and (3.7) are obtained from Eq. (B10) by using the identity

$$H^2 = \sum_{jk} \left[\left(\frac{\partial A_j}{\partial q_k} \right)^2 - \frac{\partial A_j}{\partial q_k} \frac{\partial A_k}{\partial q_j} \right] \quad (\text{B12})$$

and a few transformations that leave the integral over \mathbf{p} unchanged, namely: (i) the change of variables Eq. (3.5) (allowing the substitution of \mathcal{H} by $\mathcal{H}^0 = \mathbf{p}^2/2m + V(\mathbf{q})$) (ii) the elimination of all terms antisymmetric in \mathbf{p} , (iii) the replacement of all terms of the form $p_i^2 e^{-i\mathbf{p}^2/2m}$ by $(m/\lambda) e^{-i\mathbf{p}^2/2m}$. Note finally that the field appears only in the term $-\lambda^2 \mu_B^2 H^2/6$, which is independent of the confining potential $V(\mathbf{q})$. This is at the root of the very general applicability of the Landau result.

Appendix C. Calculation of g_E for a ring billiard

In this appendix we derive the explicit form $I_2 = g_E(I_1)$ of the energy surface E in action space for a ring geometry. The calculation reduces to the evaluation of the integral of Eq. (4.1) along two independent paths on the invariant torus. The only subtlety arises from the difficulty of visualizing the integration paths in our four-dimensional phase-space where the tori are discontinuous due to

the presence of hard walls. We closely follow the procedure used by Keller and Rubinow [66] for the circular billiard, and we refer to this work for further details.

In a circular ring (with outer and inner radii a and b) we can distinguish two types of periodic trajectories: those which do not touch the inner disk (type-I, Fig. 17(a)) and those which do hit it (type-II, Fig. 17(b)). Type-I trajectories have their caustics outside the inner disk and therefore they are unaffected by their presence. They have an angular momentum pc , with $b < c < a$ ($p = \sqrt{2mE}$). Taking as the integration path \mathcal{C}_1 the concentric circle of radius R , we have $\mathbf{p} \, d\mathbf{q} = (pc/R)dq$ and then

$$I_1 = \frac{1}{2\pi} \oint_{\mathcal{C}_1} \frac{c}{R} p \, dq = p c . \quad (C1)$$

The action variable I_1 is just the angular momentum. The straight part of the path \mathcal{C}_2 of Fig. 17(a) is chosen along a classical trajectory, where \mathbf{p} is constant and collinear with $d\mathbf{q}$. For the part along the outer circle $\mathbf{p} \, d\mathbf{q} = -(pc/a)dq$. Combining both contributions we have

$$I_2^{(I)} = \frac{p}{\pi} \left\{ [a^2 - c^2]^{1/2} - c \arccos \left(\frac{c}{a} \right) \right\} . \quad (C2)$$

Elimination c between (C1) and (C2) leads to Eq. (4.12) of the text, valid for the description in action space of the energy surface of the circular billiard [66] and the energy surface associated with type-I trajectories in the ring billiard ($pb < I_1 < pa$). We have chosen the integration paths for type-I trajectories different from those of Ref. [66] because slight modifications of them are applicable for type-II trajectories.

Type-II trajectories have their caustics in the interior of the inner disk, that is, they have an angular momentum pc , with $c < b$. Integration along the path \mathcal{C}_1 of Fig. 17(b) leads to the identification of I_1 with the angular momentum pc (similarly to Eq. (C1)). By choosing the path \mathcal{C}_2 as shown on Fig. 17(b), the action integral along this path is simply the difference $I_2^{(II)}(a) - I_2^{(II)}(b)$ (where both terms are given by Eq. (C2), except that for the second a should be replaced by b). This yields

$$I_2^{(II)} = \frac{p}{\pi} \left\{ [a^2 - c^2]^{1/2} - [b^2 - c^2]^{1/2} - c \left[\arccos \left(\frac{c}{a} \right) - \arccos \left(\frac{c}{b} \right) \right] \right\} . \quad (C3)$$

Eliminating c between (C1) and (C3) leads to Eq. (4.21) of the text.

Appendix D. Calculation of the determinant D_M at zero field for a generic integrable system

In the semiclassical approximation of the Green function (Eq. (5.2)) the amplitude D_t associated with a classical trajectory t is given by [21]

$$D_t = \left| \begin{array}{cc} \frac{\partial^2 S_t}{\partial \mathbf{q} \partial \mathbf{q}'} & \frac{\partial^2 S_t}{\partial \mathbf{q} \partial E} \\ \frac{\partial^2 S_t}{\partial E \partial \mathbf{q}'} & \frac{\partial^2 S_t}{\partial E \partial E} \end{array} \right|^{1/2} = \frac{1}{|\dot{q}_2 \dot{q}'_2|^{1/2}} \left| -\frac{\partial^2 S}{\partial q_1 \partial q'_1} \right|^{1/2} . \quad (D1)$$

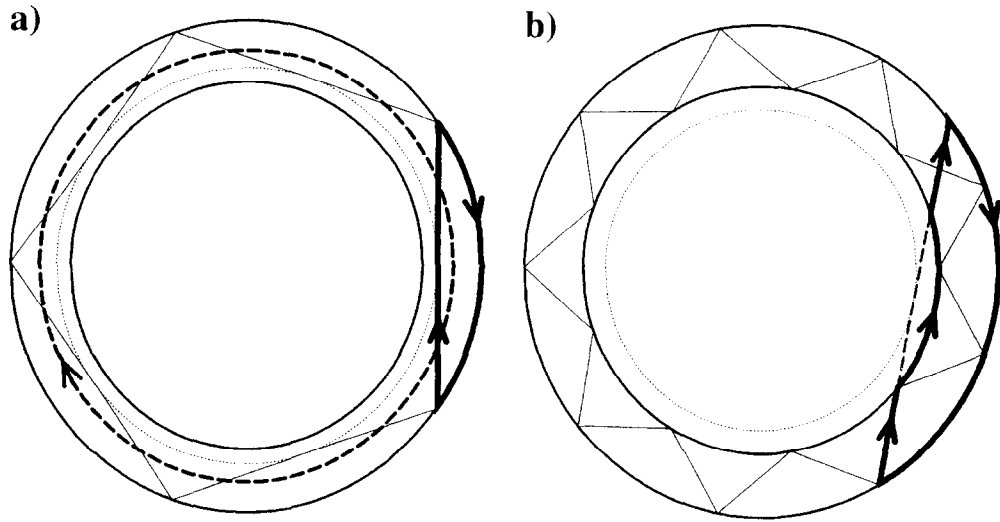


Fig. 17. Integration paths on the invariant tori used to compute the action integrals I_1 and I_2 for the circular and the ring geometries. (a) Path \mathcal{C}_1 (thick dashed) and \mathcal{C}_2 (thick solid) for the circle and type-I trajectories of the ring. The straight part of \mathcal{C}_2 is along a classical trajectory (thin solid), whose caustic (dotted) is outside the inner disk. (b) Path \mathcal{C}_2 (thick solid) for type-II trajectories of the ring. Path \mathcal{C}_1 is similar as in (a) and therefore not shown. The straight parts of \mathcal{C}_2 are along classical trajectories. We indicated one of them (solid thin) and its caustic (dotted) laying inside the inner disk. The thick-dashed line joining the straight parts of \mathcal{C}_2 is a guide to the eye putting in evidence the simple form of Eq. (C3).

Note the second equality holds not only when q_2 is taken along the orbit and q_1 in the perpendicular direction, as supposed by Gutzwiller in its original derivation [51], but also, as shown by Littlejohn, in any coordinate system (see Section III.C in Ref. [78] and Section III in [79]). Although a priori q_1 and q_2 play a similar role, their nonsymmetrical appearance on the right-hand side of Eq. (D1) (q_1 and q_2 can be exchanged without affecting the value of D_M) is due to the fact that one coordinate (here q_1) is chosen as a Poincaré surface of section, and the dependence of the other coordinate (here q_2) just expresses the conservation of energy.

Turning now to the particular problem we are concerned with, i.e. an integrable system at zero field and the diagonal part of the Green function, the above Eq. (D1) applies to D_M (except for a change $t \rightarrow M$ in the label of the orbits). Moreover, the measure $D_M dq_1 dq_2$ in Eq. (6.2) is invariant under the transformation $(q_1, q_2) \rightarrow (\theta_1, \theta_2)$ at zero magnetic field (see Ref. [70] for a more detailed discussion of this point). In other words, noting in Eq. (D1) $D_M(\mathbf{q})$ the determinant in the original \mathbf{q} coordinate and $D_M(\theta)$ the determinant defined in the same way but in the system of coordinates given by Eq. (6.5), one has $D_M(\mathbf{q})dq_1 dq_2 = D_M(\theta)d\theta_1 d\theta_2$. Therefore

$$D_M(\mathbf{q}) \left| \left(\frac{\partial \mathbf{q}}{\partial \theta} \right) \right| = \frac{1}{|\dot{\theta}_2 \dot{\theta}'_2|^{1/2}} \left| -\frac{\partial^2 S}{\partial \theta_1 \partial \theta'_1} \right|^{1/2} = \frac{1}{\dot{\theta}_2} \left| \left(\frac{\partial \theta'_1}{\partial J_1} \right)_{\theta_1} \right|^{-1/2}, \quad (\text{D2})$$

where the derivatives have to be taken at E , θ_2 , and $\theta'_2 = \theta_2 + 2\pi M_2$ constant. To compute the r.h.s. of Eq. (D2) one just needs the expression of the Poincaré mapping $(\theta_1, J_1) \rightarrow (\theta'_1, J'_1)$ between the two ($\theta_2 = \text{const.}$) Poincaré surfaces of section. Since the motion is integrable, $J'_1 = J_1$, and from

Eq. (6.5) we obtain

$$\theta'_1(J_1, \theta_1) = \theta_1 + 2\pi r u_2^2 (\alpha(J_1) - u_1/u_2), \quad (\text{D3})$$

where $\alpha(J_1)$ is the winding number of the torus labeled by J_1 . Thus

$$\left(\frac{\partial \theta'_1}{\partial J_1} \right)_{\theta_1} = 2\pi r u_2^2 \frac{d\alpha}{dJ_1}. \quad (\text{D4})$$

We recall that the function g_E introduced in Section 4 is defined by the implicit relation $H(I_1, I_2 = g_E(I_1)) = E$, which yields after differentiation $dg_E/dI_1 = -\alpha$. Therefore

$$\frac{d\alpha}{dJ_1} = u_2 \frac{d\alpha}{dI_1} = -u_2 \frac{d^2 g_E}{dI_1^2}, \quad (\text{D5})$$

from which one finally obtains

$$D_M \left| \left(\frac{\partial \mathbf{q}}{\partial \theta} \right) \right| = \frac{1}{\dot{\theta}_2} \frac{1}{|2\pi r u_2^3 g_E''|^{1/2}}. \quad (\text{D6})$$

D_M is inversely proportional to the square root of the curvature of the line $H(I_1, I_2) = E = \text{const.}$ and independent of θ .

Appendix E. Diagonal part of the Green function for a free electron in a constant magnetic field

In this section, we calculate semiclassically the diagonal part of the Green function $G(\mathbf{r}, \mathbf{r})$ for a free electron moving in a plane in a perpendicular magnetic field. The resulting classical cyclotron motion is extremely simple, but yields slight complications in the semiclassical evaluation of the diagonal part of the Green function because all trajectories starting at some point \mathbf{r} are refocused precisely at \mathbf{r} . The calculation of the prefactors deserves special attention but can be done using a slight variation of the standard techniques and yields for unconstrained systems the usual result Eq. (1.11). In addition to provide an alternative (semiclassical) derivation of the de Haas–van Alphen effect, our procedure allows to compute correctly the contribution of the cyclotron orbits for billiard systems, i.e. it takes into account the corrections due to the boundaries which appear to be necessary if the cyclotron radius r_c is not small compared to the typical dimension a of the system.

E.1. Computation of the prefactor of a Green function near a focal point

It is an old problem to obtain a correct semiclassical solution of wave equations valid also near turning points, focal points, caustics, etc., where the usual expressions are diverging. A general solution for this problem can for instance be found in the book of Maslov and Fedoriuk [80]. In this subsection, we will give the explicit form of this general theory when applied to the calculation of a two-dimensional Green function and consider in the next subsection the particular problem of a free electron in a constant magnetic field. To avoid confusion we will slightly modify our usual notations, writing $G(\mathbf{r}|\mathbf{r}')$ instead of $G(\mathbf{r}, \mathbf{r}')$. In addition, we will make more explicit what are the initial and final points by using $\mathbf{r}^i = (x^i, y^i)$ for the initial (source) point and, and $\mathbf{r}^f = (x^f, y^f)$ for

the final (observation) point. As already stated, the semiclassical evaluation of the Green function $G(\mathbf{r}^i|\mathbf{r}^f)$ yields a sum over all classical trajectories t joining \mathbf{r}^i to \mathbf{r}^f at energy E

$$G(\mathbf{r}^i|\mathbf{r}^f) = \sum_t G_t(\mathbf{r}^i|\mathbf{r}^f). \quad (\text{E1})$$

For a trajectory t starting at \mathbf{r}^i such that \mathbf{r}^f is not a focal point, one can use (cf. Appendix D, and in particular the discussion concerning the nonsymmetric role of x and y)

$$G_t(\mathbf{r}^i|\mathbf{r}^f) = \frac{1}{i\hbar} \frac{1}{\sqrt{2i\pi\hbar}} D_t \exp \left[\frac{i}{\hbar} S_t - \eta_t \frac{\pi}{2} \right], \quad (\text{E2})$$

$$D_t = \frac{1}{|y^i y^f|^{1/2}} \left| \frac{\partial^2 S}{\partial x^i \partial x^f} \right|^{1/2}. \quad (\text{E3})$$

However, the above expression is not valid near focal points where [locally, and at fixed y^f] x^f becomes independent of p_x^i . The use of the action integral $S(\mathbf{r}^i, \mathbf{r}^f)$ supposes that \mathbf{r}^i and \mathbf{r}^f can be taken as independent variables, and $\partial^2 S / \partial x^i \partial x^f$ is a priori not meaningful since x^f is entirely determined by x^i . Writing $\partial^2 S / \partial x^i \partial x^f = -(\partial x^f / \partial p_x^i)^{-1} = -\infty$ one sees moreover that D_t is, as mentioned above, in fact diverging.

To overcome this difficulty Maslov proposed a procedure to compute $G_t(\mathbf{r}^i|\mathbf{r}^f)$ using a momentum (or mixed position/momentum) representation, by defining (omitting for a moment the source point \mathbf{r}^i)

$$G_t(x^f, y^f) = \mathcal{F}_{p_x^i \rightarrow x^f}^{-1} [\tilde{G}_t(p_x^f, y^f)], \quad (\text{E4})$$

where $\mathcal{F}_{p_x^i \rightarrow x^f}^{-1}$ is the inverse Fourier transform

$$\mathcal{F}_{p_x^i \rightarrow x^f}^{-1}[\cdot] = \frac{1}{\sqrt{-2i\pi\hbar}} \int dp_x^f[\cdot] \exp \left(\frac{i}{\hbar} x^f p_x^f \right). \quad (\text{E5})$$

performing quantum mechanically the change from the mixed representation (p_x, y) to the position representation (x, y) .

Eq. (E4) is just the definition of \tilde{G}_t which remains to be evaluated semiclassically. The general theory presented in Ref. [80] (Section 5.1) can be however applied to our problem, giving

$$\tilde{G}_t(p_x^f, y^f) = \frac{1}{i\hbar} \frac{1}{\sqrt{2i\pi\hbar}} \tilde{D}_t \exp \left[\frac{i}{\hbar} \tilde{S}_t - \tilde{\eta}_t \frac{\pi}{2} \right] \quad (\text{E6})$$

where

$$\tilde{S} = S - p_x^f x^f, \quad (\text{E7})$$

$$\tilde{D}_t = D_t \left| \frac{\partial x^f}{\partial p_x^f} \right|_{p_x^f = \text{const.}}^{1/2}, \quad (\text{E8})$$

$$\tilde{\eta}_t = \begin{cases} \eta_t & \text{if } \partial p_x^f / \partial x^f > 0, \\ \eta_t + 1 & \text{if } \partial p_x^f / \partial x^f < 0. \end{cases} \quad (\text{E9})$$

Without entering into a derivation of this semiclassical formula for \tilde{G}_t , it can be checked that starting from Eq. (E6) the evaluation of the inverse Fourier transform Eq. (E4) using stationary phase approximation readily yields Eq. (E2). Far from any focal point both expressions are equivalent at the semiclassical level. Near a focal point however, Eq. (E6) still provides an accurate approximation for \tilde{G}_t because the Lagrangian manifold, on which the Green function is constructed semiclassically, has a nonsingular projection onto the plane (p_x, y) . Therefore, contrarily to Eq. (E2) which is diverging, Eq. (E4) is still a valid semiclassical approximation for G_t , provided the inverse Fourier transformation is evaluated exactly (or using uniform techniques going beyond stationary point approximation [81]).

From Eqs. (E3) and (E8) one has

$$\tilde{D}_t = \frac{1}{|\dot{y}^i \dot{y}^f|^{1/2}} \left| \frac{\partial^2 \tilde{S}}{\partial x^i \partial p_x^f} \right|^{1/2}. \quad (\text{E10})$$

This explains why the Legendre transform \tilde{S}_t of S_t has to be understood as a function of x^i and p_x^f . In practice, this means that, to compute \tilde{S}_t from Eq. (E7), the action integral S_t has to be calculated for a trajectory starting at position x^i and ending with a momentum p_x^f , and that in the additional term $x^f p_x^f$, x^f has to be interpreted as $x^f(x^i, p_x^f)$. Finally, note that for a Hamiltonian, which can be decomposed into a kinetic energy plus potential part (including the case where a magnetic field is present), $\partial p_x^f / \partial x^f$ is always negative just in front of a focal point and always positive directly after the focal point. Therefore

$$\tilde{\eta}_t = \begin{cases} \eta_t & \text{right after a focal point,} \\ \eta_t + 1 & \text{just before a focal point.} \end{cases}$$

Since precisely at focal points η_t is incremented by one unit (for a kinetic energy plus potential Hamiltonian), this implies that, when crossing a focal point, $\tilde{\eta}_t$ remains constant, keeping the value which η_t acquires after the focal point. This latter has to be taken into account for the computation of Maslov indices of a trajectory at a focal point.

E.2. Application to the cyclotron motion

Turning now to the specific problem we are concerned with, i.e. cyclotron motion and diagonal elements of the Green function, we need to calculate $\tilde{S}(x^i, y^i, p_x^f, y^f)$, where we can however restrict ourselves to $y^f = y^i$ since the partial derivatives are taken only in the x direction. Eq. (E7) states that, omitting the y 's, $\tilde{S}_n(x^i, p_x^f) = S_n(x^i, p_x^f) - x^f(x^i, p_x^f)p_x^f$, where $S_n(x^i, p_x^f)$ is the action integral along a trajectory starting at the abscissa x^i and arriving with a momentum p_x^f . But here the Poincaré map $(x^i, p_x^i) \rightarrow (x^f, p_x^f)$ is just the identity, and therefore

$$\begin{aligned} \tilde{S}_n(x^i, p_x^f) &= nS_0 - x^i p_x^f, \\ \left| \frac{\partial^2 \tilde{S}_n}{\partial x^i \partial p_x^f} \right| &= 1; \end{aligned}$$

where S_0 is given by Eq. (7.14). Noting moreover that $\dot{y}^i = \dot{y}^f$ for all trajectories, and that they pass through two focal points at each turn, one has from Eq. (E4) (omitting the Weyl part of G)

$$G(\mathbf{r}^i | \mathbf{r}^f = \mathbf{r}^i) = \sum_n \frac{1}{i\hbar} \frac{1}{\sqrt{2i\pi\hbar}} \frac{(-1)^n}{\sqrt{-2i\pi\hbar}} \exp \left[\frac{i}{\hbar} n S_0 \right] \int \frac{d\mathbf{p}_x^f}{\dot{y}^f}. \quad (\text{E11})$$

At fixed position, $d\mathbf{p}_x^f = m d\dot{x}^f$ (the vector potential eliminates). Therefore the remaining integral in Eq. (E11) is just, up to a multiplication by the mass m of the electron, an integral over the angle θ specifying the direction of the trajectory at \mathbf{r} . For unbounded motion, it simply gives a factor $2\pi m$, yielding the expected result

$$G(\mathbf{r}^i | \mathbf{r}^f = \mathbf{r}^i) = \sum_n (-1)^n \frac{m}{\hbar^2} \exp(inS_0/\hbar - i\pi/2). \quad (\text{E12})$$

In billiard systems the contribution to G of the cyclotron orbits is the same as for the unbounded motion, except that for points \mathbf{r} close to the boundary, Eq. (E12) has to be reduced by a multiplicative factor $\theta_{\text{eff}}/(2\pi)$, where θ_{eff} is the angular measure of the trajectories not affected by the boundary. The contribution to the density of states of the cyclotron orbits is thus

$$d^{\text{osc}}(E, H) = s(H) \frac{g_s A m}{\pi \hbar^2} \sum_n (-1)^n \cos(n\pi k r_c). \quad (\text{E13})$$

The multiplicative factor $s(H)$ is given by

$$s(H) = \frac{1}{2\pi A} \int d\mathbf{r} d\theta \zeta(\mathbf{r}, \theta). \quad (\text{E14})$$

The function $\zeta(\mathbf{r}, \theta)$ is defined such that $\zeta = 1$ if the trajectory started at \mathbf{r} with initial velocity along θ does not hit the boundary, and $\zeta = 0$ otherwise. Substituting in the integral above the variables (\mathbf{r}, θ) by $(\tilde{\mathbf{r}}, \tilde{\theta})$, where $\tilde{\mathbf{r}}$ specifies the center of the cyclotron orbit and $\tilde{\theta}$ the position on this orbit (the Jacobian of the transformation is equal to one) and performing the integral over $\tilde{\theta}$ since then ζ depends only on $\tilde{\mathbf{r}}$, one obtains

$$s(H) = \frac{1}{A} \int d\mathbf{r} \zeta(\tilde{\mathbf{r}}), \quad (\text{E15})$$

which yields Eq. (7.20) for the square geometry.

As a final comment, we note that the approach described here for a two-dimensional electron gas can be generalized in a straightforward manner to three dimensional systems, including cases with non-spherical Fermi surfaces.

References

- [1] L.D. Landau, Z. Phys. 64 (1930) 629.
- [2] L.D. Landau and E.M. Lifshitz, Statistical Physics (Pergamon, Oxford, 1985).
- [3] J.H. van Leeuwen, J. Phys. (Paris) 2 (1921) 361.
- [4] R.E. Peierls, Quantum Theory of Solids (Oxford University Press, Oxford, 1964); Surprises in Theoretical Physics (Princeton University Press, Princeton NJ, 1979).

- [5] E.H. Sondheimer and A. H. Wilson, *Proc. Roy. Soc.* 210 A (1952) 173.
- [6] R.E. Peierls, *Z. Phys.* 80 (1933) 763.
- [7] D. Shoenberg, *Proc. R. Soc.* 170 A (1939) 341.
- [8] D.A. van Leeuwen, Ph.D. Thesis, University of Leiden, unpublished, 1993; J.M. van Ruitenbeek and D.A. van Leeuwen, *Mod. Phys. Lett. B* 7 (1993) 1053.
- [9] A. Papapetrou, *Z. Phys.* 107 (1937) 387, L. Friedman, *Phys. Rev.* 134 A (1964) 336, S. S. Nedorezov, *Zh. Eksp. Teor. Fiz.* 64 (1973) 624 [*Sov. Phys. JETP* 37 (1973) 317].
- [10] R.B. Dingle, *Proc. R. Soc.* 212 A (1952) 47.
- [11] R.V. Denton, *Z. Phys.* 265 (1973) 119.
- [12] R. Németh, *Z. Phys. B* 81 (1990) 89.
- [13] E.N. Bogachev and G.A. Gogadze, *Pis'ma Zh. Eksp. Teor. Fiz.* 63 (1972) 1839, [*Sov. Phys. JETP* 36 (1973) 973].
- [14] D.B. Bivin and J.W. McClure, *Phys. Rev. B* 16 (1977) 762.
- [15] W. Lehle, Yu. N. Ovchinnikov and A. Schmid, unpublished.
- [16] B. Shapiro, *Physica A*, 200 (1993) 498.
- [17] M. Robnik, *J. Phys. A* 19 (1986) 3619.
- [18] M. Antoine, Thesis (Université Paris VI, unpublished, 1991).
- [19] J.M. van Ruitenbeek, *Z. Phys. D* 19 (1991) 247; J.M. van Ruitenbeek and D.A. van Leeuwen, *Phys. Rev. Lett.* 67 (1991) 641.
- [20] Y. Imry, in: *Directions in Condensed Matter Physics*, eds. by G. Grinstein and G. Mazenko (World Scientific, Singapore, 1986).
- [21] M.C. Gutzwiller, *Chaos in Classical and Quantum Mechanics* (Springer, Berlin, 1990).
- [22] O. Bohigas, in: *Chaos and Quantum Physics*, *Proc. Les Houches Summer School, Session LII, 1989*, eds. M.-J. Giannoni, A. Voros, and J. Zinn-Justin (North-Holland, Amsterdam, 1991).
- [23] C.M. Marcus, R.M. Westervelt, P.F. Hopkins and A.C. Gossard, *Chaos*, 3 (1993) 643.
- [24] H.U. Baranger, R.A. Jalabert and A.D. Stone, *Chaos*, 3 (1993) 665.
- [25] L.P. Lévy, D.H. Reich, L. Pfeiffer and K. West, *Physica B* 189 (1993) 204.
- [26] D. Mailly, C. Chapelier, and A. Benoit, *Phys. Rev. Lett.* 70 (1993) 2020.
- [27] K. Nakamura and H. Thomas, *Phys. Rev. Lett.* 61 (1988) 247.
- [28] M. Rezakhanlou, H. Kunz and A. Crisanti, *Europhys. Lett.* 16 (1991) 629.
- [29] M. Büttiker, Y. Imry and R. Landauer, *Phys. Lett. A* 96 (1983) 365.
- [30] F. von Oppen, Ph.D. Thesis (University of Washington, unpublished, 1993).
- [31] R. Landauer, in: *Coulomb and Interference Effects in Small Electronic Structures*, eds. D.C. Glattli, M. Sanquer and J. Trân Thanh Vân (Frontiers, Gif-sur-Yvette, 1994).
- [32] H.F. Cheung, Y. Gefen and E.K. Riedel, *IBM J. Res. Develop.* 32 (1988) 359.
- [33] L. P. Lévy, G. Dolan, J. Dunsmuir and H. Bouchiat, *Phys. Rev. Lett.* 64 (1990) 2074.
- [34] H. Bouchiat and G. Montambaux, *J. Phys. (Paris)* 50 (1989) 2695.
- [35] Y. Imry, in: *Coherence Effects in Condensed Matter Systems*, ed. B. Kramer (Plenum, New York, 1991).
- [36] A. Schmid, *Phys. Rev. Lett.* 66 (1991) 80; F. von Oppen and E.K. Riedel, *ibid* 84; B.L. Altshuler, Y. Gefen and Y. Imry, *ibid* 88.
- [37] V. Chandrasekhar, R.A. Webb, M.J. Brady, M.B. Ketchen, W.J. Gallagher and A. Kleinsasser, *Phys. Rev. Lett.* 67 (1991) 3578.
- [38] R.L. Schult, et al., *Superlattices and Microstructures* 11 (1991) 73.
- [39] F. von Oppen and E.K. Riedel, *Phys. Rev. B* 48 (1993) 9170.
- [40] M.V. Berry and J.P. Keating, *J. Phys. A* 27 (1994) 6167.
- [41] O.D. Cheishvili, *Pis'ma Zh. Eksp. Teor. Fiz.* 48 (1988) 206 [*JETP Lett.* 48 (1988) 225].
- [42] S. Oh, A.Yu. Zyuzin and A. Serota, *Phys. Rev. B* 44 (1991) 8858; A. Raveh and B. Shapiro, *Europhys. Lett.* 19 (1992) 109; B.L. Altshuler, Y. Gefen, Y. Imry and G. Montambaux, *Phys. Rev. B* 47 (1993) 10340.
- [43] K. Richter, D. Ullmo and R.A. Jalabert, unpublished.
- [44] N.W. Ashcroft and N.D. Mermin, *Solid State Physics* (Saunders College, Philadelphia, 1976).
- [45] J.P. Eisenstein et al., *Phys. Rev. Lett.* 55 (1985) 875.
- [46] U. Sivan and Y. Imry, *Phys. Rev. Lett.* 61 (1988) 1001.
- [47] D. Yoshioka, *J. Phys. Soc. Japan* 62 (1993) 3198.

- [48] J. Hajdu and B. Shapiro, *Europhys. Lett.* 28 (1994) 61.
- [49] H. Mathur, M. Gökçedag and A.D. Stone, *Phys. Rev. Lett* 74 (1995) 1855.
- [50] O. Agam, *J. Phys. I (France)* 4 (1994) 694.
- [51] M.C. Gutzwiller, *J. Math. Phys.* 11 (1970) 1791; *J. Math. Phys.* 12 (1971) 343.
- [52] M.V. Berry, M. Tabor, *Proc. R. Soc. Lond. A.* 349 (1976) 101.
- [53] M.V. Berry and M. Tabor, *J. Phys. A* 10 (1977) 371.
- [54] R. Balian and C. Bloch, *Ann. Phys.* 69 (1972) 76, reprinted in: Claude Bloch, *Oeuvre Scientifique*, eds. R. Balian, C. de Dominicis, V. Gillet and A. Messiah (North Holland/American Elsevier, 1975).
- [55] A.M. Ozorio de Almeida, in: *Quantum Chaos and Statistical Nuclear Physics*, Lecture Notes in Physics 263, ed. T. Seligman (Springer, New York, 1986).
- [56] A.M. Ozorio de Almeida, *Hamiltonian Systems: Chaos and Quantization* (Cambridge University Press, Cambridge, 1988).
- [57] D. Ullmo, K. Richter and R.A. Jalabert, *Phys. Rev. Lett.* 74 (1995) 383.
- [58] R.A. Jalabert, K. Richter and D. Ullmo, in Ref. [31].
- [59] F. von Oppen, *Phys. Rev. B* 50 (1994) 17151.
- [60] Y. Gefen, D. Braun and G. Montambaux, *Phys. Rev. Lett.* 73 (1994) 154.
- [61] S.D. Prado, M.A.M. de Aguiar, J.P. Keating and R. Eglydio de Carvalho, *J. Phys. A* 27 (1994) 6091.
- [62] M. Seeley, *Am. J. Math.* 91 (1969) 889.
- [63] E.P. Wigner, *Phys. Rev.* 40 (1932) 749.
- [64] I.O. Kulik, *Zh. Eksp. Teor. Fiz.* 58 (1970) 217 [*Sov. Phys. JETP* 31 (1970)1172]; and *ZhETF Pis. Red.* 11 (1970) 407 [*JETP Lett.* 11 (1970) 275].
- [65] V.I. Arnold, *Mathematical Methods of Classical Mechanics* (Springer, New York, 1984).
- [66] J.B. Keller and S.I. Rubinow, *Ann. Phys.* 9 (1960) 24.
- [67] O. Bohigas, M.-J. Giannoni, A.M. Ozorio de Almeida and C. Schmit, *Nonlinearity* 8 (1995) 203.
- [68] I.S. Gradshteyn and I.M. Ryzhik, *Table of Integrals, Series and Products* (Academic Press, New York, 1980).
- [69] M. Brack, O. Genzken and K. Hansen, *Z. Phys. D* 21 (1991) 655.
- [70] M. Grinberg, S. Tomsovic and D. Ullmo, preprint.
- [71] J.H. Hannay and A.M. Ozorio de Almeida, *J. Phys. A* 17 (1984) 3429.
- [72] E. Doron, U. Smilansky and A. Frenkel, *Physica D* 50 (1991) 367, R. Jensen, *Chaos* 1 (1991) 101.
- [73] M. Robnik in *Nonlinear Phenomena and Chaos*, ed. S. Sarkar (Adam Hilger, Bristol, 1986).
- [74] U. Eichmann, K. Richter, D. Wintgen and W. Sandner, *Phys. Rev. Lett.* 61 (1988) 2438.
- [75] V. Ambegaokar and U. Eckern, *Phys. Rev. Lett.* 65 (1991) 381.
- [76] R. Jalabert and S. Das Sarma, *Phys. Rev. B* 40 (1989) 9723.
- [77] O. Bohigas, S. Tomsovic and D. Ullmo, *Phys. Rep.* 223 (1993) 43.
- [78] R.G. Littlejohn, *J. Math. Phys.* 31 (1990) 2952.
- [79] S.C. Creagh, J.M. Robbins and R.G. Littlejohn, *Phys. Rev. A* 42 (1990) 1907.
- [80] V.P. Maslov and M.V. Fedoriuk, *Semiclassical Approximation in Quantum Mechanics* (Reidel, Dordrecht, 1981).
- [81] A.M. Ozorio de Almeida and J.H. Hannay, *J. Phys. A* 20 (1987) 5873.
- [82] A. Altland and Y. Gefen, *Phys. Rev. B* 51 (1995) 10671.
- [83] R. Kubo, *J. Phys. Soc. Japan* 19 (1964) 2127.